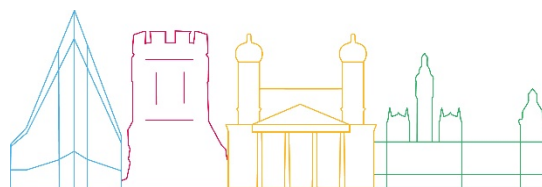




ARCH D5.1

Hazard models for impact assessment



Deliverable No.	D5.1
Work Package	WP5
Dissemination Level	PU
Author(s)	Sonia Giovinazzi (ENEA), Antonio Costanzo (INGV), Maurizio Pollino, Ludovica Giordano, Maurizio Sciortino, Antonio Di Pietro, Vittorio Rosato (ENEA), María Puig Fuentenebro, Iván Rafael Rodríguez Gelpi, Saioa Zorita, Nieves Peña (Tecnalia), Marco Materazzi (UNICAM)
Co-Author(s)	-
Contributor(s)	Manel Alemany Martínez (Càtedra L'Horta de València: Territori metropolitana- Universitat de València), Francisco Galiana Galán (Universitat Politècnica de València), Miquel Jordà Piqueras (Consorci del Consell de l'Horta de València), Emilio Servera Martínez (Las Naves)
Due date	2021-11-30
Actual submission date	2022-01-20
Status	Final
Revision	1.0
Reviewed by	Antonino D'Alessandro (INGV), Emilio Servera Martínez (Las Naves), Quintilio Piattoni (Camerino Municipality), Luisa Lavalle (ENEA)

This document has been prepared in the framework of the European project ARCH – Advancing Resilience of historic areas against Climate-related and other Hazards. This project has received funding from the European Union’s Horizon 2020 research and innovation programme under grant agreement no. 820999. The sole responsibility for the content of this publication lies with the authors. It does not necessarily represent the opinion of the European Union. Neither the REA nor the European Commission are responsible for any use that may be made of the information contained therein.

Contact

arch@iais.fraunhofer.de

www.savingculturalheritage.eu



This project has received funding from the European Union’s Horizon 2020 research and innovation programme under Grant Agreement no. 820999.

Executive Summary

This deliverable has been prepared for the European Commission-funded research project ARCH: Advancing Resilience of historic areas against Climate-related and other Hazards. It is the key output of Task 5.1 “*Hazard models for impact assessment*” within Work Package 5, WP5 “*Impact & Risk Assessment*”.

The aim of Task 5.1 has been to develop and adapt hazard models and to foresee the use of further environmental and heritage asset data collected as part of WP4 “*Hazard & Object Information Management System*” to be used for estimating the possible impacts on Historic Areas due to climate change and other hazards such as earthquakes. Toward that, hazard models described in this deliverable, as well as hazard indicators defined in WP4, will be coupled with the vulnerability models, described in Task 5.2 *Vulnerability and consequence analysis*, aiming to assess risk and impacts scenarios, co-created with the 4 ARCH pilots (as described in Task 3.4.3) and implemented and represented within ARCH Decision Support System, DSS (T5.3).

The work describes in this deliverable focused in particular on summarizing *methods, data and results* in relation to:

- Climate-change hazard maps for
 - extreme temperature assessed under different climate scenarios according to the current land use and under the hypothesis of possible future modifications of the land use;
 - pluvial flooding accounting for, digital terrain models, and urban parameters (such as building height, land cover, vegetation).
- Earthquake hazard maps for
 - ground motion shaking produced for both user-defined and real earthquake events;
 - soil characterization to support the identification of resonance effects and possible soil-structure interactions;
 - earthquake-induced mass movements and landslides.

Table of contents

Executive Summary	3
Table of contents.....	4
1. Introduction	8
1.1. Gender statement	10
1.2. Purpose of this report and relation to other deliverables	10
2. Climate-Change Hazard Models	11
2.1. Climate-change hazard models and maps for the assessment of extreme temperature impacts on socio-ecologic systems	13
2.1.1. Methods	14
2.1.2. Data	22
2.1.3. Results	33
2.1.4. Climate change effect analysis on temperature - Current land use scenario.....	33
2.1.5. Land use effect analysis - Outcomes from the grey and black land use scenarios	41
2.1.6. Concluding remarks	44
2.2. Climate-change hazard models and maps for pluvial flooding impact assessment	45
2.2.1. Methods	46
2.2.2. Data	47
2.2.3. Results	54
3. Earthquake Hazard Models for Impact assessment	62
3.1. Ground Shaking Models and Maps for impact assessment	62
3.1.1. Methods	65
3.1.2. Data	68
3.1.3. Results	71
3.2. Earthquake-induced landslide hazard models and maps for impact assessment.....	74
3.3. Earthquake-induced Soil-structure interaction: Hazard models and maps for	81
3.3.1. Seismic Microzonation (SM): methods and results	81
3.3.2. Geophysical investigation: methods and results for Camerino Municipality hill	84
3.3.3. Results: P-wave velocity maps	87
4. References.....	88
6. Annex: Thermal model maps for the grey and black scenario.....	94
6.1. Historic data	94
6.2. Near Future (2011-2040)	97
6.3. Next Future (2041-2070).....	100
6.4. Far Future (2071-2100).....	102

7. Annex: Earthquake-induced ground shaking maps 105

Table of Abbreviations

Acronym	Explanation
C3S	Copernicus Climate Change Service
CDS	Climate Data Store
DSHA	Deterministic Seismic Hazard Assessment
DSS	Decision Support System
ECMWF	European Centre for Medium-Range Weather Forecasts
EMSC	European Mediterranean Seismological Centre
EMS98	European Macroseismic Scale Intensity
GHGs	Global Concentration of Greenhouse gases
GMPE	Ground Motion Prediction Equation
HAs	Historic Areas
INGV	National Institute of Geophysics and Volcanology
IPCC	Intergovernmental Panel on Climate Change
I _{MCS}	Mercalli-Cancani-Siberg Macroseismic Intensity
I _{EMS98}	European Scale Macroseismic Intensity
LSAT	Land Surface Air Temperature
M _w	Earthquake Moment Magnitude
NCAR	National Center of Atmospheric Research
PGA	Peak Ground Acceleration
PGV	Peak Ground Velocity
PGD	Peak Ground Displacement
S _a	Elastic Spectral Acceleration
S _v	Elastic Spectral Velocity
S _d	Elastic Spectral Displacement
SIOSE	Land Cover/Land Use Information System of Spain
SM	Seismic Microzonation



SRTM Shuttle Radar Topography Mission

USGS United States Geological Survey

WPS Web Processing Service

WRF-ARW Weather Research and Forecasting-Advanced Research

1. Introduction

Sonia Giovinazzi (ENEA)

This deliverable has been prepared for the European Commission-funded research project ARCH: Advancing Resilience of historic areas against Climate-related and other Hazards. ARCH is developing decision support tools and methodologies to improve the resilience of historic areas to climate change-related and other hazards. These tools and methodologies are developed with the pilot cities of Bratislava (Slovakia), Camerino (Italy), Hamburg (Germany), and València (Spain), via a co-creative approach, involving local policy makers, practitioners, and community members. The resulting solutions will be combined into a collaborative disaster risk management platform for guided resilience building, and will include:

- an information management system for relevant geo-referenced properties of historic areas;
- an information management system for geo-referenced data regarding hazards and risks relevant for historic areas
- a Decision Support System (DSS) for risk and impact analysis of historic areas;
- an inventory of resilience building measures and appropriate financing sources;
- a visual planning tool for resilience pathways;
- a resilience assessment framework to identify resilience weak points and formulate resilience action plans.

The aim of Task 5.1, whose results are reported in this Deliverable, i.e. D5.1 “*Hazard models for impact assessment*”, has been to develop and adapt hazard models to be used for estimating the possible impacts on Historic Areas due to climate change and other hazards, such as earthquakes. Towards that Task 5.1 has been processed and exploited the hazard data collected as part of WP4 “*Hazard & Object Information Management System*”.

To fully understand the purpose of this report and its relation to other ARCH deliverables it is worth briefly reminding which are the determinants of risk assessment, namely: Hazard,

Assessing risk for Damages and Impacts induced by Natural Hazards in HAs

Impacts and damages to the built and natural environment, as well as to the social, economic and intangible dimensions of the Historic Areas, HAs, potentially induced by climate changes and other hazards can be estimated by convoluting:

- the assessment of the hazards that might potentially affect the HA location;
- the characterisation of the elements, both tangible and intangible, included in the different dimensions of the HA, exposed to those hazards;
- the assessment of the vulnerabilities of the HA’s exposed elements to each specific hazard identified.

Exposure and Vulnerability; and how impacts can be estimated as a function of those determinants for Historic Areas (HAs).

The abovementioned concept, specifically customized for HAs, is universally recognized [1] , [2], [3], [4], [5], [6], by and can be summarized in the following Equation:

$$Impacts \approx Hazard * Exposure * Vulnerability (1)$$

where the symbol * has the meaning of convoluting and the symbol \approx has the meaning of numerical approximations.

An important aspect to be highlighted about risk and impact scenario assessment is in fact the incomplete knowledge in each one of the three abovementioned determinates, i.e. hazard assessment, exposure characterization and vulnerability assessment; these uncertainties, that necessarily combines into an *expanded uncertainty* affecting the impact assessment do not necessarily have to be quantified [7], and in the ARCH project has been quantified only to a certain extent. However, it is imperative to be aware and make any potential users aware about the gaps in knowledge and resulting uncertainties and about the fact that because of that an impact assessment is just targeting the estimation of “*the potential for adverse impacts and consequences*”, where the word “*potentia*” is used to make clear and explicit the uncertainty affecting the assessment.

The same concept of assessing risk for impact as convolution of hazard, exposure and vulnerability is clearly represented in Figure 1.

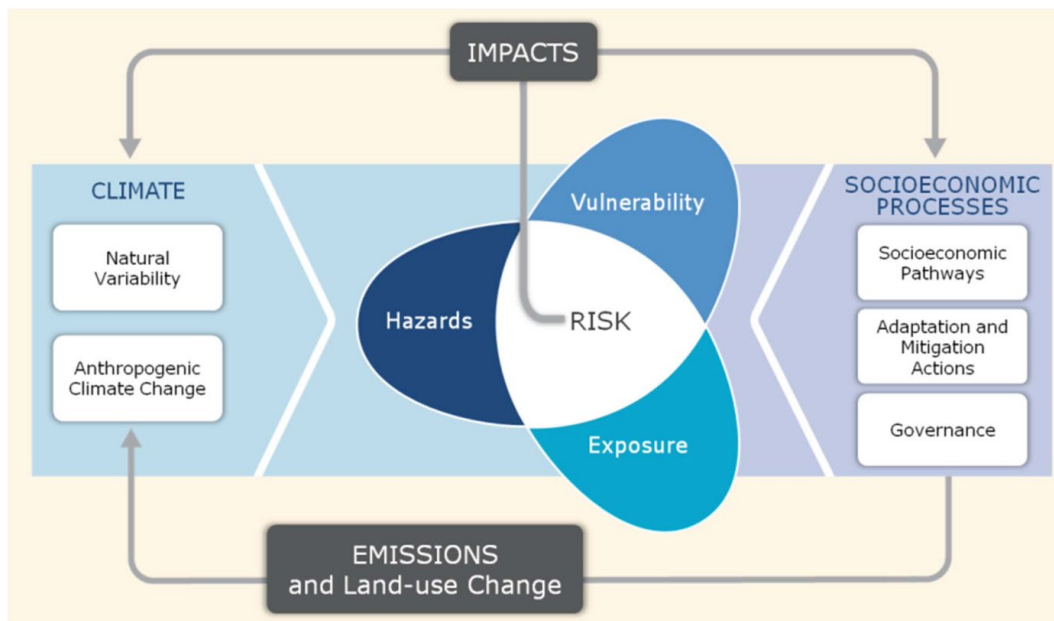


Figure 1. Assessing Risk for Impacts by convoluting hazard, exposure and vulnerability according to IPCC Assessment Report number 5, IPCC AR5 [7].

1.1. Gender statement

This document has been developed taking into consideration the guidance on gender in research provided in the Project Handbook (D1.2)¹ as well as State-of-the-Art report number 5 of deliverable D7.1² on “Gender aspects in conservation and regulation of historic areas, disaster risk management, emergency protocols, post-disaster response techniques, and techniques for building back better”.

1.2. Purpose of this report and relation to other deliverables

Task 5.1 and Deliverable D5.1 of the ARCH Project have been focusing on the assessment of the Hazard that refers to the possible, future occurrence of natural or human-induced physical events that may have adverse effects on vulnerable and exposed elements. The intensity or recurrence of natural hazard events can be partly determined by environmental degradation and human intervention in natural ecosystems. Landslides or flooding regimes associated with human-induced environmental alteration and new climate change-related hazards are examples of such socio-natural hazards, that have been analyzed in ARCH Project.

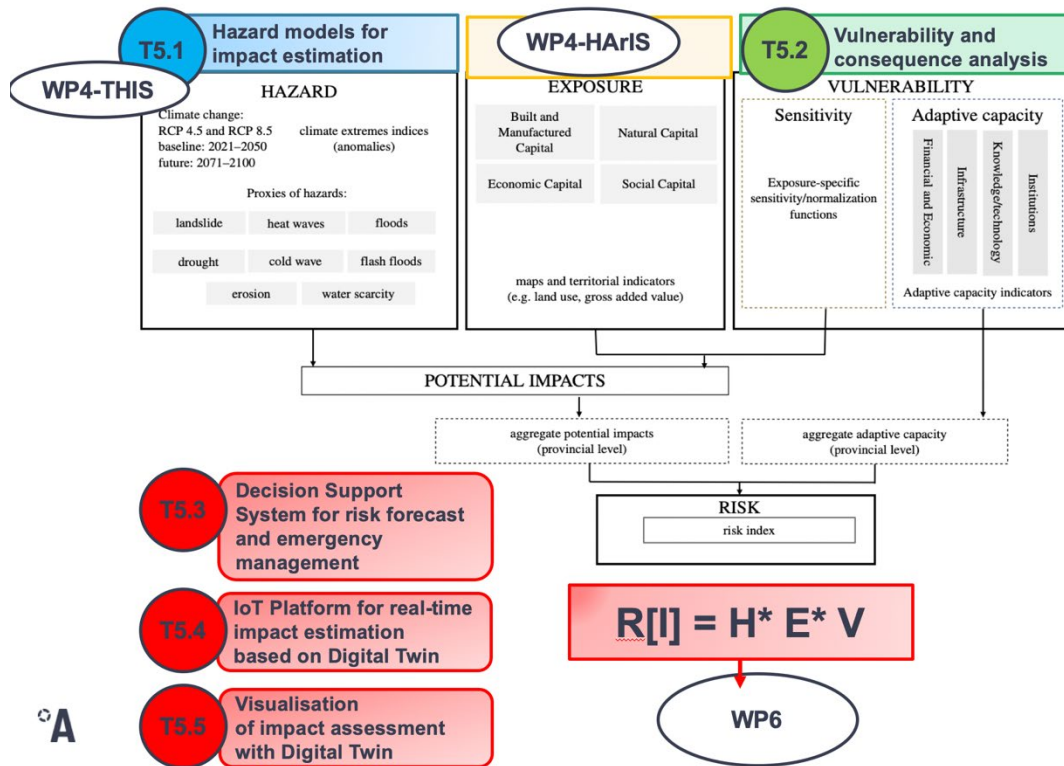


Figure 2. Methodological framework for the Climate Risk Index Assessment adapted from [8].

With reference to a different graphical representation (Figure 2) of the same risk concept already expressed in Equation 1 and represented in Figure 1, it is easily possible to explain

¹ D. Lückerrath, "ARCH D1.2 Project Handbook," H2020 ARCH, GA no. 820999, 2019.

² V. Rebollo, T. Rangil-Escribano and E. Chapman, "ARCH D7.1 State-of-the-Art report no. 5: Gender aspects in conservation and regulation of historic areas, disaster risk management, emergency protocols, post-disaster response techniques, and techniques for building back better," H2020 ARCH, GA no. 820999, 2019

how the purpose and content of this report is related to the ARCH work packages, WPs, and the other deliverables of the ARCH project.

WP4 provides data to WP5 for hazard, exposure and vulnerability assessment. WP5 provides to WP6 the inputs for identifying where and for estimating to what extent resilience interventions are needed. In turn WP6 provides to WP5, as an input, the resilience strategies to be tested in term of both *ex-ante* scenarios (i.e. scenarios in current conditions) and *ex-post* impact scenarios (i.e. scenarios after the implementation of resilience strategies); this in order to quantify the benefits, in term of diminished impacts as well as raising opportunities, resulting from the implementation of resilience strategies.

As such, D5.1 is directly related to the following deliverables and ARCH tools:

- *D3.3, City baseline report; D3.4, Report on co-creating the information systems; D3.5, Report on co-creating the Impact and Risk Assessment*: providing the co-creation context and the inputs from the pilot cities on the impact scenarios of interest for the cities and therefore on the needed hazard assessment;
- *D4.1, Sensing and Repositories; and D4.2 Historic Area Information Management System (HARIS tool)*: proving the data needed for the exposure characterization;
- *D4.3 Threats and Hazard Information Management System (THIS tool)*: providing further data and indicators for hazard mapping;
- *D5.2, Handbook on heritage asset vulnerability*: providing the models for the vulnerability assessment;
- *D5.3, Decision Support System for risk forecast and emergency management*: describing the system where the hazard assessment will be embedded to be convoluted with the exposure characterization and vulnerability assessment in order to estimate potential risk and impacts.
- *D6.1, Inventory of preparation, safeguarding, conservation & management, and response & recovery options*: providing a collection of possible resilience strategies for different kind of hazards to be tested in *ex-post* scenarios.
- *D6.2, Assessment of long-term implementation options*: providing, among other things a literature review and quantification on an hazard specific evidences of the benefits brought by different resilience options to be used for calibrating the models embedded in the ARCH DSS tools.

2. Climate-Change Hazard Models

María Puig Fuentenebro, Iván Rafael Rodríguez Gelpi, Nieves Peña, Saioa Zorita (Tacnalia); Emilio Servera Martínez (Las Naves)

The interrelation between land use and the climate is complex, however it is clear that while climate may shape the landcover and thus land use, land use practices affect the global concentration of greenhouse gases (GHGs)³. Furthermore, land use change is an important climatic driver and non-climatic driver e.g. for biodiversity loss which will impact ecosystems and, thus, again indirectly affecting land use.

³ <https://unfccc.int/topics/land-use/the-big-picture/introduction-to-land-use>

According to the Intergovernmental Panel on Climate Change (IPCC) Special Report on Climate Change and Land⁴, land is both a source and a sink of GHGs and plays a key role in the exchange of energy, water and aerosols between the land surface and atmosphere. Moreover, according to the same report, the globally averaged Land Surface Air Temperature (LSAT) has risen faster than the global mean surface temperature (combined LSAT and sea surface temperature) from the preindustrial period (1850–1900) to the present day (1999–2018). According to the single longest and most extensive dataset, from 1850–1900 to 2006–2015 mean land surface air temperature has increased by 1.53°C (very likely range from 1.38°C to 1.68°C) while global mean surface temperature has increased by 0.87°C (likely range from 0.75°C to 0.99°C).

As it is showed in Figure 3, land surface features such as albedo and emissivity regulate the amount of solar and long-wave radiation absorbed by land and reflected or emitted to the atmosphere. “Surface roughness influences turbulent exchanges of momentum, energy, water and biogeochemical tracers. Land ecosystems modulate the atmospheric composition through emissions and removals of many GHGs and precursors of Short-lived climate forces (SLCFs), including biogenic volatile organic compounds (BVOCs) and mineral dust. Atmospheric aerosols formed from these precursors affect regional climate by altering the amounts of precipitation and radiation reaching land surfaces through their role in clouds physics”².

Therefore, a sustainable land management can contribute to reducing the negative impacts of multiple stressors, including climate change.

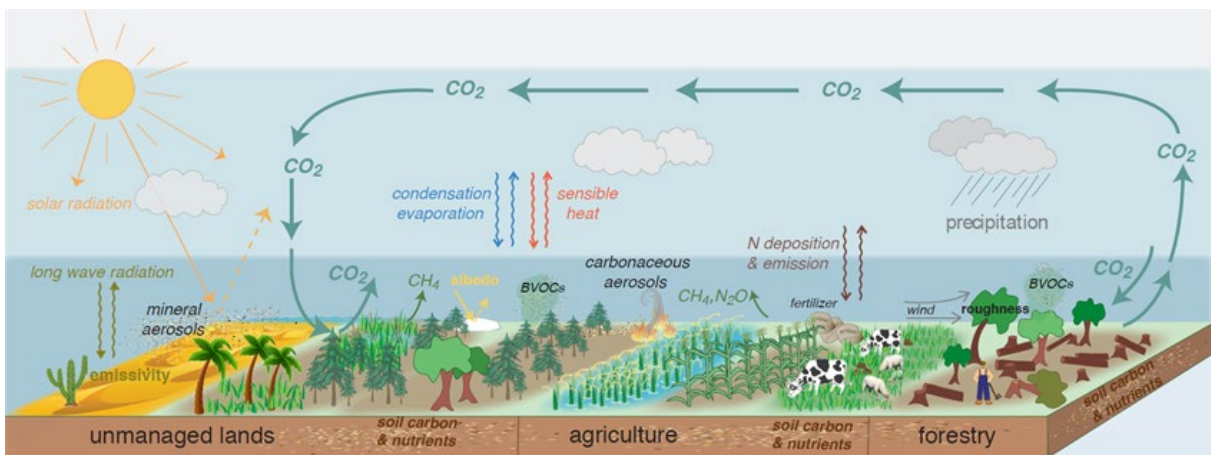


Figure 3. The structure and functioning of managed and unmanaged ecosystems that affect local, regional and global climate. Source: IPCC, 2019⁵

⁴ IPCC, 2019: Climate Change and Land: an IPCC special report on climate change, desertification, land degradation, sustainable land management, food security, and greenhouse gas fluxes in terrestrial ecosystems [P.R. Shukla, J. Skea, E. Calvo Buendia, V. Masson-Delmotte, H.-O. Pörtner, D. C. Roberts, P. Zhai, R. Slade, S. Connors, R. van Diemen, M. Ferrat, E. Haughey, S. Luz, S. Neogi, M. Pathak, J. Petzold, J. Portugal Pereira, P. Vyas, E. Huntley, K. Kissick, M. Belkacemi, J. Malley, (eds.)]. In press.

⁵ IPCC, 2019: Climate Change and Land: an IPCC special report on climate change, desertification, land degradation, sustainable land management, food security, and greenhouse gas fluxes in terrestrial ecosystems [P.R. Shukla, J. Skea, E. Calvo Buendia, V. Masson-Delmotte, H.-O. Pörtner, D. C. Roberts, P. Zhai, R. Slade, S.

On the other side, the frequency and intensity of some extreme weather and climate events have increased as a consequence of the global warming and, according to the IPCC's latest report⁶, this will continue to increase under medium and high emission scenarios (high confidence).

Ad hoc *Climate Indicators* have been identified, measured and represented for the four pilots in ARCH HARIS tool (ARCH Deliverable D4.3) as part of the ARCH project for characterizing climate-change induced hazards encompassing: Sea Level Rise; Air quality Biodiversity loss / Crop yield losses; Extreme events (Drought/Floods, Extreme Temperatures, Heatwaves); Pluvial Flooding; and Rock Displacement. Similarly ad hoc climate services have been developed customizing specific application of the Copernicus Climate Data Service CDS Toolbox⁷. Building on the work done as part of WP4, Task 5.1 has targeted the assessment of climate induced natural hazards where: the human intervention in natural ecosystems, in term of land use and land cover, has a strong influence and needs therefore to be represented and accounted for; and whose impacts might strongly affect socio-ecologic systems.

In the following the work done for modelling extreme temperature hazard maps for the assessment of the impacts on socio-ecologic systems and pluvial flooding hazard maps is described in the following sub-sections; reference is made to the pilots of València and Bratislava respectively. The work has been developed with reference to the following relevant international work, in particular from [8] to [15] for modelling extreme temperature and hazard maps and from [16] to [24] for modelling pluvial-induced flood in urbanized areas.

2.1. Climate-change hazard models and maps for the assessment of extreme temperature impacts on socio-ecologic systems

Heat-related events, commonly referred to as heatwaves, have been made more frequent or intense due to anthropogenic GHG emissions in most land regions and the frequency and intensity of drought has increased. These heat-related events may cause several impacts such as thermal discomfort, lack of working productivity, loss of viability and crop yield, more energy consumption or health related problems. To reduce or at least mitigate these impacts, governments need added-value information regarding the risks of extreme temperatures to take proper decisions to prepare, protect and prevent cities and their socio-ecological systems. In order to deepen on this matter and understand how heat-related hazards may impact the socio-ecological system of the “Huerta de València” or “Horta de València” (hereinafter the Huerta), one of the target cultural heritage landscapes identified for ARCH in València, and at the same time understand the thermal ecosystem services provided by the Huerta, a study to analyze the effect of climate change (under the RCP 8.5 scenario) and land use was conducted to assess the evolution of the temperature at meso-scale. Meteorological simulations were performed to understand the behavior of extreme temperatures in possible future scenarios, unfavorable (more urban development declining orchards) and optimistic

⁶ IPCC, 2021: Summary for Policymakers. In: Climate Change 2021: The Physical Science Basis. Contribution of Working Group I to the Sixth Assessment Report of the Intergovernmental Panel on Climate Change [Masson-Delmotte, V., P. Zhai, A. Pirani, S. L. Connors, C. Péan, S. Berger, N. Caud, Y. Chen, L. Goldfarb, M. I. Gomis, M. Huang, K. Leitzell, E. Lonnoy, J.B.R. Matthews, T. K. Maycock, T. Waterfield, O. Yelekçi, R. Yu and B. Zhou (eds.)]. Cambridge University Press. In Press.

⁷ CDS toolbox documentation: <https://cds.climate.copernicus.eu/toolbox/doc/index.html>

(increasing the green area) land use scenario. The changes in the futures scenarios were considered by analysing the land cover of the urban and peri-urban areas of València.

The outputs of this study can be important to take adequate planning decisions in order to evaluate the response of policies and strategies in future city configurations for mitigating extreme urban temperatures or its impact in the population.

2.1.1. Methods

2.1.1.1. Thermal modelling

The regional and mesoscale meteorological model used for the study has been the Weather Research and Forecasting-Advanced Research (WRF-ARW) version 4.2, developed by the National Center of Atmospheric Research (NCAR). It is a universally used community mesoscale model and a state-of-the-art atmospheric modelling system that is applicable for meteorological research, climate scenarios and numerical weather prediction. WRF is a fully compressible and non-hydrostatic model with terrain-following hydrostatic pressure coordinate. Different options that WRF offers can be combined in many different ways. WRF has different parameterizations for microphysics, radiation (long and short wave), cumulus, surface layer, planetary boundary layer and land surface as physical options. There are a large number of options available, including the ability to work with multiple nests. This makes it possible to focus the meteorological simulations for an area of smaller extension and with higher resolution than that presented by the meteorological data available as initial and boundary conditions. Such increase in resolution implies an improvement in the simulation of the study meteorological phenomena that take place in the nested domain. Within this work WRF-ARW system was configured for operational forecast with the optimum options to work with high resolution domains.

WRF model domains configuration was built over a mother domain, D0n, (referred to as D01 in Figure 4) with 5 km spatial resolution, centred at 39.472°N, 0.389°W (València city). It comprises part of the west Iberian Peninsula with an important zone of sea space, and with a domain size of 460 × 460 km². The first nested domain (referred to as D02), with a spatial resolution of 715 m, covers València province with a domain size of 126 × 126 km². The third domain (referred to as D03) with 102 m of spatial resolution covers València city and surroundings areas with a domain size of 20 × 20 km². There are 33 vertical levels, with 8 in the first kilometre.

Topography data from the Shuttle Radar Topography Mission (SRTM) project⁸ with 3 arc-seconds of horizontal resolution (approx. 100 m for the studied region) was used to generate the topography for the high-resolution simulation domain (D03).

⁸ <https://www2.jpl.nasa.gov/srtm/>



Figure 4. WRF Domain configurations for meteorological simulations

Information regarding the land use/land cover was taken from Land Cover/Land Use Information System of Spain, (SIOSE) database⁹. With 3 arc-second of horizontal resolution. SIOSE data was remapped to the United States Geological Survey (USGS) 33 land use categories, with which the WRF works. The USGS land use classification considers 3 different urban categories (Figure 5): the High Intensity Residential includes highly developed areas where people reside in high numbers (apartment complexes, row houses, etc.); the Low Intensity Residential includes areas with a mixture of constructed materials and vegetation where population densities are lower than in high intensity residential areas (single-family housing units, etc.); and Industrial/Commercial, which includes infrastructures (roads, railroads, airports, harbours, etc.) and all other built areas that do not fit into the residential categories.

The initial and boundary conditions (meteorological forcing) for the operational configuration over domain D01 were supplied by the ERA5 reanalysis¹⁰. ERA5 is the 5th generation European Centre for Medium-Range Weather Forecasts (ECMWF) atmospheric reanalysis of the global climate covering the period from January 1950 to present. It is produced by the Copernicus Climate Change Service (C3S) at ECMWF. ERA5 combines vast amounts of historical observations into global estimates using advanced modelling and data assimilation systems. ERA5 provides hourly data of a large number of atmospheric, land and oceanic climate variables. The data cover the Earth on a 30 km grid and resolve the atmosphere using 137 vertical levels. Several episodes of extreme urban temperature were used as input data for the modelling (see sections 2.1.1.2 and 2.1.1.3 for further detail). A validation of the model for each event was performed by comparing the observed temperature for the event (at Spanish Meteorological Agency (AEMET) meteorological stations corresponding to València's airport and València Viveros which is define as "city centre" throughout the text¹¹) and the ones

⁹ <https://www.siose.es/>

¹⁰ <https://www.ecmwf.int/en/forecasts/datasets/reanalysis-datasets/era5>

¹¹ <https://opendata.aemet.es/centrodedescargas/productosAEMET?>

given by the WRF-ARW model as seen in Figure 6. Daily simulations were performed, with a spin-up of 24 hours. In heat wave simulation case, the spin up was 12 hours.

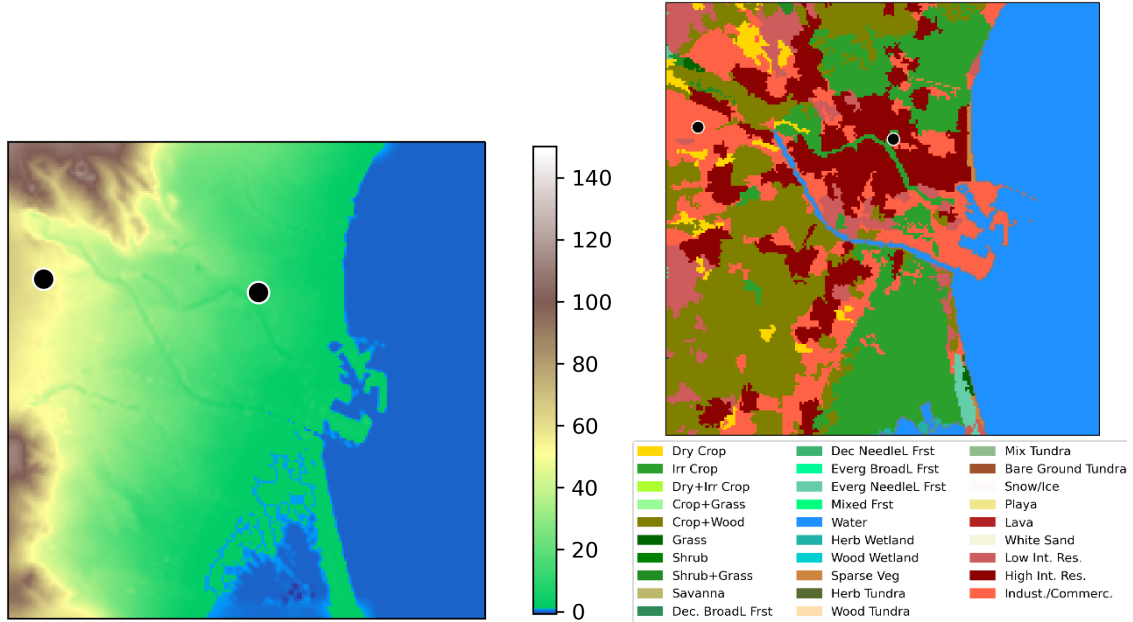


Figure 5. Topography and Land use data (USGS 33-categories) for València city domain (D03)

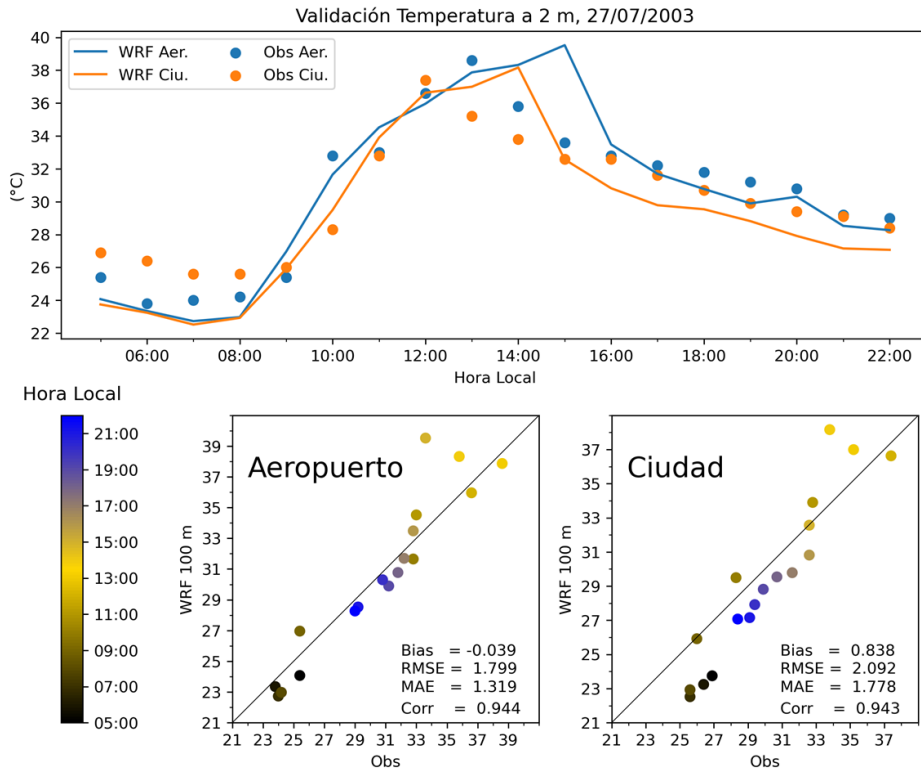


Figure 6. Graphical representation of the model validation using the airport (“Aeropuerto”) and City Centre (“Ciudad”) meteorological station’s data.

2.1.1.2. Typical summer days characterization

The methodology for analysing and characterizing the current and future urban climate regarding extreme temperatures is based on the K-means unsupervised classification algorithm, which is explained in detail in deliverable D4.3 *Threats and Hazard Information System*, section 6.6.4, and which is summarized in Figure 7. The algorithm groups objects into groups based on their characteristics. The grouping is done minimizing the sum of the distances between each object and the group or cluster centroid. The algorithm assigns the nearest centroid based on the squared Euclidean distance.

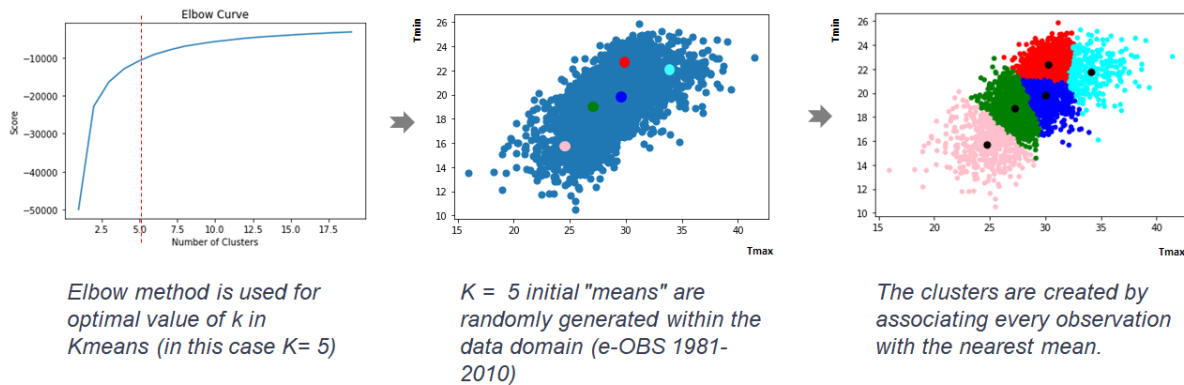


Figure 7. Graphical summary of the two initial steps of the methodology- (based on Figure 32 of D4.3 *Threats and Hazard Information System*)

This methodology was used to cluster and identify the most extreme type of events in summer in València (cyan cluster in Figure 7), named as “*tropical days*’ on the basis of daily maximum temperature, daily minimum temperature and the daily temperature range observed in València during the last 30 years (1981-2010) in the summer periods (June, July, August, September). The observations were obtained from CDS (Climate Data Store) e-OBS dataset that contains daily gridded land-only observational information over Europe. The information stored come from the station network of the European Climate Assessment & Dataset (ECA&D). All station data are sourced directly from the European National Meteorological and Hydrological Services (NMHSs) or other data holding institutions. The algorithm requires an input dataset (observations) and a pre-selected value of K (number of clusters we want it to make). The K input value has been set to 5, based on the elbow curve outcomes (Figure 8). This curve shows the mean distance between data points and their centroid. Since the value of the mean will decrease as we increase the value of K , we should use the mean distance to the centroid as a function of K and find the "elbow point" where the rate of decline "sharpen" ($K=5$). Considering $K=5$ for the València observed data series (e-OBS), the algorithm uses an iterative process in which the groups are adjusted to produce the final result. This implies that the algorithm seeks to find relationships between the observations (T_{max} and T_{min}) to produce the 5 clusters (see Figure 9), which each cluster refers to a collection of data points aggregated together because of certain similarities. Every data point is allocated to each of the clusters through reducing the in-cluster sum of squares.

Being extreme heat events the main interest to be modelled, the focus was put on the most *extreme hot days* (named *tropical days* and represented as the cyan cluster in Figure 9). The modelling exercise was developed with “tropical type of days” and how they evolve considering climate change (RCP 8.5) as explained below.

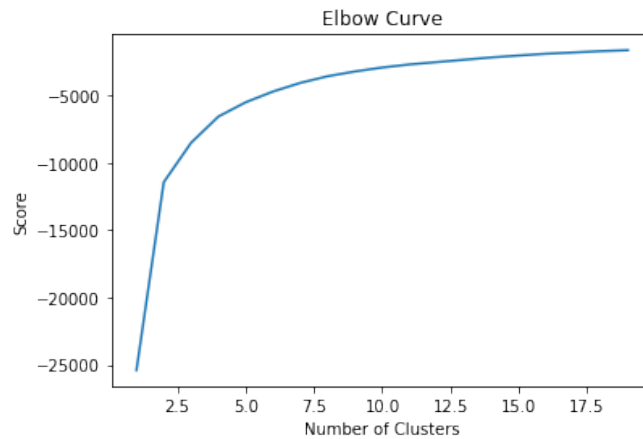


Figure 8. Elbow curve for València data

Figure 9. Clusters identified by the K-means for València dataset, where cyan cluster is related to the typical extreme hot summer days (named as “Tropical days”)

Table 1 shows the total numbers of days that fall into the above selected cluster (Tropical days) as well as the average *daily maximum temperature*, *Tmax*, and *average daily minimum temperature*, *Tmin* (centroids) considering the collection of data points aggregated together.

Table 1. Period 1981-2010: Number of Days/Year, total tropical days, Tmax and Tmin

Period	Characterization	Days/year	Total days	Tmax*	Tmin*
1981-2010	Tropical days	10,47	314	34,09	21,74

*average/mean

The above characterization of typical extreme hot summer days (named as “Tropical days”) allows to look for a specific real day, named *historical representative day* as, that matches with the values of *Tmax* and *Tmin* in Table 1 identified with 23rd July 2002. This day is assumed to be the first input for the WRF-ARW simulation of a **typical “tropical day”** or extreme summer day.

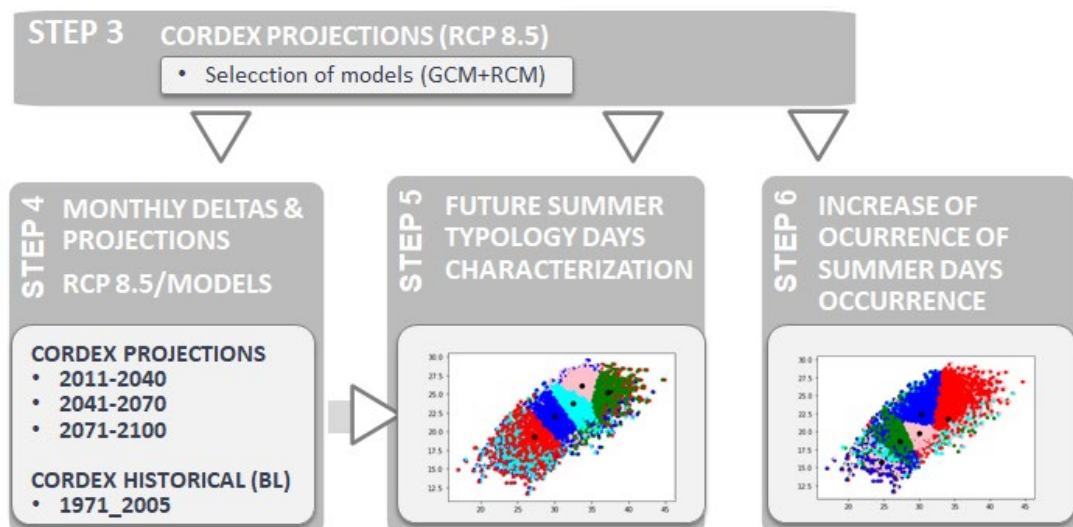


Figure 9. Methodology applied for future summer days characterization (Source D4.3)

The methodology follows by characterizing the same typologies of summer extreme hot days, but considering climate change projections of temperature (Steps from 3 to 6 in Figure 9). This was done considering three future periods 2011-2041, 2041-2070 and 2071-2100 and the worst-case emission scenario (RCP8.5). Step 3 and Step 4 are explained in detail in Deliverable 4.3 *Threats and Hazard Information System*. As for Step 5, an analysis of the future summer extreme days characterization, similarly to what done with the historical observations (Step 1 and 2), was undertaken using several bias adjusted CORDEX models projections as an input for the K-means algorithm, which groups are produced per projections. For each model projection and period a cluster (data points aggregated together) and centroid were identified, and therefore, an average and standard deviation was calculated. Table 2 summarize the average values of the ensemble of models.

Table 2. Characterization of the parameters associated to the typical tropical day for each considered period in XXI century

Periods	Type of day	Days/ year	Total days/ period	Tmax (mean)	Tmin (mean)
2011-2040	Typical tropical days	10,6	318	35,10	22,94
2041-2070		11,15	334,50	35,81	23,84
2071-2100		11,08	332,50	37,36	25,52

The above information allows to select the specific historical days that match with the above *Tmax* and *Tmin* values using the following formula:

$$(|Tmax_{obs} - Tmax_{pt}| + |Tmin_{obs} - Tmin_{pt}|) < 0.5^{\circ}C$$

The dates that best match the temperature conditions described in Table 3 are shown below:

Table 3. Representative historic days which characterize best the tropical days for each temporal period

Period	Representative tropical day for the selected period
2011-2040	20/08/2000
2041-2070	11/08/2003
2071-2100	27/07/2003

On the other hand, the K-means cluster was also used to graphically represent the increase of occurrence of the historical centroids (Step 6). The outcomes are not used for the WRF-ARW simulation but are interesting from the point of view of being aware about how many hot

days, as the ones we are having now are going to happen in the future. The graphical representation of the above criteria for the selected dates can be seen in Figure 10.

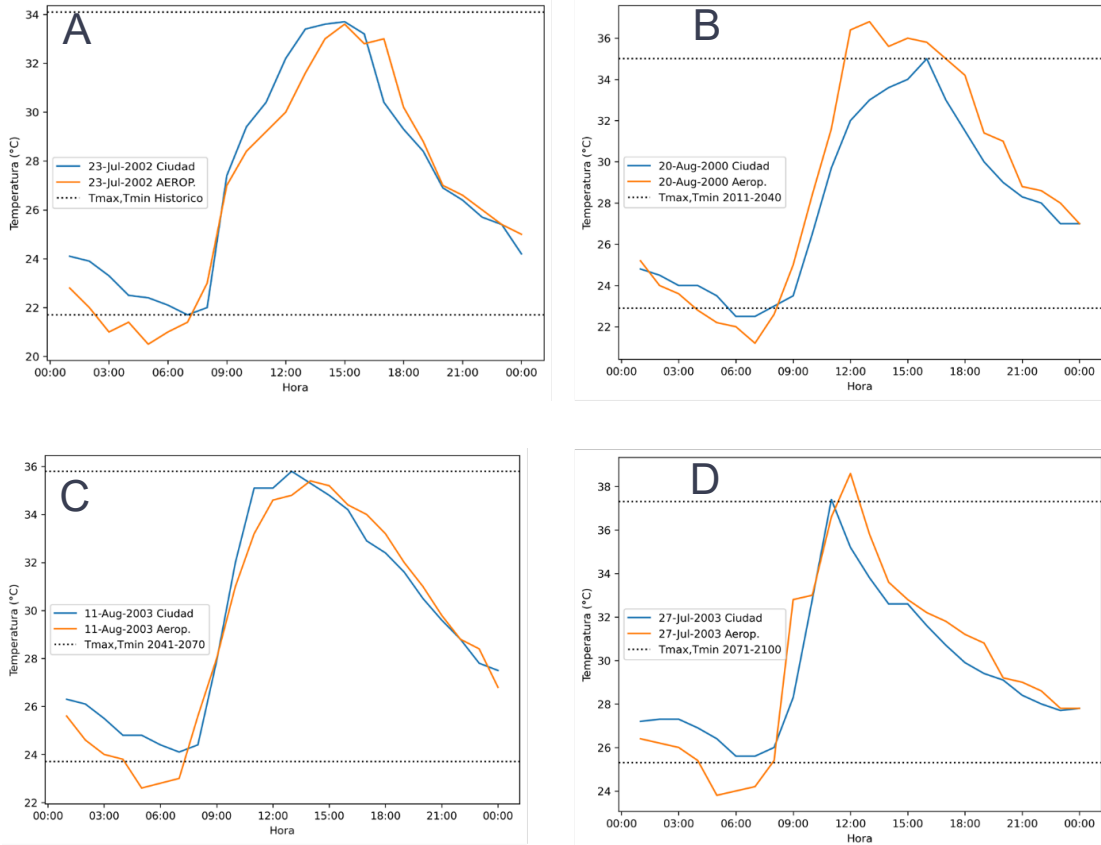


Figure 10. Graphical representation of the hourly temperature of the selected dates to characterize each representative tropical day. Dashed lines characterize the temperature thresholds for each period. (A) corresponds to values of typical day characterizing the historic period, (B) corresponds to values of the typical day characterizing the period 2011-2040, (C) corresponds to values of the typical day characterizing the period 2041-2070 and (D) corresponds to values of the typical day characterizing the period to 2071-2100.

According to the analysed data, the number of tropical days would be more than five times greater at the end of the century, while the number of tropical nights would also grow, but at a smaller rate (Figure 11).

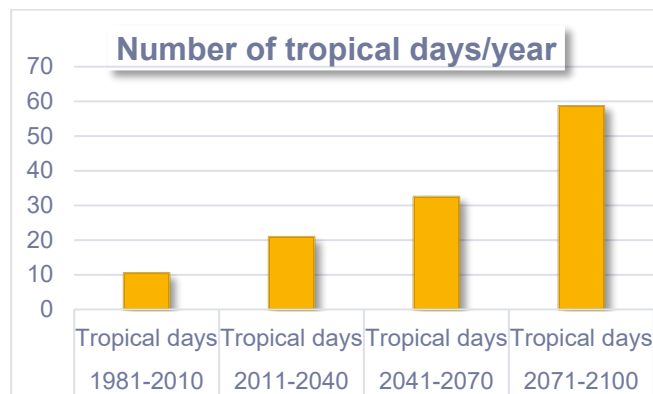


Figure 11. Evolution of the number of historical tropical days, as characterized in Table 2, in València

Extreme hot days produce several negative impacts in cities, due to captured heat by buildings, roads and other infrastructures. The heat island effect is most intense during the day, but the slow release of heat from the infrastructure can keep cities much hotter than surrounding areas. However, consecutive extreme hot days under specific conditions (heatwaves) may have even more adverse impacts in agriculture, human health, lack of productivity or tourist activity among other important for València.

These impacts will grow under an increased global warming, where more rapid heatwave trends will likely produce more severe and possibly irreversible impacts. To reduce or at least mitigate these impacts, added-value information regarding the risks of these extreme temperature events (heatwaves) is needed to take proper decisions to prepare, protect and prevent the city and citizens. Therefore, heatwaves have also been considered as a specific hazard in València, and have been characterized considering historical observations and future climate change projections of temperature following the same methodology explained in 2.1.1.2, but considering the climate parameters that specifically characterize a heatwave event.

There are multiple characteristics to heatwaves, including their *intensity, frequency, duration, timing and spatial extent*. But, specifically in València, the *Heat Wave Duration index (HWD)* was selected as the most representative to measure the impact of climate change in agriculture, other human activities and health. Therefore, heatwaves in ARCH have been characterized considering the following parameters (detailed described in D4.3):

- *Intensity of the heatwave*: Maximum temperature reached; and Global Intensity, i.e. average of the temperature maximum reached of all days during the heatwave event
- *Duration and Frequency of the heatwave*: Average Heatwave duration; Number of Heat Waves per period.

This characterization of heatwaves and their representation in a comprehensible and accessible way is a crucial challenge, in particular for delivering scientific support to policy makers. In order to fulfil this need, a method for analysing the heatwaves in València has been defined and developed following the approach of a previous research made in France [10]. For Valencia the heatwave definition used was based on the Spanish Meteorological Agency but updated to consider also the temperature minimum and months from May to September (being the most critical ones in València): “*A heatwave day is a day when both the daily minimum and maximum temperatures exceed the 95th and 90th percentile respectively for at least 3 consecutive days between the months of May and September*”.

For the historical period, the statistical analysis performed was done considering the historical timeframe of 1981-2010 of the e-OBS dataset available at CDS. As mentioned before, one of the key points of the heatwave definition is the establishment of the threshold values linked to the T_{max} and T_{min} for València. In the ARCH project, the study has been done for this geographical area (see Figure 13) from which the percentiles 95 and 90 of T_{max} and T_{min} have been calculated:

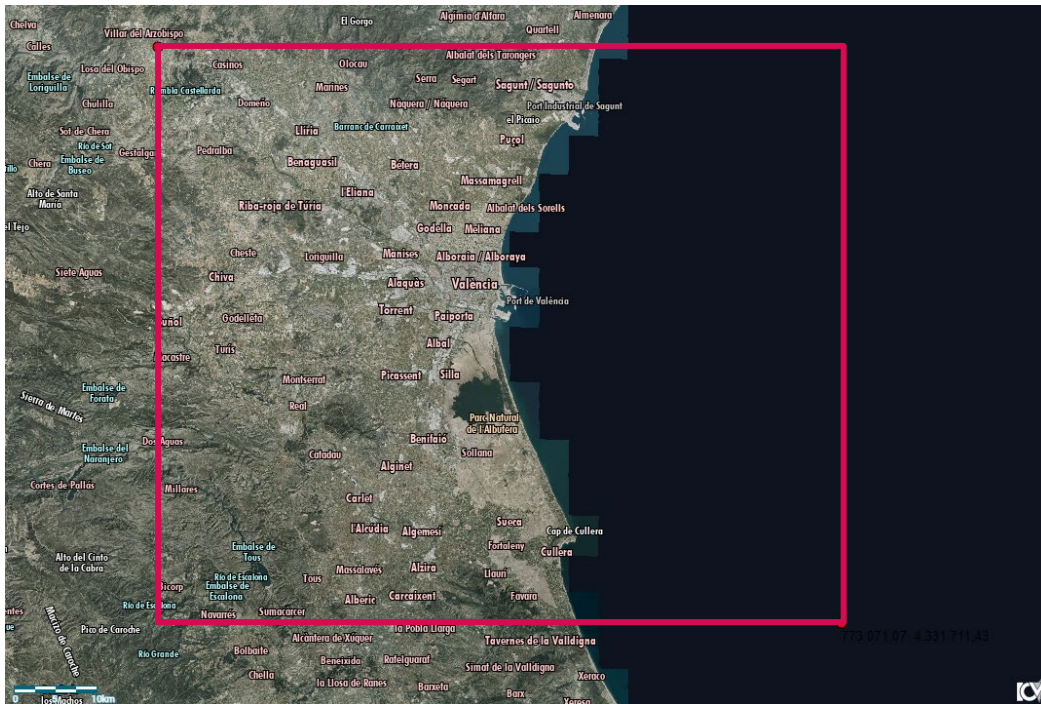


Figure 10. Red box showing the analysed area (NW: -0° 80'57.5", 39° 7'18.7", SE: 0° 15'53.3", 39° 09'18.7") (Mapa base imagen 2020 CC BY 4.0 © Institut Cartogràfic Valencià, Generalitat)

As it was explained in Tables 28 to 36 of the section 6.6.3. of Deliverable 4.3 *Threats and Hazard Information System*, the evolution of heatwaves based on the historical and projected statistics of the key selected parameters (duration, global intensity and maximum temperature reached) change along the four studied periods from 2011 to 2100. In the initial period (1981-2010), most of the heatwaves are between 3 to 5 days long, but in the last period (2071-2100) their duration would increase, reaching even durations of 30 days. The maximum reached temperature for the future projected heatwaves events also increased. Considering this evolution, it was decided to study the historical heatwave of 11 days as the best characterization of the future heatwaves, and therefore the historical representative heatwave event considered as an input for the WRF-ARW simulation is the one which occurred from 31/07/2003 until 16/08/2003.

2.1.2. Data

2.1.2.1. Land use data

Within the ARCH project, a participatory scenario construction to analyse some potentially plausible future evolution of trends in land use in València was performed. This methodology has been previously seen to increase awareness, facilitate greater stakeholder involvement and can be considered as an “interactive dialogue in problem, planning and decision making” [13]. Las Naves (ARCH Partner representing València City) developed a set of qualitative storylines based on approved policy instruments and available land use maps (data from year

2015¹², developed by the SIOSE project¹³), which are visualized in Figure 14 and can be summarized as following:

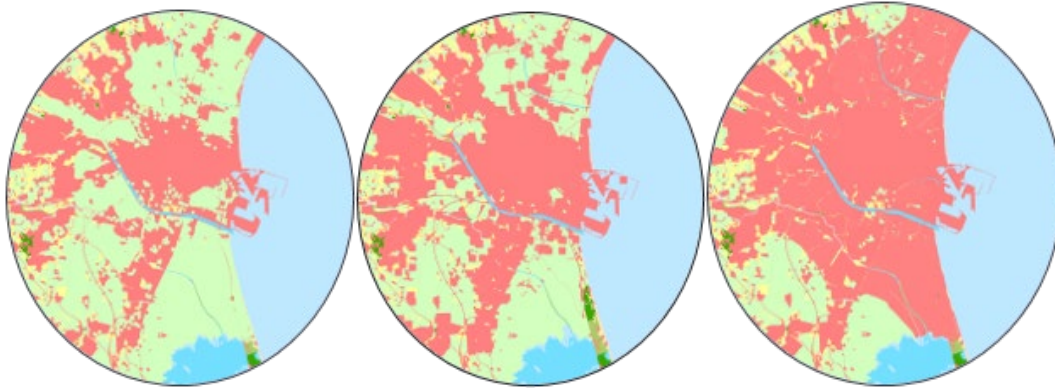


Figure 14. Schematic representation of the hypothetical: Green, Grey and Black scenarios

- **Green Scenario:** a realistic possible future scenario where areas linked to urban fabric may be incorporated to the Huerta (orchard) land classification (irrigated arable crops). These lands are or may be part of a future planning and revitalisation strategy of the orchard heritage area of València.
- **Grey Scenario:** a realistic possible future scenario where mainly areas that are now agriculturally abandoned or in the early stages of urban development may become part of the urban building environment. This may happen if further urbanization of these areas happens.
- **Black Scenario:** A hypothetical scenario where several regulations around orchard heritage areas would be withdrawn and urban expansion would take place over currently protected areas.

The steps of the methodology are summarized in Figure 15 and described in the following:

¹² http://icv.gva.es/auto/aplicaciones/icv_geocat/#/search?uuid=SpaicvSIOSE2015CV_2015&lang=spa

¹³ SIOSE produces high spatial and temporal resolution LC/LU data of the Spanish territory. <https://www.siose.es/>

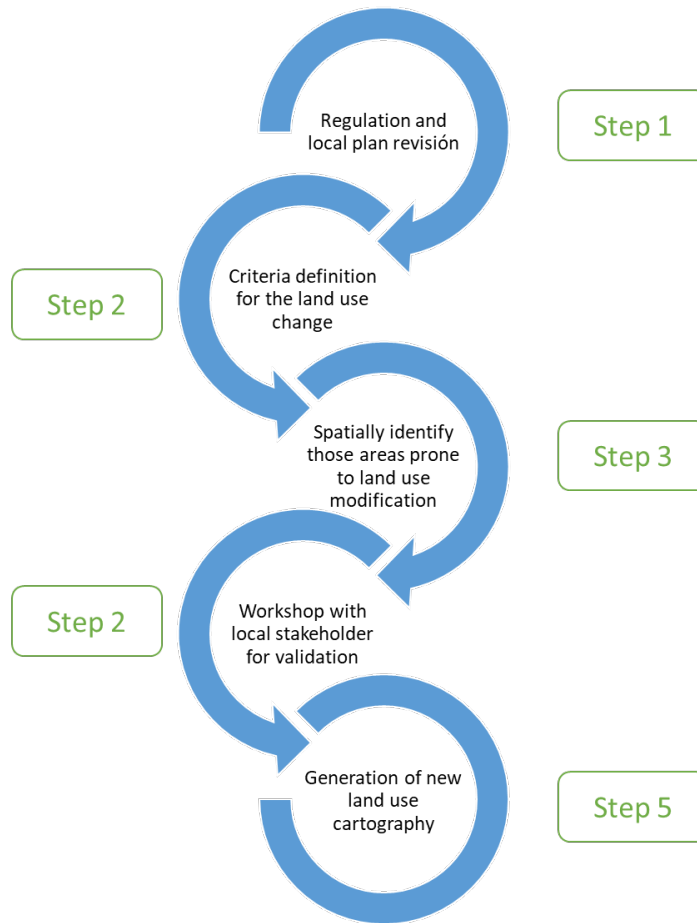


Figure 15. Methodological steps for the development of land use scenario cartography

STEP 1 & 2: The following regulation and plans, related to urban and land use planning of the orchards, green infrastructure and municipalities included in the study area, were revised:

- Plan de acción territorial de Ordenación y Dinamización de la Huerta de València (hereinafter called “PATODHV”): Regional land use plan for the protection of the València Huerta¹⁴. The following areas were analysed:
 - Recovery areas and sectors included in the articles 30 and 33 from the normative part of the PATODHV¹⁵.
 - Special plans included within the PATODHV actions catalogue, e.g., Horta Rovella and Campanar¹⁶.
 - Green infrastructure within the orchards of València: areas identified under article 15 from the normative part of the PATODHV (also available in the PATODHV proposed planning mapping chapter¹⁷), orchards of special

¹⁴ <http://politicaterritorial.gva.es/es/web/planificacion-territorial-e-infraestructura-verde/pat-horta-de-Valencia>

¹⁵ <https://politicaterritorial.gva.es/auto/planes-accion-territorial/PATHorta/04%20Normativa.pdf>

¹⁶ <https://politicaterritorial.gva.es/auto/planes-accion-territorial/PATHorta/03%20Objetivos,%20Estrategias%20y%20Acciones%20Dinamizadoras.pdf>

¹⁷ <https://politicaterritorial.gva.es/auto/planes-accion-territorial/PATHorta/06%20Planos%20de%20ordenaci%c3%b3n.pdf>

protection (articles 17 to 19 from the normative part of the PATODHV), areas of natural value (identified in article 20 from the normative part of the PATODHV, such as the Natura 2000 network) and areas of territorial and functional connection (articles 22 to 25 from the normative part of the PATODHV)

- Approved urban planning¹⁸. Special attention was given to:
 - Land affected by court judgments
 - Rural land, already approved for urban development, but where development has not taken place yet
 - Urban land where development has not taken place yet
 - Areas where green spaces are planned, but have not been implemented yet
 - Land proposed for development by the municipality, but where development was denied by other authorities
- Regional green infrastructure. The following areas were analysed, among other:
 - Wetlands of international importance under the Ramsar Convention¹⁹
 - Natural parks²⁰
 - Flooding risk areas²¹
- Local green infrastructure. Areas of landscape interest included in approved municipal green infrastructure plans²².
- Other sources of information, such as 2020 aerial photographs²³ which allowed for manual correction by photo-interpretation of mistakes made in the SIOSE 2015 land use maps used, and also to update areas where land use has changed since 2015.

Further to the identification of the typology of the land use prone to a reclassification in the future another technical criterion was included: those areas smaller than 2 ha were not considered due to the thermal modelling resolution.

STEP 3. Several spatial analysis processes developed via a desktop Geographical Information System (GIS) allowed to preliminarily identify, based on those sources and criteria mentioned in the Steps 1&2, 1039 points in the study area where a potential land use change could be included in the alternative scenarios developed. These scenarios can be summarized as follows:

- Study area: 42981.58 Hectares
- Preliminary green scenario:
 - 739 points identified
 - Most common type (over 117 points): planned green spaces, not implemented yet
- Preliminary grey scenario:
 - 300 points identified

¹⁸ http://icv.gva.es/auto/aplicaciones/icv_geocat/#/search?uid=spa_icv_plan_zonificacion&lang=spa

¹⁹ http://icv.gva.es/auto/aplicaciones/icv_geocat/#/search?uid=spa_icv_epp_ramsar&lang=spa

²⁰ http://icv.gva.es/auto/aplicaciones/icv_geocat/#/search?uid=spa_icv_epp_parques_naturales&lang=spa

²¹ http://icv.gva.es/auto/aplicaciones/icv_geocat/#/search?uid=spa_icv_orde_patricova_peligrosidad_inun&lang=spa

²² http://icv.gva.es/auto/aplicaciones/icv_geocat/#/search?uid=spa_icv_orde_paisaje_pol&lang=spa

²³ http://icv.gva.es/auto/aplicaciones/icv_geocat/#/search?uid=spaicv0202_2020CVL0025&lang=spa

- Most common type (over 110 points): Rural land, already approved for urban development, but where development has not taken place yet

A preliminary black scenario was also developed, based on the total urban development of areas currently protected under the orchards of special protection and areas of natural value typologies of the PATODHV, as previously described.

STEP 4. After this preliminary revision a workshop was planned in order to validate the employed methodology, identify potential sources of information which could be used in the development of the alternative land use scenarios and, finally, identify additional potential areas which could not be automatically identified by the methodology and data sources used, but that based on the knowledge of relevant local and regional stakeholders could also be subject to a land use change which might be relevant to the thermal modelling assessment.

A GIS web app (Figure 16) was prepared to be used in the workshop. It could be accessed from any web browser and would allow the invited stakeholders to use an online map where they could check the land use change potential points as proposed in the preliminary scenarios developed, while also considering and being able to review all the spatial layers used for the analysis. This tool was also developed with the necessary functionalities to allow the local stakeholders to simultaneously edit a new layer during the workshop, where new points and comments could be introduced, in order to improve the preliminary scenarios developed.

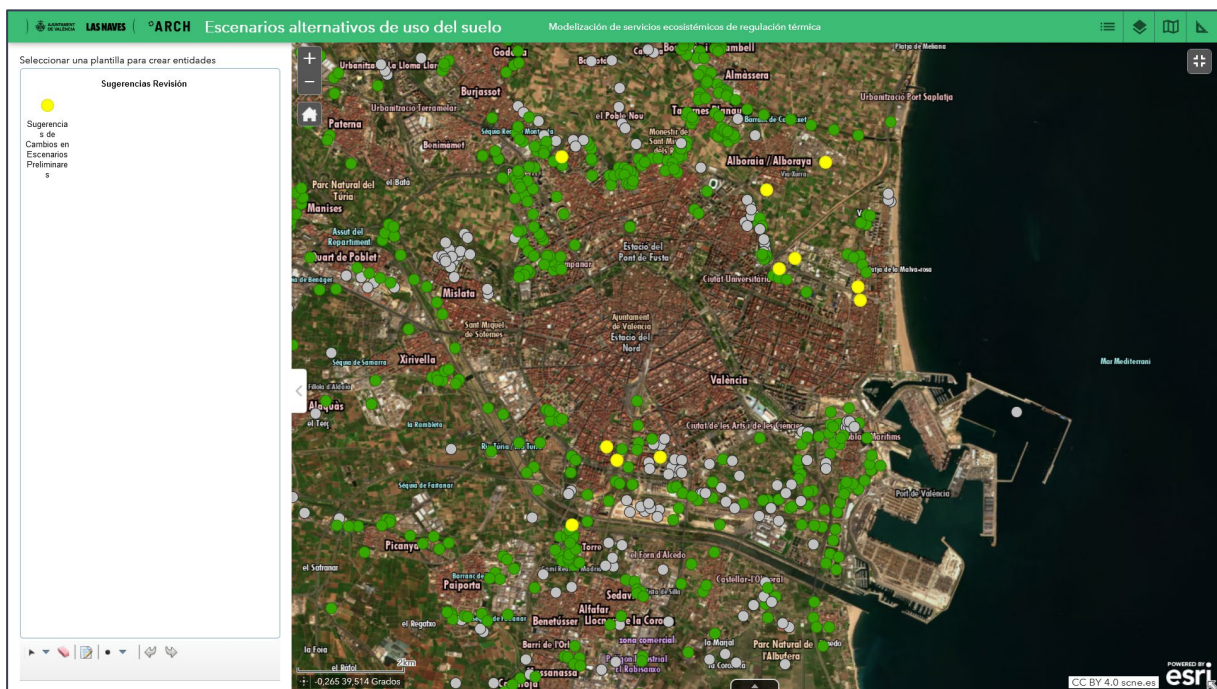


Figure 16. GIS Web app interface. Green points and grey points represent potential areas of land use change included in the preliminary green and grey scenarios, respectively, as developed prior to the workshop. Yellow points represent potential additional land use change points proposed by stakeholders during the workshop by means of the editing functionalities of the GIS web app.

Local and regional stakeholders who had previously signed up in order to take part of the working group WG3 from the València ARCH local partnership (24), which aims at “Exploring the influence of the Huerta and the Albufera on València’s urban resilience”, were invited to take part in the workshop. Representatives from Alba and Augsburg, cities working with València in the ARCH Mutual Learning Framework25 were also invited to attend as listeners, if desired. The workshop was developed online on the 27th September 2021, on the MS Teams platform, and gathered a variety of stakeholders (see Table 4).

Table 4. List of participants in the land use workshop. * City participating in the “Mutual Learning Framework” within ARCH project, invited to participate as workshop listener.

Organization	Name (Acronym)
Alba, Italy*	DA
Alba, Italy*	SB
Cátedra L'Horta de València: territorio metropolitano	MA
Conselleria d'Agricultura, Desenvolupament Rural, Emergència Climàtica i Transició Ecològica / D.G. Canvi Climàtic	VS
Consorci del Consell de l'Horta de València	MJ
Universitat Politècnica de València	FG
Universitat Politècnica de València	MV
ICLEI	IB
Las Naves	LG
Las Naves	MM
Las Naves	ES
Tecnalia	NP
Tecnalia	SZ

During the workshop, the thermal modelling methodology, potential results and characteristics were presented. The preliminary methodology followed to identify areas where land use may change in the future (Steps 1&2) was also explained, along with the obtained initial results. The GIS web app was introduced, the link was shared, and editing permits were granted during the workshop. It was explained that the web app use would be mainly aiming at the "grey" and "green" scenarios. The “black” scenario would only be discussed briefly at the end of the

²⁴ https://savingculturalheritage.eu/fileadmin/user_upload/Deliverables/D3.2_ARCH_local_work_plan-València.pdf

²⁵ <https://savingculturalheritage.eu/mutual-learning>

workshop as it represents a worst-case scenario of extensive urban development which wouldn't need as much detail as the other two scenarios.

After the explanation of the functionalities and content of the GIS app, stakeholders spent twenty minutes in the review of the preliminary scenarios available, as well as suggesting new areas to be considered via the online, simultaneous edition of a specific layer developed to store such stakeholder suggestions (Figures 17 and 18).

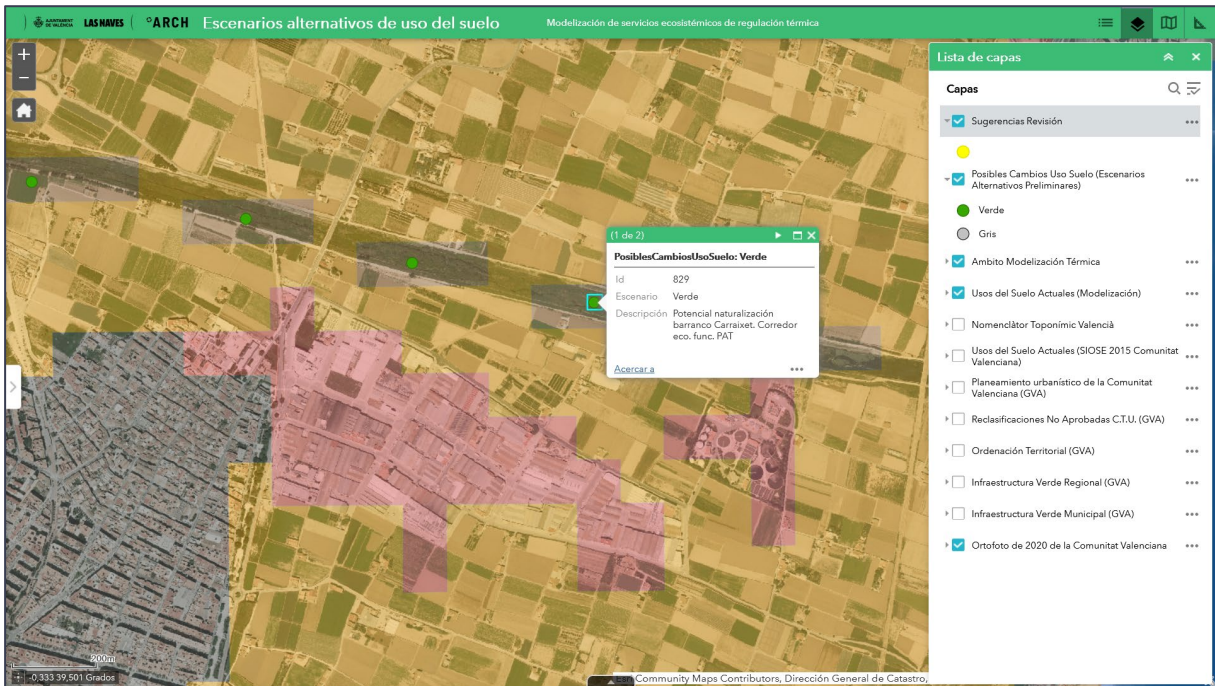


Figure 17. GIS Web app interface (detail showing the layers that the stakeholders could activate and obtain info about, on the right, as well as the data available on one of the points identified within the preliminary green scenario, on the pop-up box).

Workshop participants agreed on the general methodology and criteria presented. However, they also suggested the consideration of complementary sources of data both for the “green” and “grey” scenario. As an example, it was suggested to incorporate to the “grey” scenario the Common Rural Areas²⁶ as defined in the PATODHV, which represent priority areas for urban growth.

During the editing part of the workshop, a total of 36 additional points to be considered during the development of the alternative land use scenarios were proposed by stakeholders, as shown in Figure 16 and Figure 19 (yellow points). For each of them, a suggested scenario and additional comments could also be introduced (Figure 18). After the editing part of the workshop ended, the “edit” functions in the app were disabled to prevent from further changes in the co-created layer.

26

http://icv.gva.es/auto/aplicaciones/icv_geocat/#/search?uuid=spa_icv_orde_pathuerta_zonas_rurales_com&lang=spa

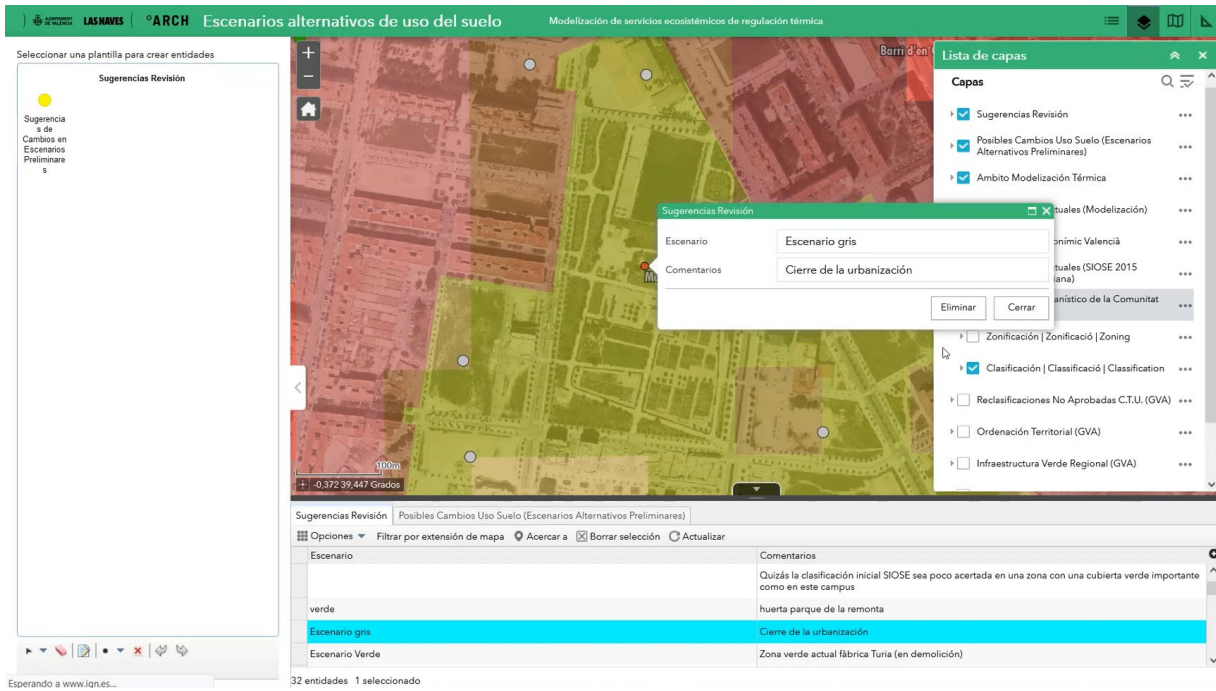


Figure 18. GIS Web app interface detail showing data available on one of the points suggested by the stakeholders during the workshop.

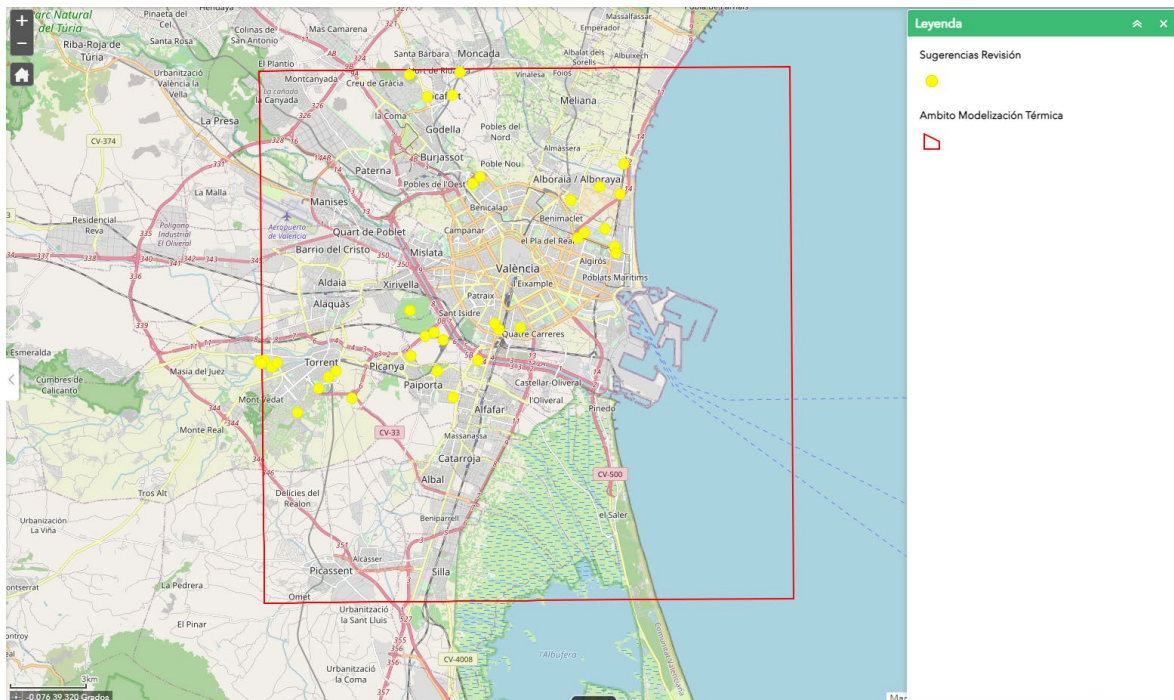


Figure 19. GIS Web app interface (in yellow, the final points suggested by the stakeholders to be additionally considered during the development of the alternative land use scenarios; in red, the thermal modelling area) (Map background ©Open Street Maps contributors, CC-BY-SA)

The participants to the workshop finally briefly discussed on the “black” scenario, understood as a worst-case hypothetical scenario. Stakeholders agreed on removing from it the potential urban growth over the areas of natural value typologies of the PATODHV, as it was understood that the protection of such areas under additional, well established, protected areas regulations

and plans would make it extremely difficult for urban development to occur there. Therefore, it was decided that the black scenario would then be defined based only on the total urban development of the areas currently protected under the orchards of special protection PATODHV categories.

STEP 5. After the workshop, the final land use alternative scenarios were developed by means of a desktop GIS. The information co-created during the workshop by the stakeholders was downloaded as a shapefile, as an additional input to be processed by the desktop GIS and therefore considered during the mentioned works.

The exact areas where land use change would take place, needed to be defined for each of the considered scenarios. Specifically, three polygon shapefiles should be created, each of them showing the land use changes related to one of the considered alternative scenarios (i.e. black, grey and green). Those polygon layers would then be used to update the current land use SIOSE map, thus producing three alternative land use maps for the whole thermal modelling area. In each of those alternative land use maps current land use from the SIOSE map would be still considered as valid for all of those areas where changes were not proposed under the specific alternative scenario. The black scenario (shown later in Figure 20) was firstly developed, since it was the simplest one. A series of spatial analysis operations were performed in order to extract the areas currently protected under the orchards of special protection PATODHV categories and assign them with the code 112, corresponding to the SIOSE “urban expansion area” category. Finally, that spatial layer was used to update the current SIOSE land use shapefile in order to change the land use category of such polygon areas, leaving the rest of the analysis area unchanged.

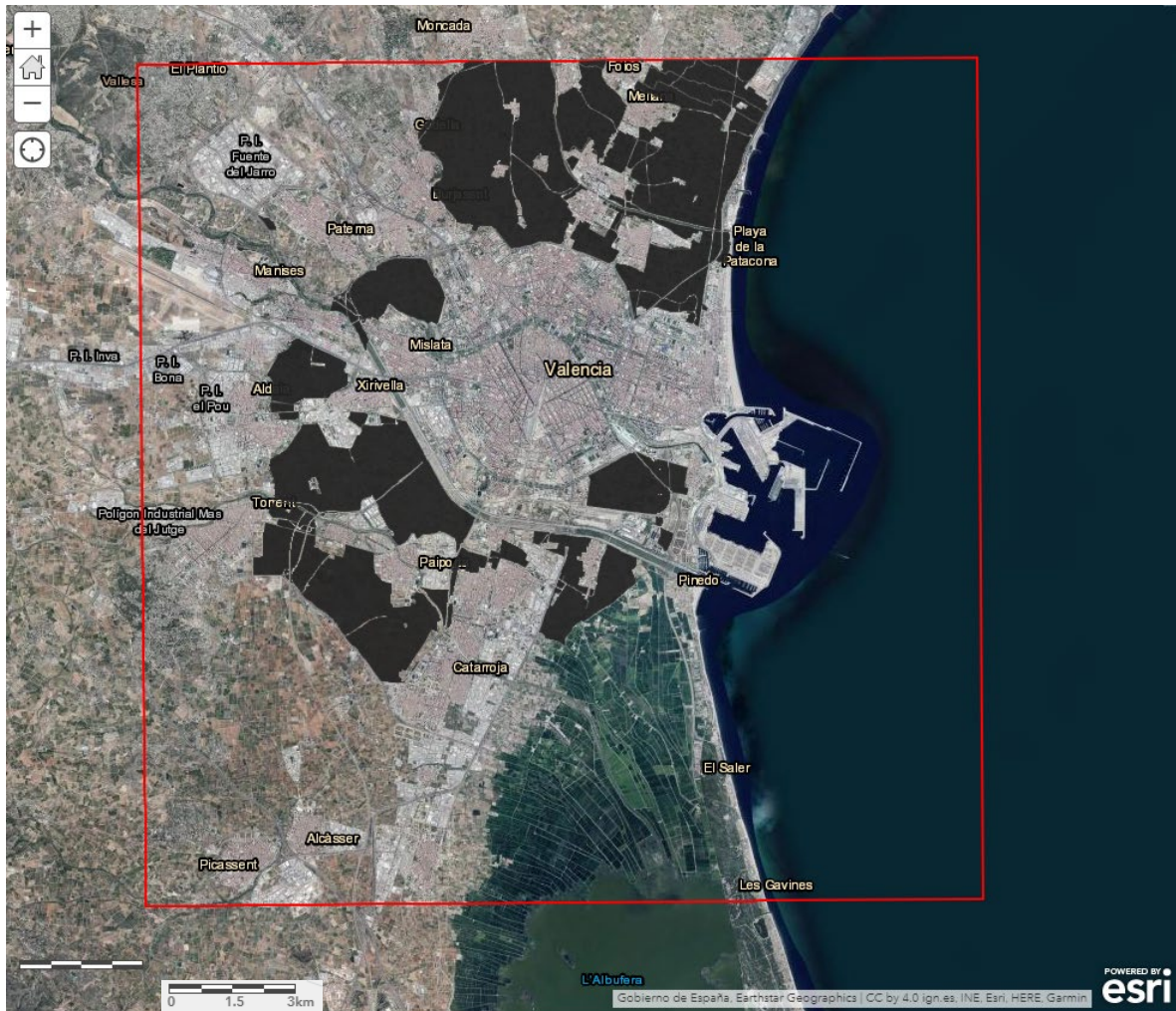


Figure 20. Alternative “black” land use scenario change areas. In black, areas currently protected under the orchards of special protection PATODHV categories which would change its land use from agricultural to urban.

The preliminary green (Figure 21) and grey scenarios (Figure 22), as well as the stakeholder suggestions, were available only as point data, as has been already mentioned. In order to update the original land use SIOSE map with the potential land use changes, for each of those points which marked a land use change location, a polygon should be produced, in order to precisely define the exact area subjected to land use under each considered scenario. Several data sources, such as the national cadastral database²⁷, the SIOSE land use map, aerial photo interpretation, or some other polygon spatial data sources mentioned under the Step 1&2 section were used in order to produce the green and grey land use change areas. Green areas were assigned the 210 SIOSE code, corresponding to irrigation arable crops, while grey areas were assigned with the code 112, corresponding to the SIOSE “urban expansion area” category, as previously done with the black scenario. Finally, both spatial layers were used to update the current SIOSE land use shapefile in order to change the land use category of such polygon areas, leaving the rest of the analysis area unchanged, and therefore creating the final green and black land use Scenarios (Figure 43).

²⁷ <https://www.sedecatastro.gob.es/Accesos/SECAccDescargaDatos.aspx>

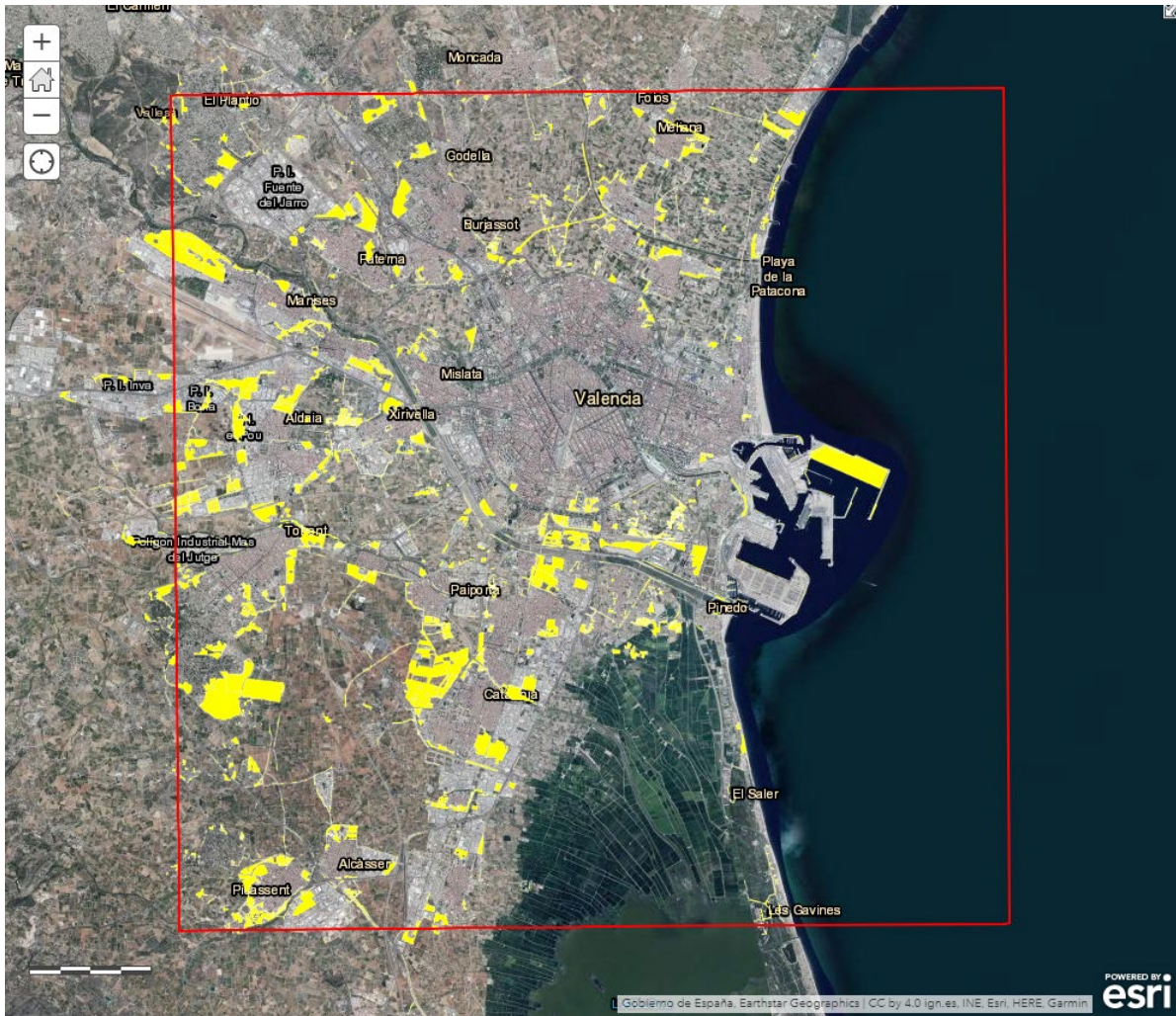


Figure 22. Alternative “grey” land use scenario change areas. In yellow, agricultural or natural areas which would change its land use to urban in the grey scenario.

2.1.3. Results

The result of the simulations consists of NetCDF files which include meteorological hourly data with special focus on temperature values. From the NetCDF files various graphics were derived to showcase different temperature-related indexes along the climate scenario evolution, based on RCP 8.5 climate projections. These graphics allow to spatially analyse (i) the thermal distributions which may help to identify hot-spots or areas with higher exposure to the extreme temperature hazard, ii) hazard trends and (iii) to assess the ecosystem services provided by l’Horta de València (one of the primary objectives of the study). This analysis may also help to assist decision making in the areas of the agriculture heritage, thermal comfort of the population and /or planning.

2.1.4. Climate change effect analysis on temperature - Current land use scenario

Outcomes of the current land use scenario are provided in terms of different metrics: namely *Tmax*, *Tmin*, % of night hours with $T > 20^{\circ}\text{C}$, Heat index and Cooling Degree Days. The current land use scenario was used as well to analyse the thermal impact of climate change, RCP 8.5 scenario, in València.

2.1.4.1. Maximum temperature

Figure 23 represents the maps corresponding to the maximum daily temperature T_{max} , in each pixel for the four analysed representative tropical days to each RCP 8.5 period and the heat wave event. As observed the maximum daily temperature increases along the century. According to the modelling exercise, the temperature increase will be most severe at the end of the century (2071-2100). The absolute T_{max} increase between the historical and far future period was around 8 °C both in the city centre and at the airport. This significant temperature increase will result in important impacts in many sectors such as health, agriculture and tourism.

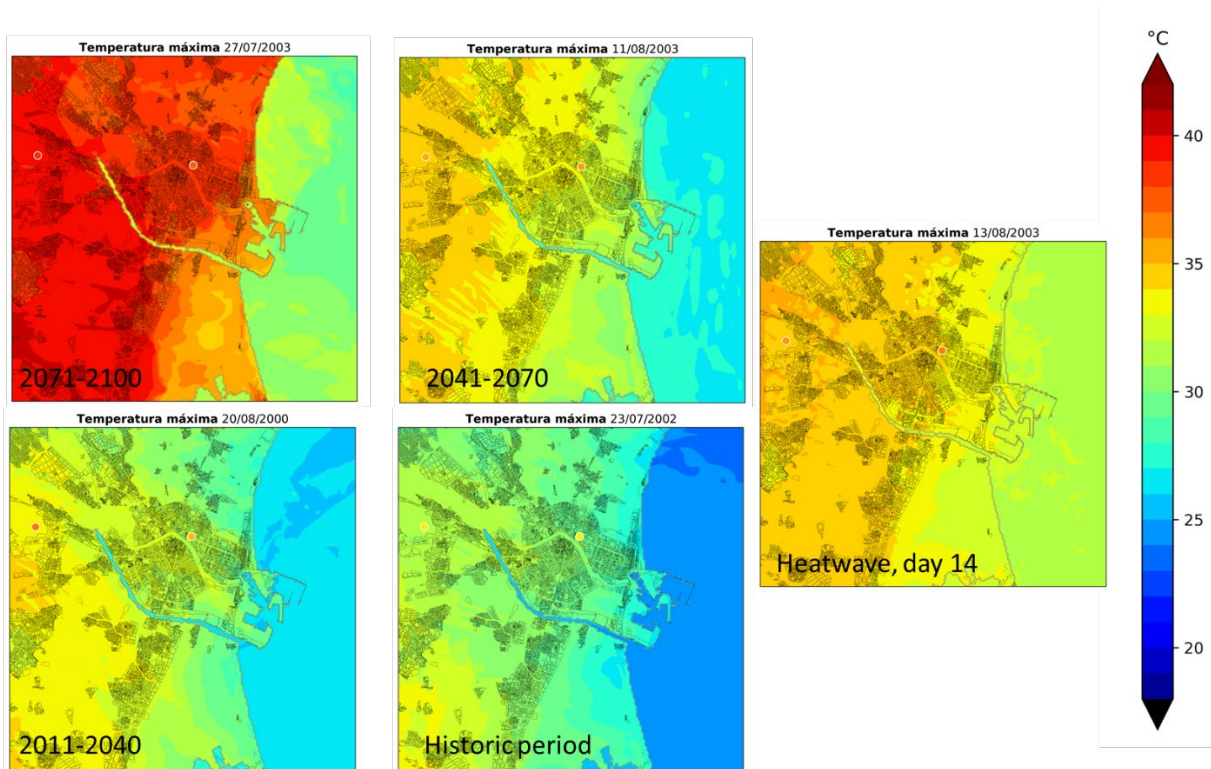


Figure 113. Spatial representation of T max for each of the studied periods

2.1.4.2. Minimum temperature

Figure 24 represents the maps corresponding to the minimum daily temperature T_{min} in each pixel. As for T_{max} the minimum daily temperature increases along the century, but at lower rate. The absolute T_{min} increase between the historical and far future period results in increases ranging from 0.5 and 3 °C both in the city centre and at the airport. Despite the T_{min} increase is not as high as T_{max} the results indicate that nocturnal comfort may decline impacting on health and well-being.

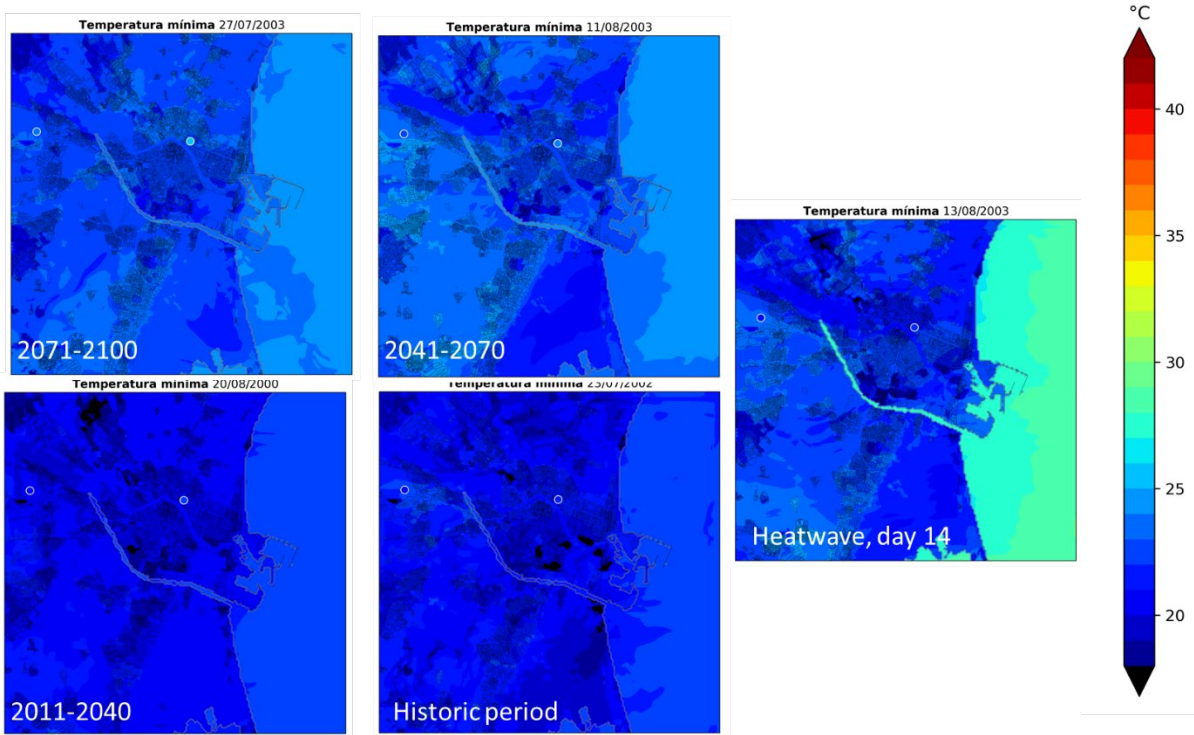


Figure 24. Spatial representation of T min for each of the studied periods

2.1.4.3. Thermal oscillation

Figure 25 represents the thermal oscillation, *i.e.* $\Delta T = T_{max} - T_{min}$ difference between the maximum T_{max} and minimum temperature T_{min} in each pixel. As a result of a higher increase of T_{max} with respect to T_{min} over the time periods, the thermal oscillation also increases along the century.

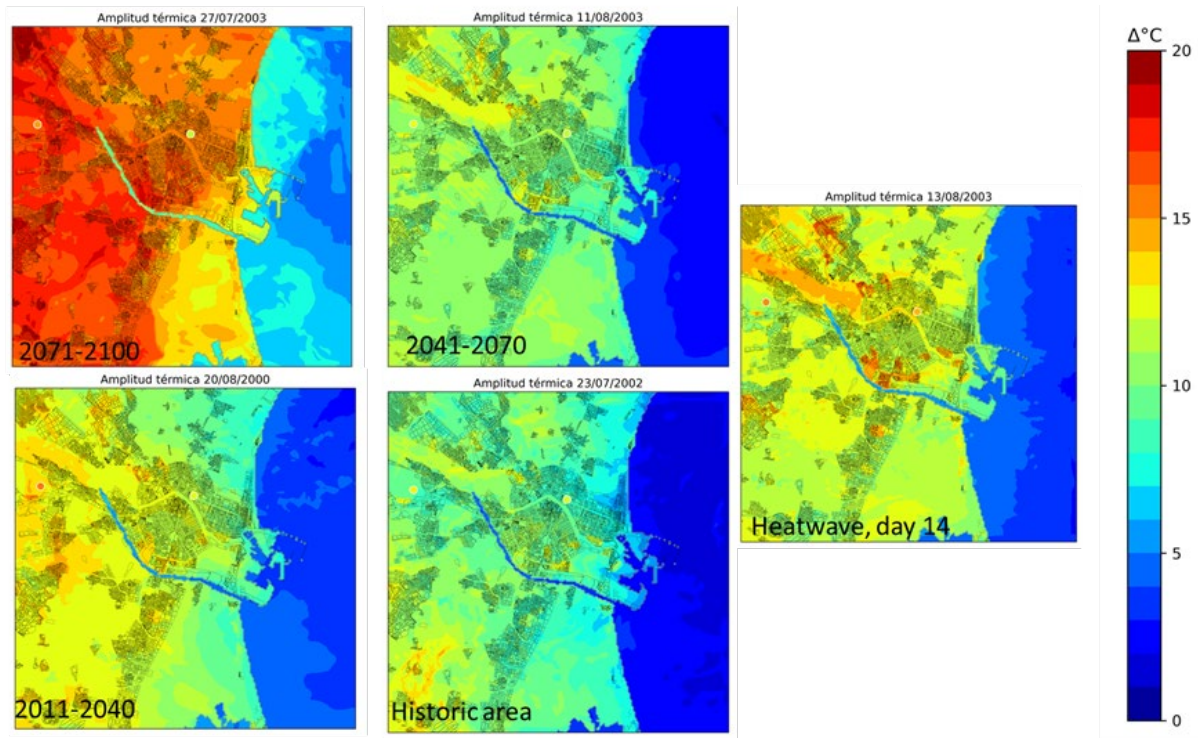


Figure 25. Spatial representation of the daily thermal oscillation for each of the studied periods

2.1.4.4. Heat Index

The perception of heat feel by a person through the skin is expressed according to a combination of meteorological parameters, usually temperature, wind and relative humidity. There are a number of indices that attempt to quantify this effect and, although they are not only a temperature variable, they are also expressed in degrees. One of the indices for expressing thermal comfort due to high temperatures is the heat index. The US National Weather Service²⁸ explains that the equation characterizing heat index is obtained by multiple regression analysis [14]. The heat index is calculated using the temperature and relative humidity variables. The heat index value is linked to the impacts on the body given by those environmental condition as reported in Table 5.

Table 12. Heat Index ranges and associated impacts. Source: US National Weather Service²⁹

Classification	Heat Index (T ranges)	Effect on the body
Caution	27°C - 32°C	Fatigue possible with prolonged exposure and/or physical activity
Extreme Caution	33°C - 39°C	Heat stroke, heat cramps, or heat exhaustion possible with prolonged exposure and/or physical activity
Danger	40°C - 53°C	Heat cramps or heat exhaustion likely, and heat stroke possible with prolonged exposure and/or physical activity

²⁸ <https://www.wpc.ncep.noaa.gov/html/heatindex.shtml>

²⁹ <https://www.wrh.noaa.gov/psr/general/safety/heat/heatindex.png>

Extreme Danger	54°C or higher	Heat stroke highly likely
-----------------------	----------------	---------------------------

Temperatures increase along the century, specially towards the end of it, as well as the heat index (Figure 26). While in the past València has not reach extreme caution threshold in the far future (2071-2100) it is likely that areas of the city will suffer from up to 10 hours of extreme caution. Furthermore, as observed in Figure 27, in the far future, daytimes around 15:00 will likely experience from extreme precaution to danger situations. Heat index is lower close to shore and Albufera due to the proximity to water that act as a buffer. As previously described, tropical days will be more likely to happen. Thus, it is important to adapt and strengthen current extreme heat event protocols and guidelines as well as further prepare to better cope with these extreme events.

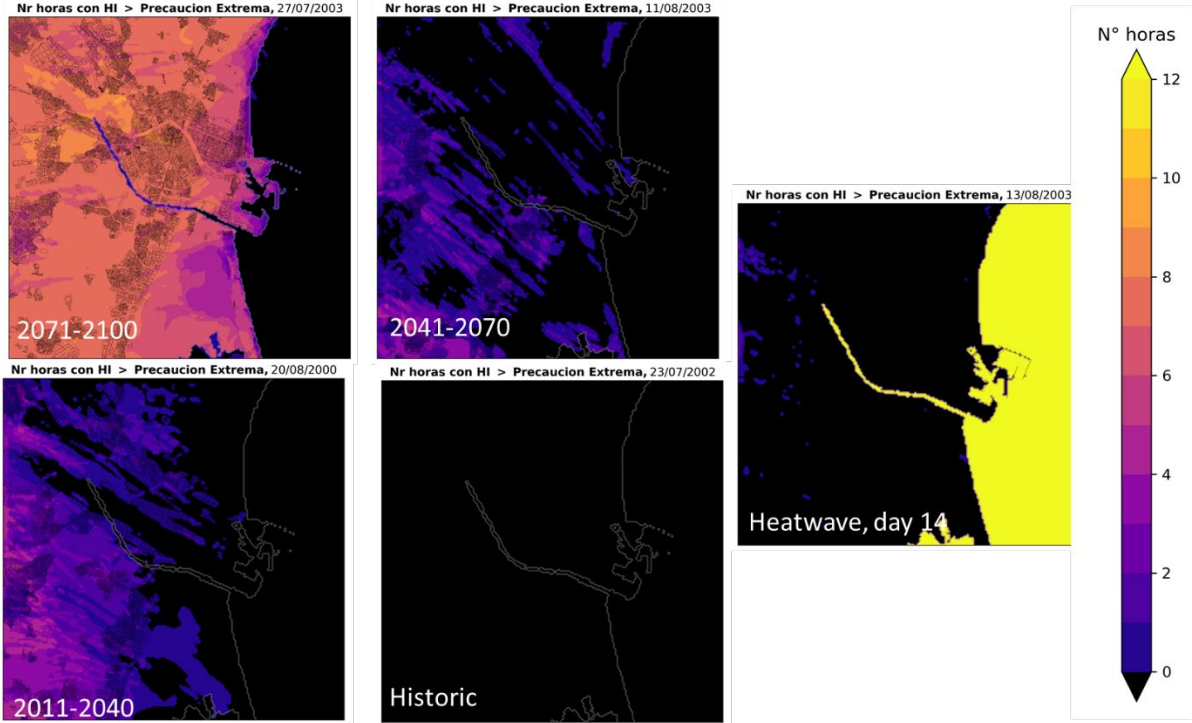


Figure 13. Number of daily hours that exceed the *extreme caution* threshold.

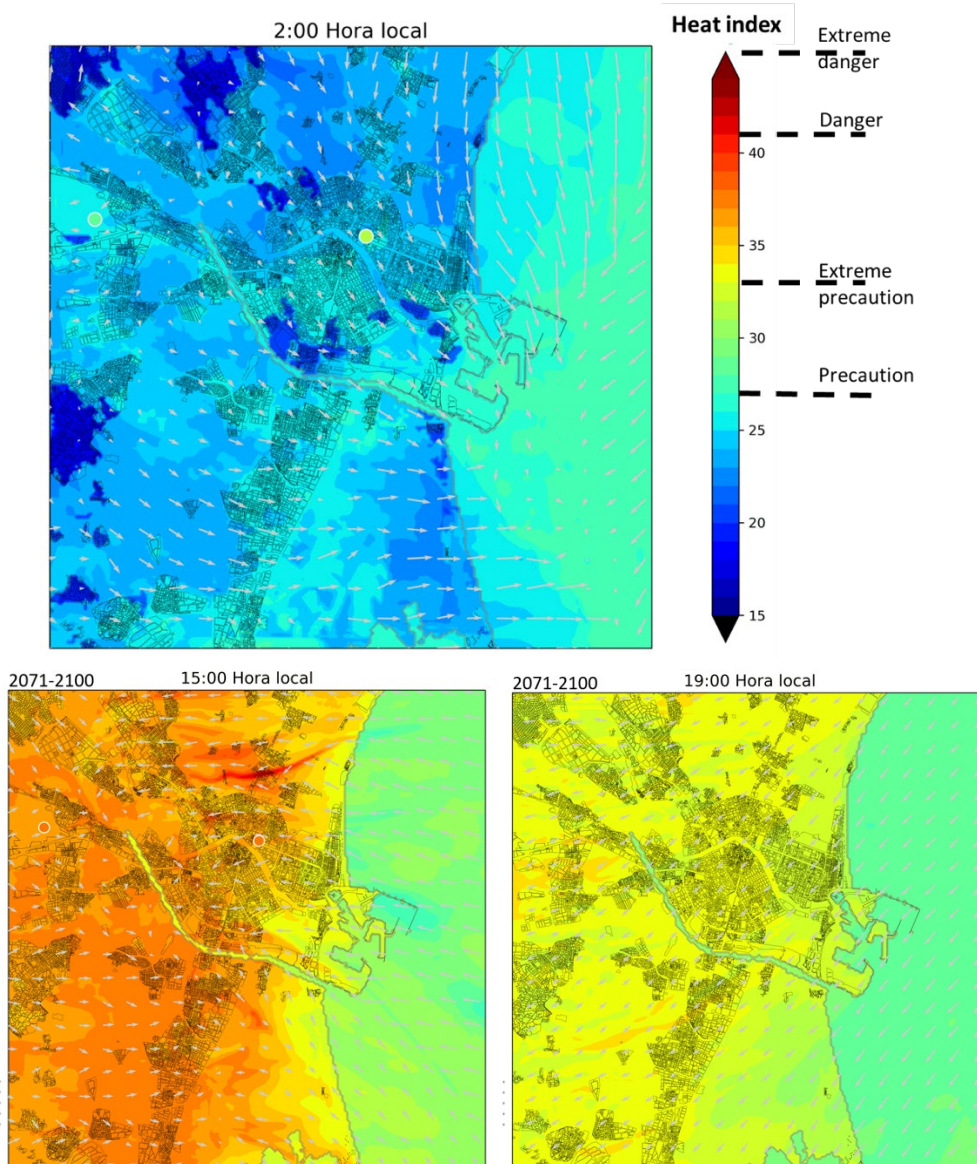


Figure 14. Heat index conditions at three different times for the representative typical day for the period comprising 2071-2100

2.1.4.5. % of night hours with $T > 20^{\circ}\text{C}$

Further to studying representative tropical days for each period of the century, a heatwave event was studied as these types of events will be more frequent in the future (section 2.1.1.3). The modelled historic heatwave event did not show as high temperatures as the tropical days nor reaching *extreme caution* threshold to the same extent. However, the impacts of prolonged heat are also known³⁰. However, heat exposure during the night is not often assessed and identified as important. A recent study demonstrated the importance of the effect of night-time temperatures in increasing the risk of mortality (7). Therefore, a specific index (% of night hours with $T > 20^{\circ}\text{C}$, in each pixel) to assess the night temperatures over the heatwave was analysed

³⁰ https://www.unisdr.org/files/1145_ewheatwave.en.pdf

within this study and represented in Figure 28. As observed almost all night-time for the 2003 heatwave (16 days) exceeded 20 °C and often being above 22 °C in the city centre.

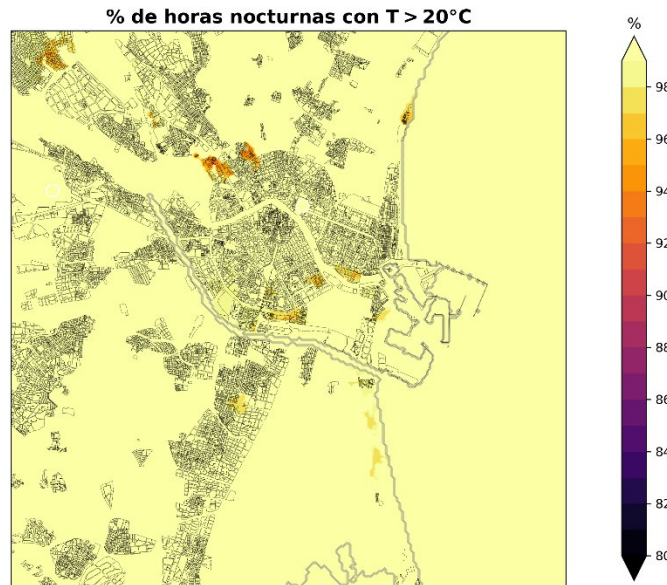


Figure 15. % of night hours with T> 20°C

2.1.4.6. Cooling degree days (CDD)

Cooling degree days (CDD) are a measure of how hot the temperature was on a given day or during a period of days. In other words, CDD is a measure of how much (in degrees), and for how long (in days), the outside air temperature was *above* a certain level (In Spain, this threshold is set at 26 °C³¹). CDD is used to assess the energy consumption required to *cool* buildings. Despite this index may not be directly related to the studied historic area within València, it was considered that it may be useful for the residential, tourism, climate change related stakeholders to assist on the relevant decision making related to climate change mitigation and adaptation. Figure 29 shows the areas with highest CDD which corresponds to the city of València and inland part reaching 40 CDD for the city centre and almost 50 CDD for the airport (Figure 30).

³¹ <https://escenarios.adaptecca.es/doc/datos.pdf?v=2021>

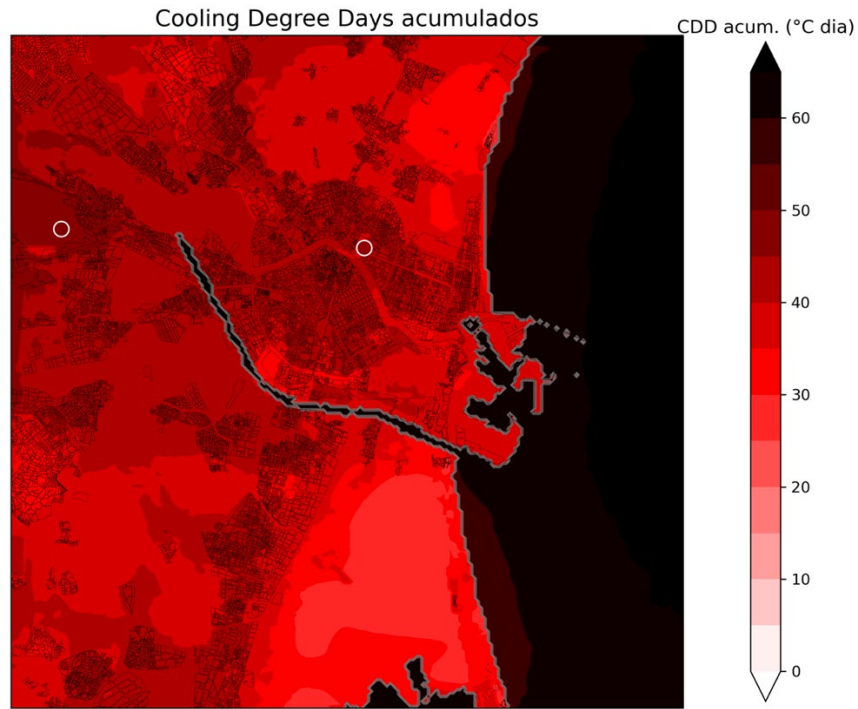


Figure 16. Cooling Degree Daily CDD map for València

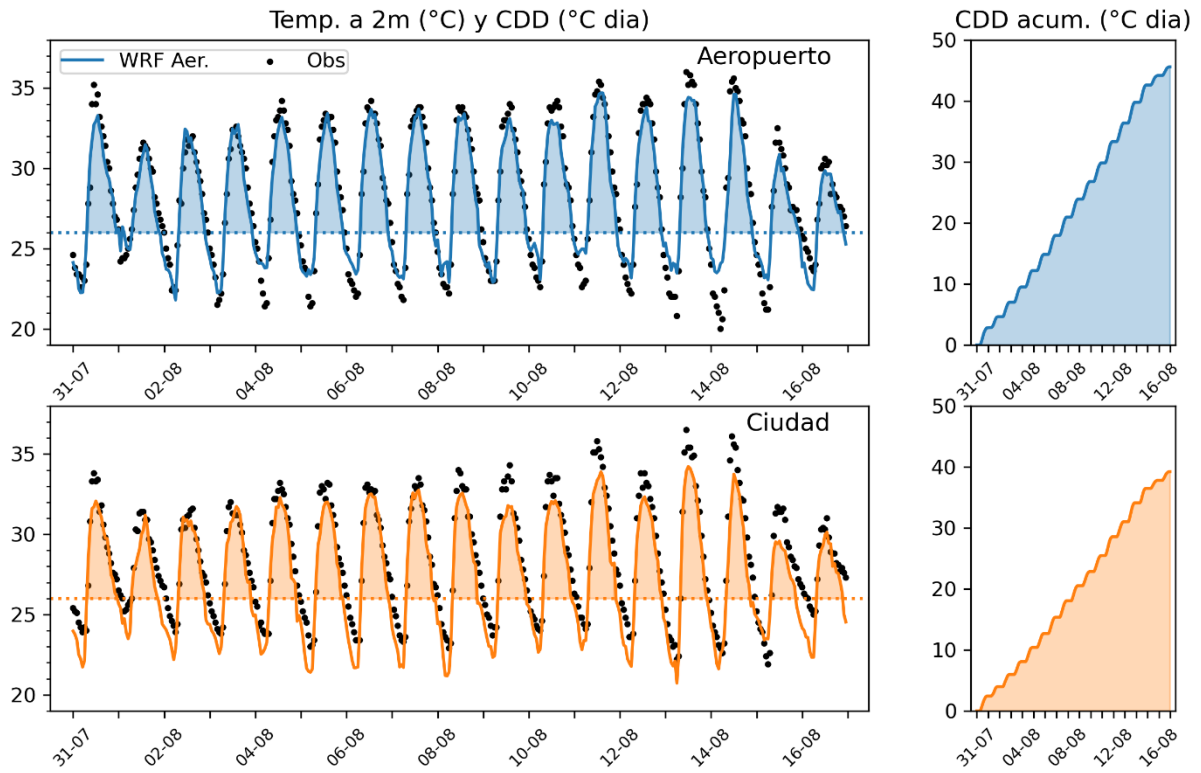


Figure 17. Hourly distribution of CDD and HDD for the heatwave event.

2.1.5. Land use effect analysis - Outcomes from the grey and black land use scenarios

As explained above, further the current land use scenario, two additional land used scenarios have been used as an input for the thermal modelling: The grey scenario, a realistic possible future scenario where mainly areas that are now abandoned or in the process of land use change may become part of the urban building environment. And a black scenario, a hypothetical scenario where several regulations around orchard heritage areas would be withdrawn and urban expansion would take place over the Huerta. Figure 31, Figure 32, Figure 33 described the land use classification according to WRF-ARW. To the right it can be seen the percentage of area of each type of land use. The *irrigation crop* and *crop+wood* type of land use decrease in favour of *high intensity residential* and *industrial/commercial* areas. In the case of the grey scenario the artificialized area would increase by nearly a 5% while for the black scenario the artificialized area would reach nearly a 13% increase.

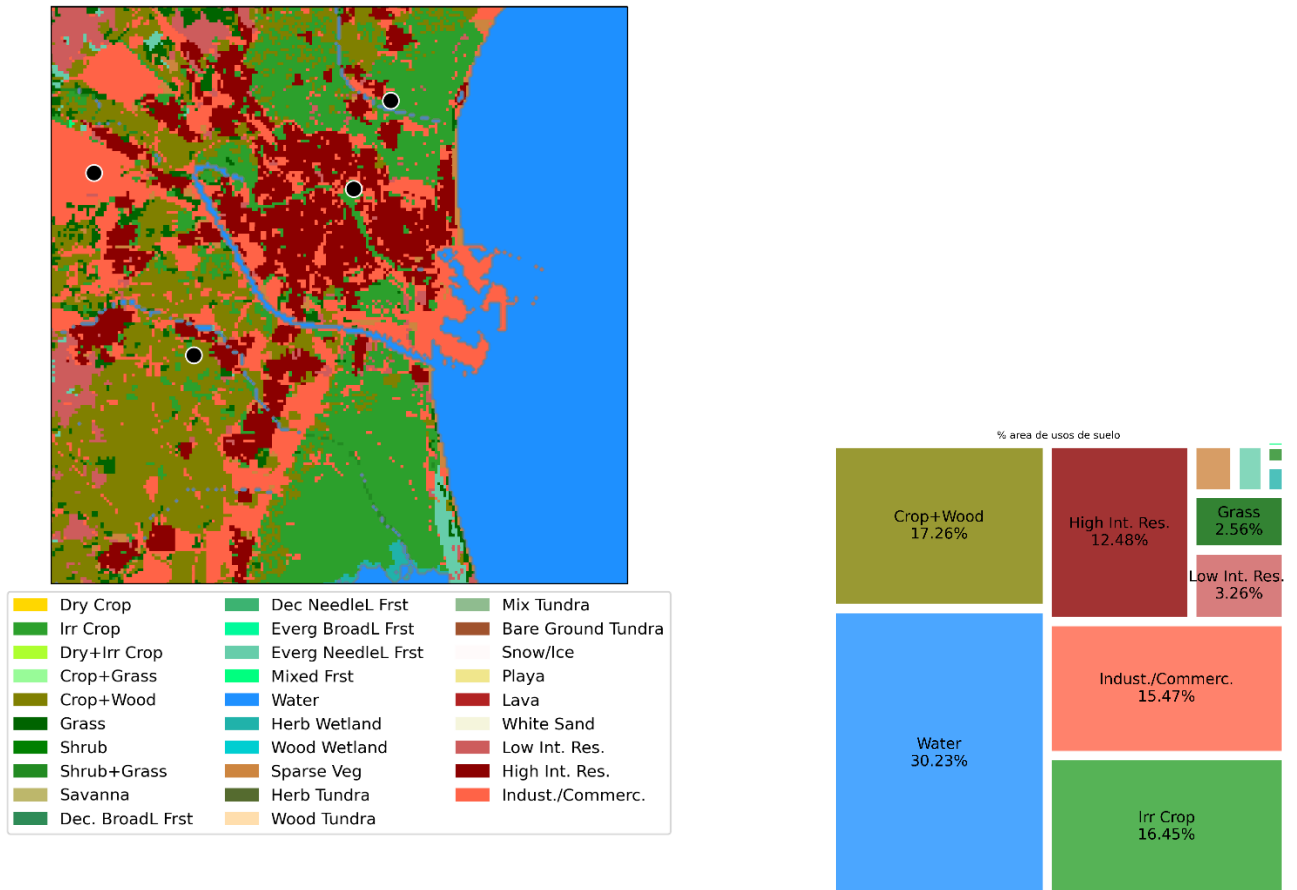


Figure 18. Current land use scenario in Valencia.

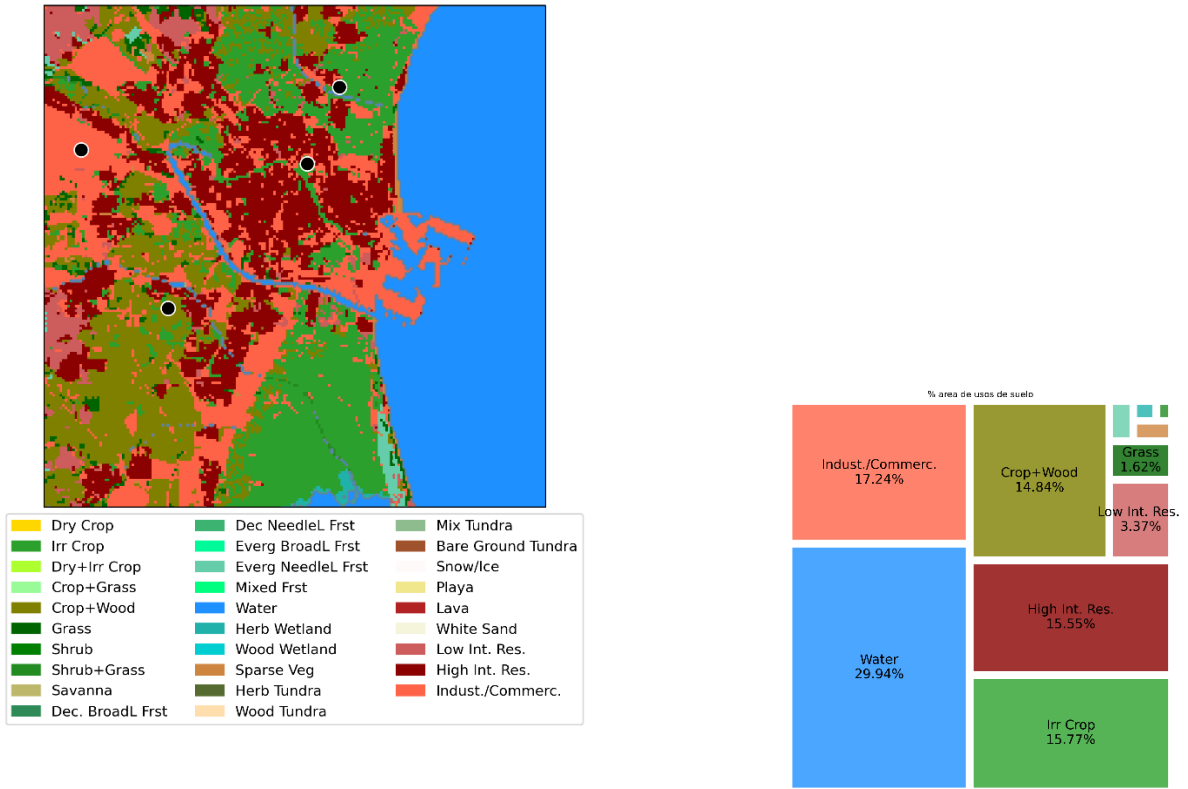


Figure 19. Grey land use Scenario

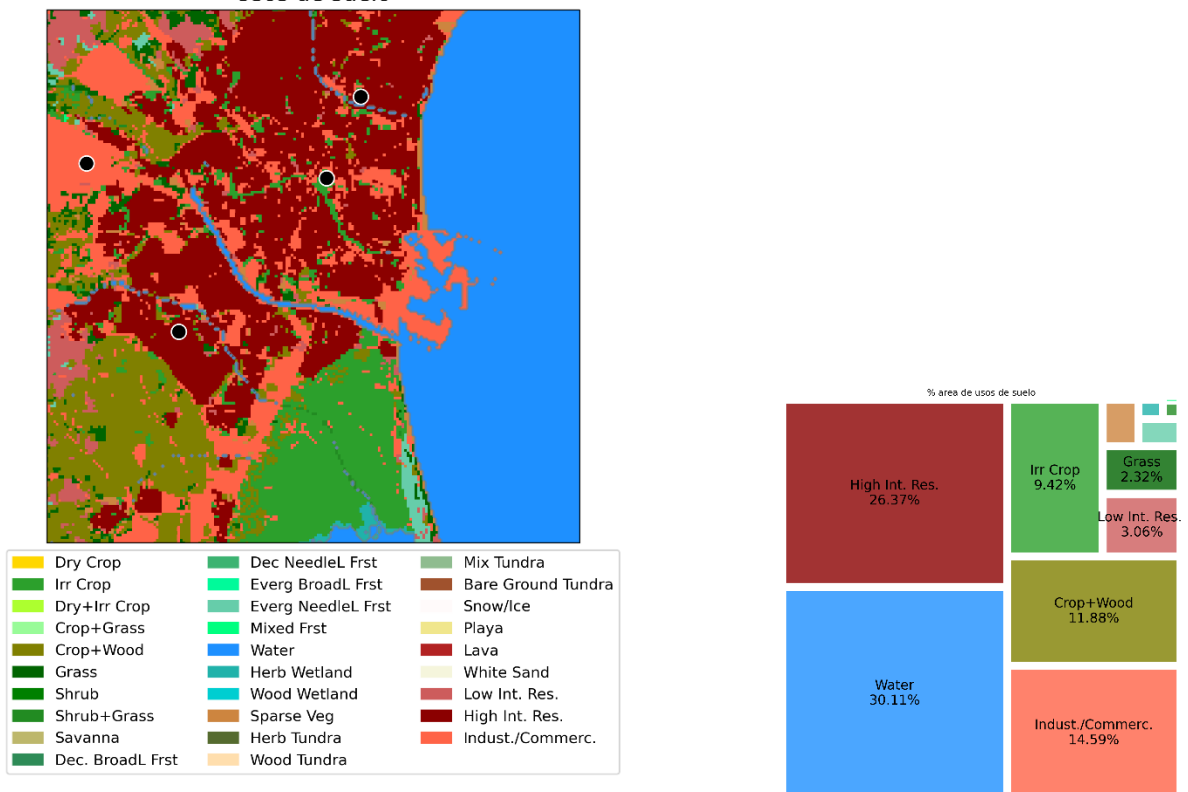


Figure 20. Black land use Scenario

To better observe and numerically analyse the differences between the scenarios 4 geographical points (P1, P2, P3 and P4) have been selected as observe in Figure 34.

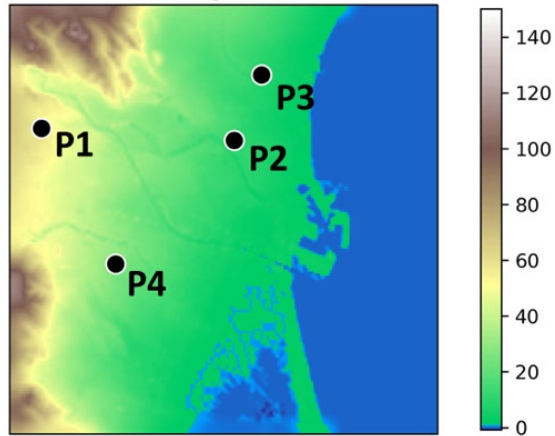


Figure 21- Selected geographical points

The outcomes of the modelling exercise indicate four main conclusions:

- Only the black scenario, compared to the actual scenario, presented significant changes in temperatures ($> 0.5 \text{ }^{\circ}\text{C}$)
- The artificialization of the land use would affect more strongly the minimum temperature values. The black scenario increased night-time temperatures (minimum temperatures) up to $2 \text{ }^{\circ}\text{C}$ for the historic period (Figure 35)
- Points 3 and 4 showed relevant minimum temperatures increase, as a result of more land used change around them, while no significant temperature effect was observed in Points 1 and 2.
- Land use buffer on temperature increase was more obvious for the historic period with milder temperatures

	Temperature difference, °C (Black-actual scenario)			
	P1	P2	P 3	P4
23/07/2002 2:00	0,02	-0,03	0,88	0,96
23/07/2002 3:00	0,12	0,38	0,81	0,23
23/07/2002 4:00	-0,44	0,41	0,8	0,24
23/07/2002 5:00	0,15	0,12	0,97	0,76
23/07/2002 6:00	0,09	0,42	1,99	0,94
23/07/2002 7:00	0,2	0,21	0,57	1,19
23/07/2002 8:00	0	0,85	0,13	-0,01
23/07/2002 9:00	-0,08	0,06	0,24	-0,25
23/07/2002 10:00	-0,04	0,03	0,02	-0,3
23/07/2002 11:00	0,22	0,13	-0,08	-0,36
23/07/2002 12:00	0,08	-0,08	0,06	-0,62
23/07/2002 13:00	-0,04	-0,06	0,1	-0,48
23/07/2002 14:00	0,18	0,12	0,23	-0,11
23/07/2002 15:00	-0,2	0,17	0	-0,16
23/07/2002 16:00	-0,08	-0,01	0,23	-0,12
23/07/2002 17:00	0,08	-0,08	0,06	-0,18
23/07/2002 18:00	-0,06	0,08	0,3	0,1
23/07/2002 19:00	0	-0,05	0,53	-0,03
23/07/2002 20:00	0	-0,04	0,68	0,22
23/07/2002 21:00	0,3	0,07	1,16	1,28
23/07/2002 22:00	0,18	0,24	1,51	1,34
23/07/2002 23:00	-0,18	-0,01	1,54	0,67
24/07/2002 0:00	0,14	0	1,61	1,04
24/07/2002 1:00	0,06	0,18	1,57	0,95

Figure 22. Hourly temperature (°C) difference between de black and actual land use scenario for the four selected points. Data corresponding to the historic period

Next step would be to model the green scenario to better understand not only the artificialization of the land but to understand the ecosystem services provided by green areas such as Albufera and more specifically the Huerta de València.

It has to be noted that this research exercise aims at understanding the implications of land use on the temperature in València and surroundings at meso-scale using a meteorological modelling. This means that changes on land use at microscale level, either by greening or artificializing a site, will not be captured by this specific simulation model. Other type of modelling exercises at microscale level should be done for this later purpose.

2.1.6. Concluding remarks

The outcomes of this research exercise (identification of hot-spots areas, temperature trends as a result of climate change and land use), together with other valuable municipal and project information (e.g. GrowGreen³²) may support València municipality on the development of cross-sectoral policies and strategies dealing with health, adaptation to climate change, planning, among others to better prepare and mitigate extreme urban temperatures. This modelling exercise can be complementary to the micro-scale modelling to support the adoption of resilience measures.

³² <https://growgreenproject.eu/>

2.2. Climate-change hazard models and maps for pluvial flooding impact assessment

Pluvial flooding is a major problem since it leads to numerous direct and indirect impacts and it causes social, economic, and environmental damages all over the world. Modelling and simulations of pluvial flooding are crucial tools for local water managers to improve the decision-making regarding flood risk management and flood mitigation strategies.

The purpose of this study is to predict and characterize pluvial flooded areas using the hydraulic numerical modelling of MIKE FLOOD Screening Tool under different scenarios. The specific objectives of the study are the following:

- Develop the methodology and procedure for setting the hydrodynamic model.
- Map the flooding areas under different scenarios.
- Implement these results in a GIS environment for visualization.

The study site (Figure 36) has a total area of 9.59 km² and it is bordered by the river Danube to the west, Karlova Ves borough to the north, the New Town borough to the north and Ruzinov borough to the east and south.



Figure 23. Location of Old Town in Bratislava city.

The study area contains the Old Town (Staré Mesto) of Bratislava city, capital of Slovakia (Figure 36) The Old Part of Bratislava includes the historical and administrative centre in the southern-eastern section and contains the medieval core of Bratislava with many historical buildings as well as other elements of tangible cultural heritage (e.g. Ápponyi House, Pálffy Palace, Bratislava Castle, Saint James's Chapel, Fishermen's Gate among others).

These monuments and surrounding areas are exposed and vulnerable to climate related hazards (e.g. high extreme temperatures, pluvial flooding from intensive precipitation). Pluvial flooding events are among the main hazards affecting this area. In the last decades, the city has experienced frequent episodes that have threatened the historical monument reserve. The reason for this may be influenced by a sewage water and rainwater sewage system that date back to 2008 and are not suitable for the amount of urban development occurred in the past

10 years, which has resulted in an increase of impermeable land-cover. Hence the importance of knowing the areas most exposed to pluvial flooding in order to help policy making in planning for the mitigation of potential pluvial flooding impact on the historic area.

2.2.1. Methods

2.2.1.1. MIKE 21 FLOOD Screening Tool

For this study, MIKE 21 FLOOD Screening Tool (MIKE 21 FST, Figure 37), a hydrodynamic model, has been applied to determine the hydrodynamic processes within the Bratislava’s Staré Mesto urban area. This model has been previously applied and has shown to be effective for urban flooding mapping [16], [17],[18],[19].

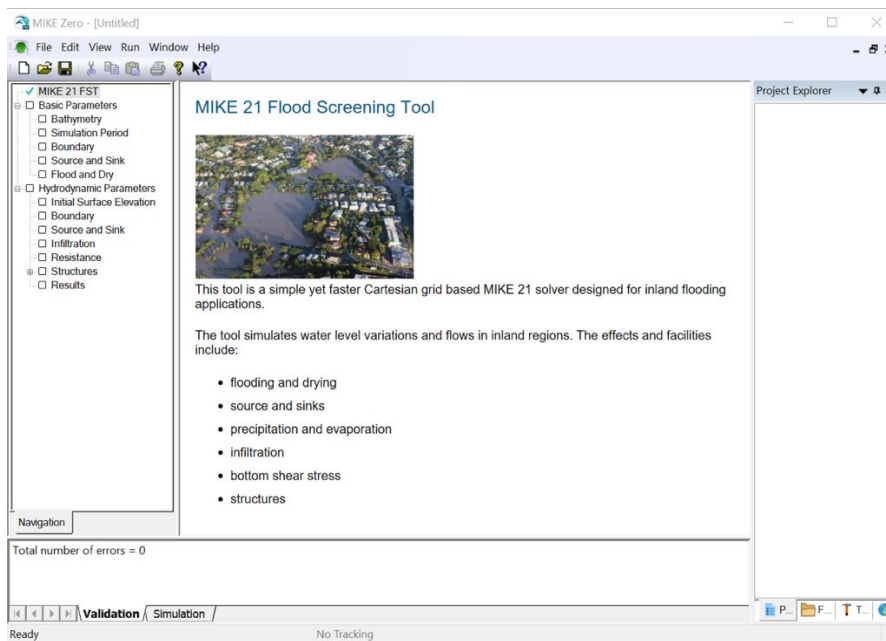


Figure 24. Mike 21 FST User Interface.

MIKE 21 FST was developed by the Danish Hydraulic Institute, DHI, and it is based on the MIKE 21 Flow model (MIKE 21 HD)³³. MIKE 21 FST allows simulating water level variations and flows in inland regions, including effects and facilities, such as bathymetry, sources and sinks, evaporation, flooding and drying, bottom shear stress, among others.

The following equations describe the flow and water level variations [19]:

$$\frac{\partial \zeta}{\partial t} + \frac{\partial p}{\partial x} + \frac{\partial q}{\partial y} = \frac{\partial d}{\partial t} \quad (2)$$

$$\frac{\partial p}{\partial t} + gh \frac{\partial \zeta}{\partial x} + \frac{gp\sqrt{p^2 + q^2}}{c^2 \cdot h^2} = 0 \quad (3)$$

³³ Despite the numerical engine of both models (MIKE 21 FST and MIKE 21 HD) is the same, MIKE 21 FST differs on the following (DHI, 2017): The convective terms are omitted from the model, as well as the viscous terms in the governing equation; Wind, atmospheric pressure variation, Coriolis and wave radiation stresses are neglected.

$$\frac{\partial q}{\partial t} + gh \frac{\partial \zeta}{\partial y} + \frac{gp\sqrt{p^2 + q^2}}{C^2 \cdot h^2} = 0 \quad (4)$$

where $h(x,y,t)$ is water depth, $d(x,y,t)$ is the time varying water depth (m), $\zeta(x,y,t)$ is surface elevation, $p,q(x,y,t)$ are flux densities in x- and y-directions, $C(x,y)$ is Chezy resistance, g is gravity, x,y are space coordinates and t is time.

2.2.2. Data

MIKE 21 FST model requires as input meteorological and spatial data. This data, which can be divided into basic and hydrodynamic parameters, determines the structure of the model. Table 6 provides a summary of them. A description of each parameter can be found hereafter.

Table 6. Parameters to set up MIKE 21 FLOOD Screening Tool

Basic parameters	Hydrodynamic parameters
Bathymetry	Initial surface elevation
Simulation period	Water level at the boundary
Flood and dry	Source and Sink
Location of model boundaries	Infiltration
	Resistance
	Results

Bathymetry, refers to the topographic information of the terrain and provides height data with respect to the mean sea level. In this study, the Digital Elevation Model (DEM) was used to represent the terrain, together with buildings and constructions. This DEM, which is detailed in *ARCH D4.1 Sensing and Repositories* (section 5.4 for further details), presented a resolution of 1 m x 1 m which was converted to a resolution of 2 m x 2 m in order to achieve the viability of the simulation process and the required computational capacity (Figure 38). The correction of the DEM, despite being quite time-consuming, it is of a high importance as a non-detailed DEM can lead to a false representation of the topography and, by extension, to distortions in the model.

The procedure of correction was carried out through an iterative process, which consisted on a four-step procedure. Initially, a first test was done running MIKE model with the original DEM. Secondly, the results of water level were analysed mainly focusing on the areas where water was accumulated. Thirdly, the critical points were verified checking satellite images. Finally, necessary adjustments and corrections were developed with DEM editing.

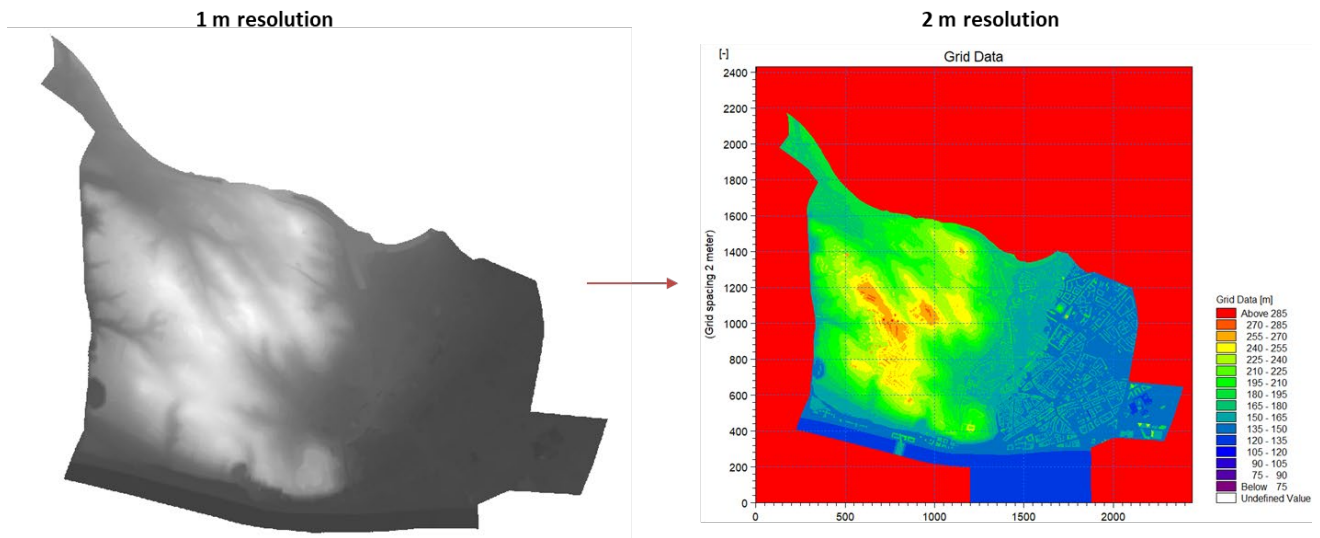


Figure 25. Transformation of MDE resolution from 1 m to 2 m.

Within the corrections that were developed, tunnels, pedestrian subways and new development areas were among the main areas that needed correction in the DEM (Figure 39).

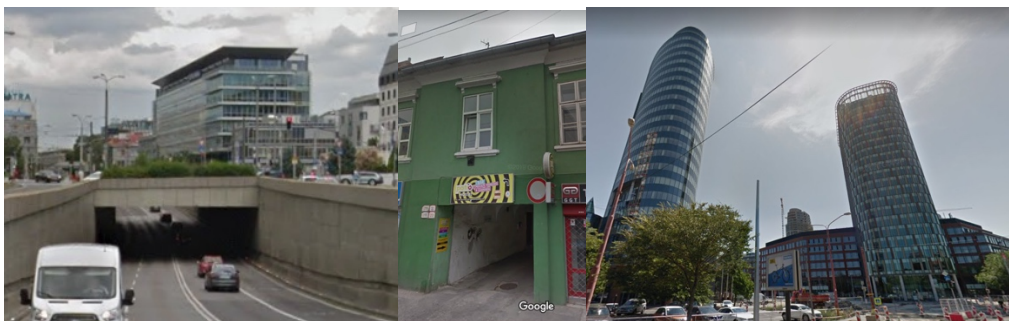


Figure 39. Examples of locations of Bratislava that needed correction in the DEM.

Simulation period, corresponds to the simulation time of the flood model and involves the following parameters:

- The time step range is the number of steps that the simulation should cover.
- The time step interval is the amount of time that is incremented between each time step. A small-time step results in a higher stability of the model.
- Identify minimum geographical unit of analysis
- The simulation start date is the date and time corresponding to the start of the simulation and corresponds with the date of the designed rain events (see Source and Sink section for further details)

Table 7 presents the values that were chosen for the model for each rain event.

Table 7. Simulation period parameters.

Parameter of simulation period	1 h rain event	2.5 h rain event
Time step range	0-90,000	0-90,000
Time step interval	0.3	0.3
Simulation start date	23/07/2010 22:40	04/08/2011 04:10

Flooding and drying depth, refer respectively to: the water depth at which the point of the grid will enter into the calculation; and the minimum water depth allowed in a point before is taken out of calculation. In the present work, the recommended values were used [19]. Drying depth was set at 0.001 m and flooding depth at 0.005 m.

Location of model boundaries, represents the contact points of the model grid with the boundaries. In this study, they were identified automatically by the program. The resulting boundary points are shown in the figure below in white arrows (Figure 40).

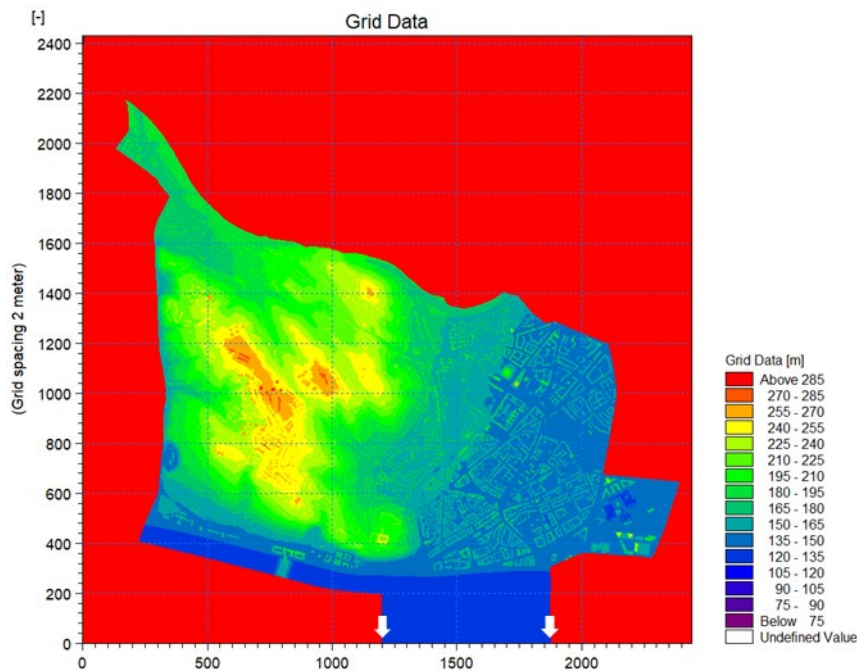


Figure 26. Boundary positions in the study area represented by white arrows.

Initial surface elevation, provides information about the initial water level. In this study, the initial surface level was set to a constant value, which corresponds to the water level of the Danube River.

Water level at the boundaries, specifies the level of the surface or flow at the boundary point detected above. In the present study a constant value of water level was set, which coincided with the water level of the Danube River.

Source and Sink dialog, where evaporation and precipitation rates are specified. In this work, a constant value is given for evaporation and two different scenarios are set for precipitation rates.

Precipitation rate (in mm day) is the forcing factor that feeds the hydraulic model and refers to an intense precipitation event, which is defined for a given duration. Both scenarios were considered from the historical precipitation records of the meteorological stations of Koliba and Letisko. They belonged to the most intense events for a duration of 1 and 2.5 hours over the period between 2007 and 2018 (Figure 41 and Figure 42).

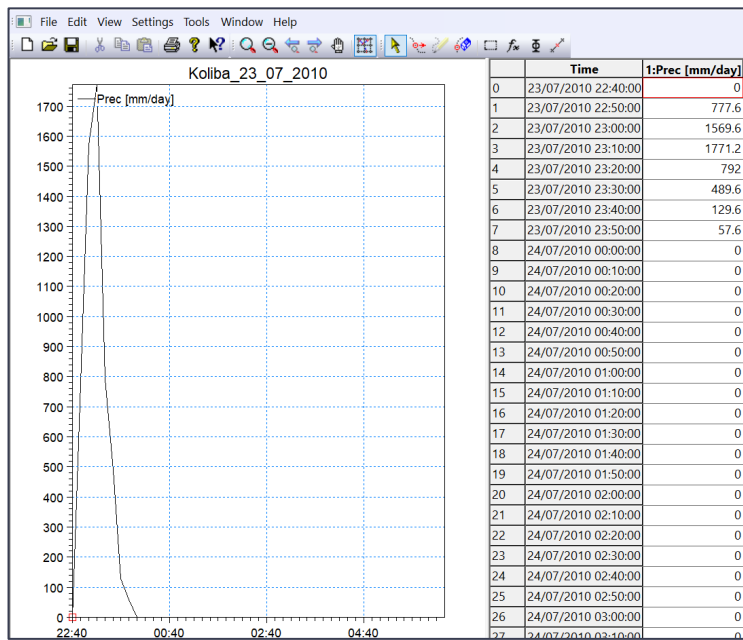


Figure 27. Precipitation rate (in mm/day) of 1 h rain event at Koliba station.

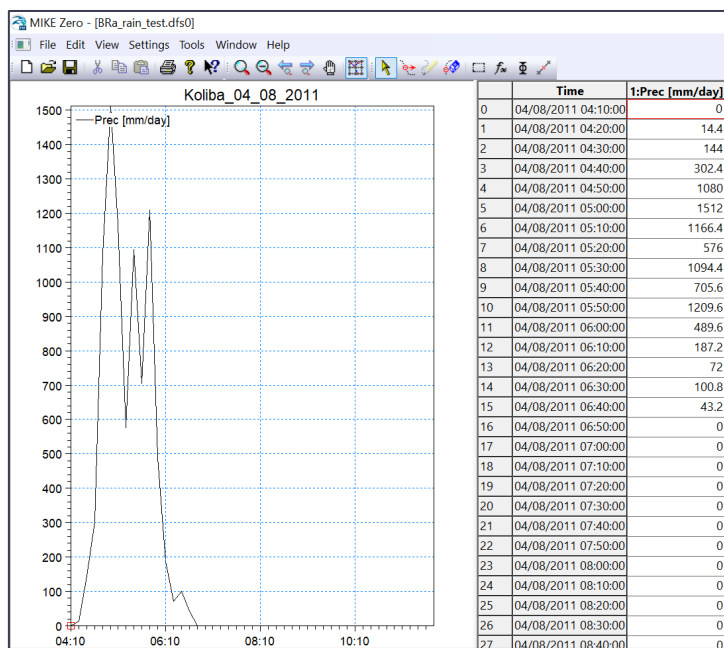


Figure 28. Precipitation rate (in mm/day) of 2.5 h rain event at Koliba station.

In addition to the rainfall events, two different “What If” scenarios were considered in the study. A first one, where the entire drainage system is saturated. This represents the worst-case scenario and implies that the system is not able to absorb rainwater and, as a result, runoff depends on the infiltration and roughness of the terrain. On the hand, a second scenario, in which the street drainage system is saturated; however, the drainage systems of buildings are working and draining water into the public system. As a result, a total of 4 simulations were carried out as summarized in Table 8.

Table 8 Description of the scenarios considered in MIKE FST

Nº	Scenario description
1	Entire drainage system is saturated under the most intense raining event of 1 hour
2	The street drainage system is saturated under the most intense raining event of 1 hour; however, the drainage systems of buildings are working and draining to the public systems
3	Entire drainage system is saturated under the most intense raining event of 2.5 hour
4	The street drainage system is saturated under the most intense raining event of 2.5 hour; however, the drainage systems of buildings are working and draining to the public systems

Resistance, refers to the roughness of the terrain and is represented by Manning or Chezy number³⁴. In general, high vegetation areas show a high bed resistance, while urban fabric areas show a low resistance. In the present work, Manning numbers in Table 9 were estimated using the land use and land cover of the Urban Atlas [20] in combination with standard Manning’s roughness coefficient tables [21].

Table 9. Average values of Manning’s roughness coefficient based on the Urban Atlas of 2018

Land use and land cover	Manning’s n
Continuous urban fabric	0.033
Discontinuous dense urban fabrics	0.035
Discontinuous medium density urban fabrics	0.037
Discontinuous low-density urban fabrics	0.038
Industrial, commercial, public areas	0.033
Fast transit roads	0.033

³⁴ <https://www.hydroreview.com/world-regions/dimensionally-homogeneous-form-of-the-chezy-and-manning-equations/#gref>

Roads	0.033
Railways	0.033
Port areas	0.033
Land without current use	0.04
Green urban areas	0.1
Sports and leisure activities	0.025
Forests	0.1
Water	0.05

The resulting grid for the study area is presented in Figure 43. It is worth mentioning that the Manning number used in MIKE 21 is the reciprocal value of the Manning number.

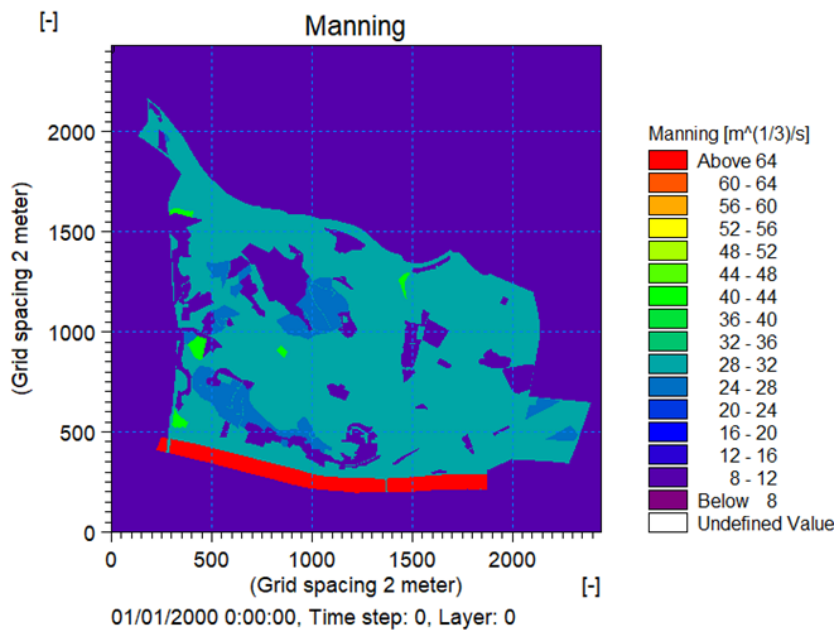


Figure 29. Manning's roughness coefficient for the study area

Infiltration, describes the flow of water from the surface zone to the infiltration zone below the ground level. In the present study, infiltration parameter was also defined based on the land use of the study area as it is considered one of the prime factors affecting infiltration behaviour and its spatial variability [22], [23],[24].

Table 10 summarizes the average values of Horton infiltration capacity based on the land use/land cover of the Urban atlas [20] and Figure 44 presents the infiltration coefficient for the Old Part of Bratislava.

Table 10. Average values of Horton infiltration capacity based on the Urban Atlas of 2018.

Land use and land cover	Horton's infiltration capacity
Continuous urban fabric	2.7
Discontinuous dense urban fabrics	15
Discontinuous medium density urban fabrics	19.8
Discontinuous low-density urban fabrics	36
Industrial, commercial, public areas	2.7
Fast transit roads	2.7
Roads	2.7
Railways	2.7
Port areas	2.7
Land without current use	19.8
Green urban areas	45
Sports and leisure activities	2.7
Forests	45

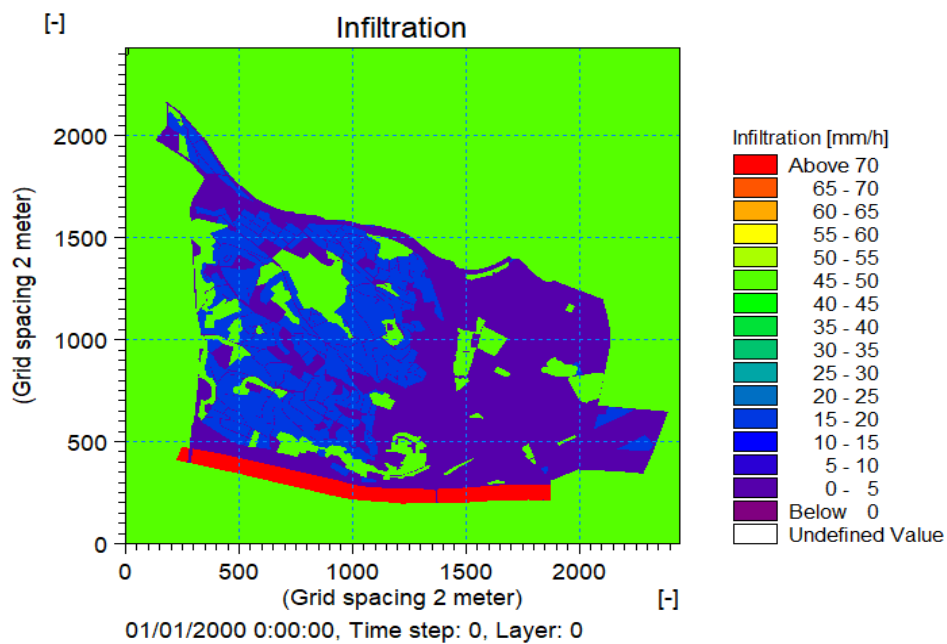


Figure 30. Horton's infiltration capacity for the study area.

Once the necessary parameters were introduced into the model, the four different scenarios were run. As a result, inundation statistics were obtained and stored as a *dfs file*, containing the following variables as separate items in the output file:

- Maximum water depth.
- Time at maximum water depth.
- Maximum flux magnitude.
- Time at maximum flux magnitude.
- Maximum current speed.
- Current direction at maximum current speed.
- Time at maximum current speed.
- Duration above threshold (optional).

From this file, the maximum water level [m] and maximum current velocity [m/sec] were extracted and visualized in a GIS environment; in this sense, the period of greatest severity of each scenario was represented.

2.2.3. Results

In general, the results show that the low-lying areas of the Old Town of Bratislava city would be flooded under the different scenarios. Inundation areas would appear specially in the streets of some major roads, such as the intersection between Staromestská and Suché mýto, Nábřežie armádneho generála Ludvíka Svobodu, Šulekova, Kozia, Klariská and Farská streets, as well as in several parks, such as Medická záhrada and Horský parks (Figure 45).

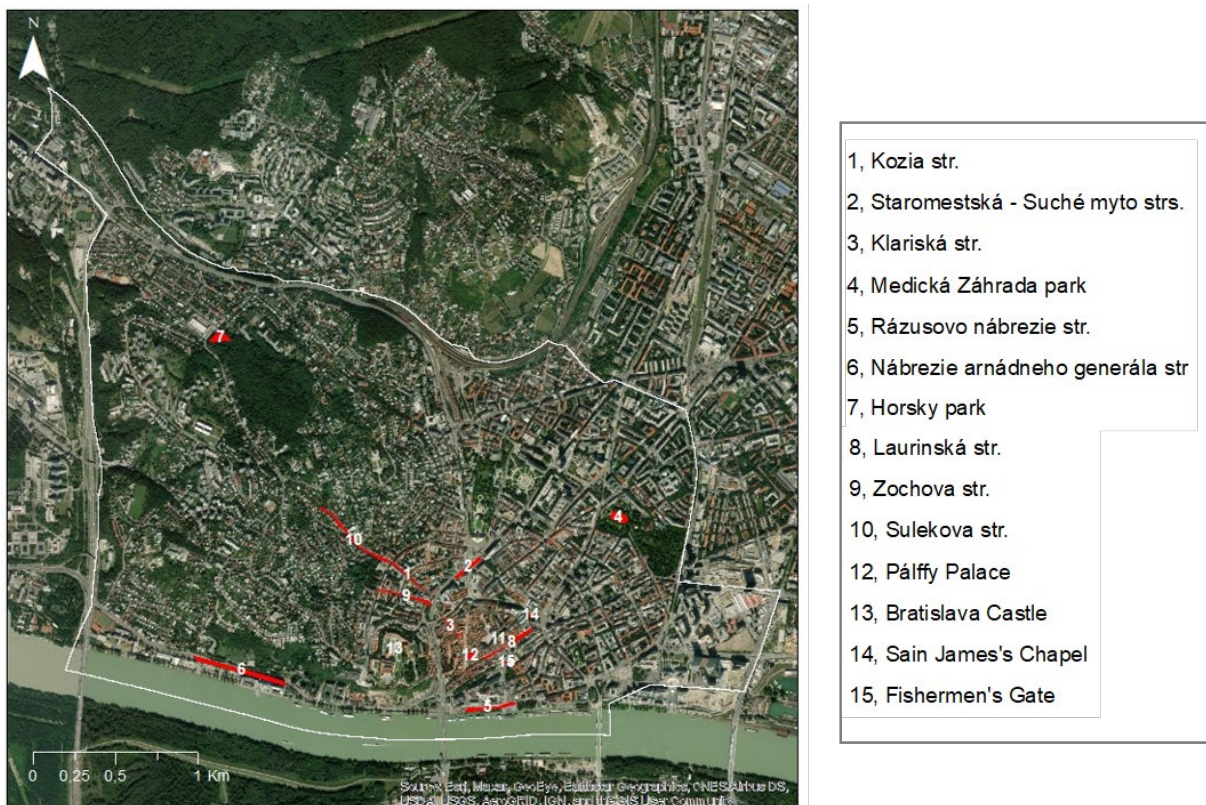


Figure 31. Areas where flooding parameters were assessed for the different scenarios.

The identified scenarios experience differences in maximum water level and current velocity. Regarding water depth, the rainfall event of 2.5 hours presents greater depths compared to 1-hour rainfall event, while the “*What If*” scenarios, show higher water depths when the entire drainage system is saturated (as expected).

Table 11 summarizes the results of water depth at the target historic areas identified for ARCH (see ARCH D3.3 City baseline report – Bratislava for further details³⁵), as well as at other locations of the Old Town under the developed scenarios. Water level maps for the entire study site are shown from Figure 46 to Figure 49.

Table 11. Maximum water level (in m) at different locations under the different scenarios

Location	Maximum water level (m)			
	Scenario 1	Scenario 2	Scenario 3	Scenario 4
Celtic pottery kiln, Ápponyi House	0.72	0.33	1.16	0.35
Celtic mint, Pálffy Palace	0.67	0.21	1.02	0.27
Celto-Roman structures, Bratislava Castle	0.21	0.17	0.25	0.2
Saint James’s Chapel	0.19	0.19	0.26	0.26
Fishermen’s Gate	0.5	0.37	0.62	0.54
Staromestská and Suché mýto streets	3.44	2.95	4.49	3.96
Šulekova street	2.32	2.12	1.89	1.87
Zochova street	1.51	1.44	1.53	1.52
Klariská street	3.28	3.23	3.26	3.19
Kozia street	2.51	2.5	2.35	2.18
Laurinská street	1.1	0.97	1.23	1.14
Nábřežie armádneho generála Ludvíka Svobodu street	0.57	0.54	0.55	0.53
Rázusovo Nábřežie street	0.81	0.79	0.86	0.83
Medická záhrada park	1.02	0.74	1.38	1.10
Horsky park	2.3	0.26	2.32	2.3

35

https://savingculturalheritage.eu/fileadmin/user_upload/Deliverables/ARCH_D3_3_City_baseline_report_Bratislava.pdf

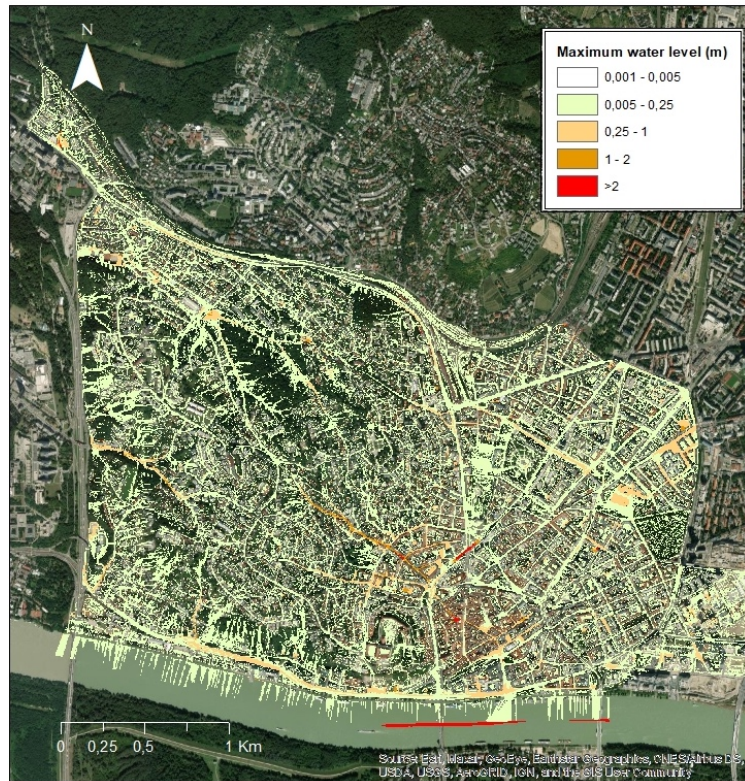


Figure 32. Results of water level under scenario 1 (entire drainage system is saturated under the most intense raining event of 1 hour).

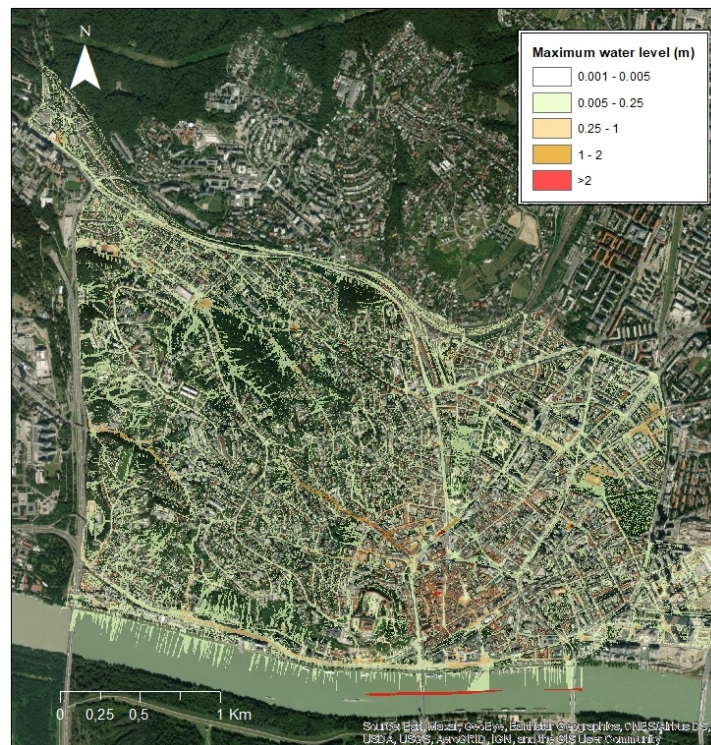


Figure 33. Results of water level under scenario 2 (street drainage system is saturated under the most intense raining event of 1 hour; however, the drainage systems of buildings are working and draining to the public systems).

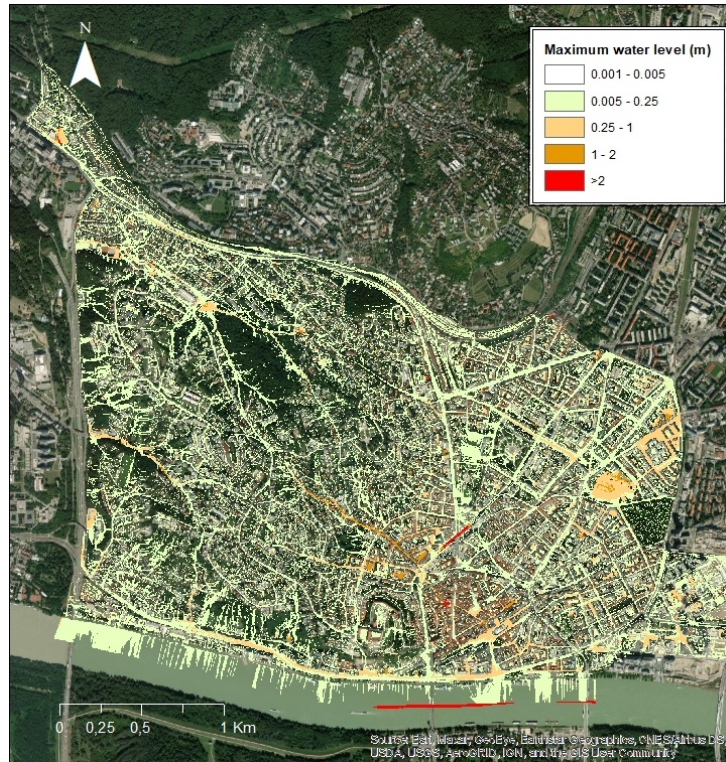


Figure 34. Results of water level under scenario 3 (entire drainage system is saturated under the most intense raining event of 2.5 hour)

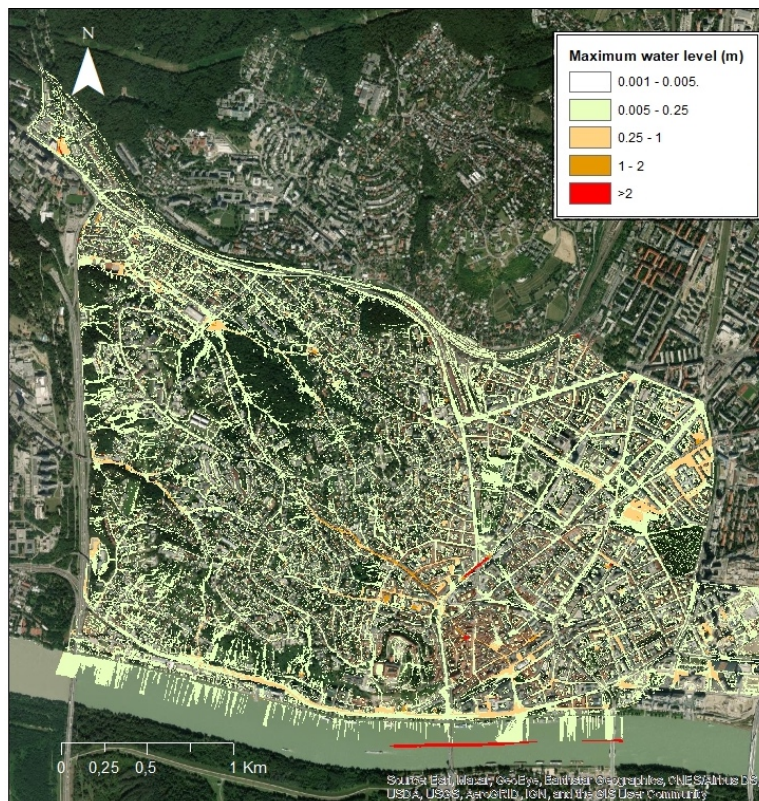


Figure 35. Results of water level under scenario 4 (street drainage system is saturated under the most intense raining event of 2.5 hour; however, the drainage systems of buildings are working and draining to the public systems).

It is worth mentioning that these results coincide with previously developed studies in the area, which state a high exposure to pluvial floods at Laurinská, Panská street, Klariská as well as at Kapucínska streets (Figure 50).



Figure 36. Results of Streberová et al (2020) regarding pluvial flooding in the historical monument preservation reserve.

With regards to the maximum current velocity, results show the highest values at the steepest streets (e.g. Šulekova, Zochova, Kozia and Klariská streets) and the lowest values at the flattest streets or target historic areas (e.g. Saint Jame’s Chapel, Bratislava Castle and Fishermen’s Gate). On the other hand, results of the different scenarios present no significant differences between them. This is clearly seen at Saint James’s Chapel or the Áppobyi House, where the differences are less than 0.11 m/sec. Table 12 summarizes the results of maximum current velocity at the target historic areas identified for ARCH (see ARCH D3.3 City baseline report – Bratislava for further details), as well as at other for different locations of the Old Town under the developed scenarios. Current velocity maps for the entire study site are shown from Figure 51 to Figure 54.

Table 12. Maximum current velocity (in m/sec) at different locations under the different scenarios

Location	Maximum current velocity (m/seg)			
	Scenario 1	Scenario 2	Scenario 3	Scenario 4
Celtic pottery kiln, Ápponyi House	0.57	0.68	0.5	0.57
Celtic mint, Pálffy Palace	0.85	0.74	0.79	0.63
Celto-Roman structures, Bratislava Castle	0.48	0.16	0.45	0.14
Saint James's Chapel	0.11	0.11	0.1	0.1
Fishermen's Gate	0.36	0.2	0.36	0.22
Staromestská and Suché mýto streets	1.5	1.4	1.4	1.35
Šulekova street	5.05	5.06	5.06	5.09
Zochova street	5.06	5.07	5.04	5.03
Klariská street	3.01	2.95	2.99	2.89
Kozia street	5.05	5.09	5.06	5.07
Laurinská street	0.84	1.27	0.79	1.1
Nábřežie armádneho generála Ludvíka Svobodu street	1.18	1.09	1.08	0.83
Rázusovo Nábřežie street	0.85	0.83	0.83	0.82
Medická záhrada park	0.25	0.21	0.27	0.23
Horsky park	0.9	0.87	0.78	0.75

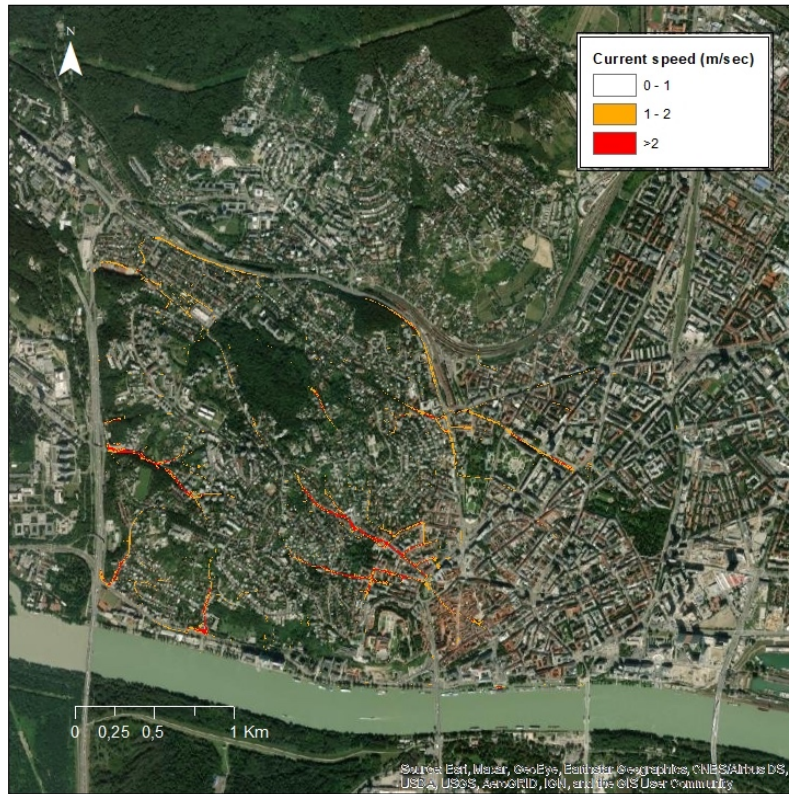


Figure 37. Results of current velocity under scenario 1 (entire drainage system is saturated under the most intense raining event of 1 hour).

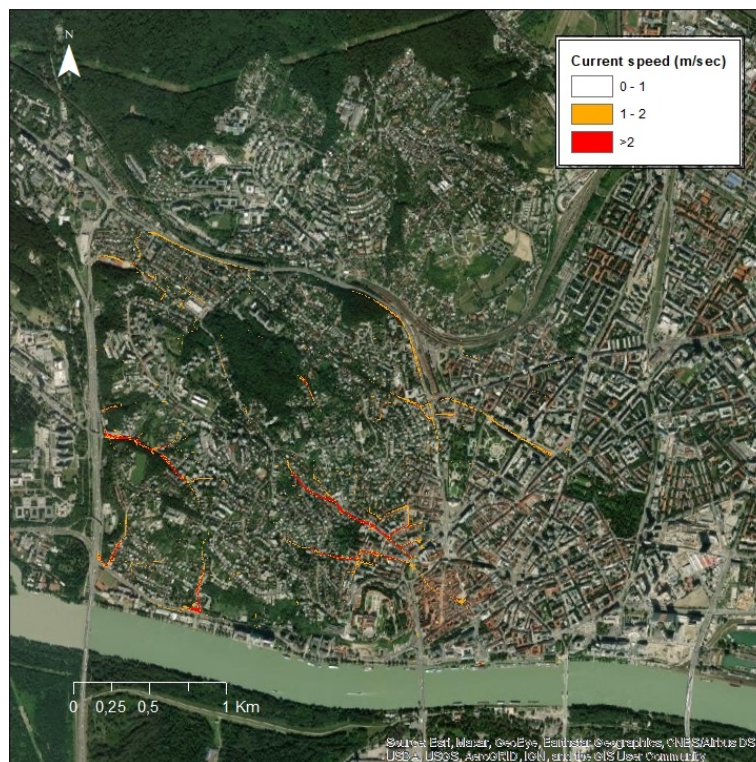


Figure 38. Results of current velocity under scenario 2 (street drainage system is saturated under the most intense raining event of 1 hour; however, the drainage systems of buildings are working and draining to the public systems).

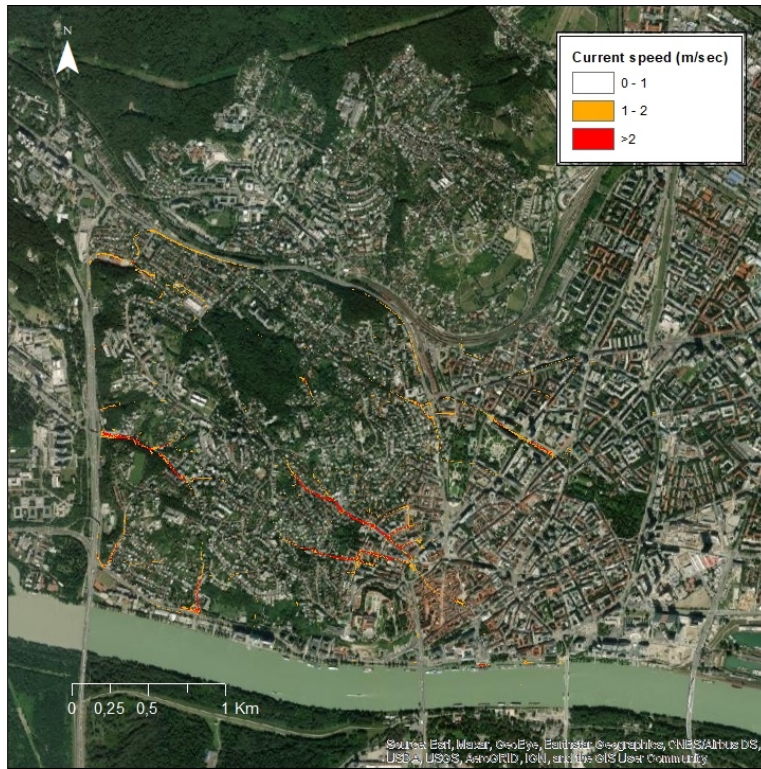


Figure 39. Results of current velocity under scenario 3 (entire drainage system is saturated under the most intense raining event of 2.5 hour).

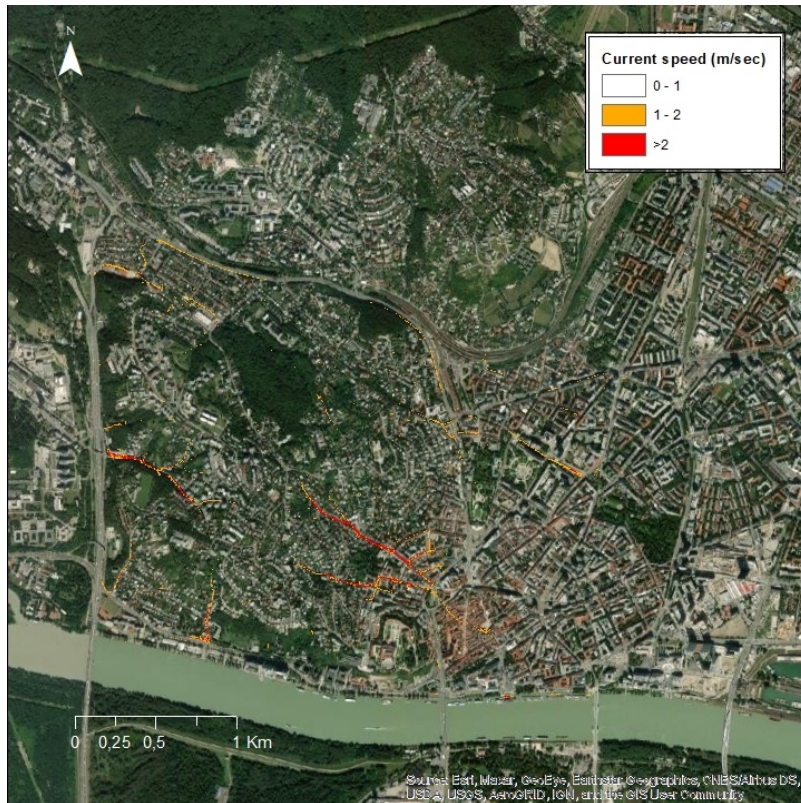


Figure 40. Results of current velocity under scenario 4 (street drainage system is saturated under the most intense raining event of 2.5 hour; however, the drainage systems of buildings are working and draining to the public systems).

3. Earthquake Hazard Models for Impact assessment

3.1. Ground Shaking Models and Maps for impact assessment

Ground motion is the movement of the earth's surface produced by the waves that are generated by earthquakes (due to sudden slip or rupture on a fault) or explosions (due to sudden pressure at the explosive source) travelling through the earth and along its surface; ground motion can be amplified by particular soil or morphology conditions of the territory. Figure 55 exemplifies the factors that influence the intensity and extent of ground motion generated by an earthquake, i.e.: 1) the characteristics of the seismogenetic source (such as location; geometry; activity that will influence the position of the hypocentre (and of the epicentre, i.e. the hypocentre projection on the surface) and the amount of the energy released at the sudden slip or rupture on a fault, referred to as Earthquake Moment Magnitude, M_w , and measured according to the Richter scale [25];) the distance between the earthquake source and the site of interest (e.g., points A, B, C, D in the picture); 3) the local site conditions including the soil type profile and the morphology of the territory.

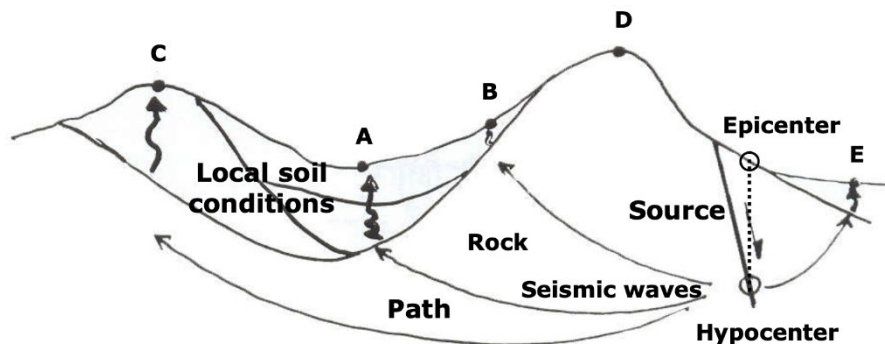


Figure 55. Example of factors that influence the intensity and extent of the ground motion generated by an earthquake.

A seismic hazard analysis and the consequent production of ground shaking models and maps are the basic inputs for developing earthquake damage and impact scenarios. Ground shaking models allow to estimate the severity of the ground shaking generated in different areas of the territory by an earthquake event. Ground shaking maps (reported also a seismic hazard map in the following) provide a graphical representation, via a selected metric, of the earthquake ground-shaking motion resulting after running ground shaking models; ground shaking maps should be readable by the stakeholders and suitable for the next steps of the seismic risk and impact analysis (that will be described in D5.3).

Two universally recognized approaches exist for seismic hazard assessment and ground shaking map modelling and representation: the Deterministic Seismic Hazard Assessment (DSHA) and the Probabilistic Seismic Hazard Assessment (PSHA). The DSHA considers each seismogenetic source separately; PSHA combines the contributions from all the relevant seismogenetic sources and allows characterizing the rate at which earthquakes and particular levels of ground motions might occur in the territory under analysis. For both the methods the information to be collected and the steps to be run for the ground motion assessment are the same, namely: the identification of the potential seismogenetic sources and their

characterization in terms of locations, geometry, activity and potential energy that can be released; and secondly the representation of the ground motion propagation from the point/plan of the seismogenetic sources in the surrounding area by a suitable Ground Motion Predictive Equation (GMPE) taking into consideration the morphological and the geological amplification effects (referred to as site effects).

DSHA and deterministic impact scenario approaches allow for the estimation of the expected ground motion and its related consequences separately for any different selected seismic that stakeholders might consider interesting to analyse (e.g. the maximum historical event known in the area surrounding the HA under analysis, or the maximum earthquake compatible with the known seismogenetic framework). On the other hand, PSHA approaches allow for the estimation of the probability of occurrence of a certain ground motion and the relative consequences in a certain time frame due to all of the possible seismogenetic sources that might generate an earthquake in the HA. The selection of either the DSHA, or the PSHA or both of them depends on the goal of the study [26, 35], in general terms:

- DSHA provides an estimate of the expected ground motion for a single earthquake event, that can be real or defined by the end-user; if there is the interest to assess more than one seismic event a hazard model and map is generated for each one of the events of interest. DSHA are implemented for assessing deterministic impact scenarios (by combining seismic hazard maps with exposure and vulnerability assessment) assessed that are useful for supporting “*what if analysis*”. Deterministic impact scenarios will provide to the stakeholders an estimation on the possible consequences that a specific earthquake event or a range of different kind of earthquake events analysed might cause on an HA; these estimates are useful to inform and guide an aware mitigation planning and emergency and response management. Stakeholders might be interested to perform *what-if analyses* based on user-defined scenarios to find data and evidence regarding “*what would happen if an earthquake, equal (max historical known earthquake) or stronger than the one already occurred centuries ago in this historic area, would strike again?*” [36].
- PSHA estimates the likelihood that various levels of earthquake-induced ground motions will be exceeded at a given location in a given future time period. The results of such an analysis are expressed as estimated probabilities per year or estimated annual frequencies. PSHA computes ground motion maps by considering the contribution from all potential seismic sources in the area under analysis collectively and the likelihood of the possible seismic events generated by those potential sources. PSHA maps are used for the seismic design of building and infrastructures³⁶, therefore each country has them available. Seismic hazard models and maps for Italy are made available through a WebGIS from INGV publically accessible and available for data download³⁷. Figure 56 provides a screenshot of such a WebGIS that has been queried for Camerino Municipality. It is worth highlighting that different shortcomings of the use of PSHA for seismic design purposes have been highlighted [37], and alternative approaches are under investigation [38]. Further to their use for design purposes PSHA

³⁶ Seismic design is ruled in Europe by Eurocode 8, i.e. EC8 defining Performance requirements, ground conditions and seismic action

³⁷ http://esse1-gis.mi.ingv.it/mps04_eng.jsp

maps can be used for a relative comparison of the seismic risk level among different structures or different geographical areas. This can inform stakeholders on where to prioritise intervention or resources allocation in the case of resource constrains. As an exemple the Italian Bridge Guidelines³⁸ recently issued use seismic ground motion values from PSHA maps as part of their proposed approach for screening the risk of bridges and viaducts nationwide and for attributing to each bridge a class of attention. As a furthe exemple PSHA have been used for the National Risk Assessment NRA [39] for Italy that was developed at the end of 2018 by the Italian Department of Civil Protection (DPC) in response to the specific requirement of the Sendai Framework for Disaster Risk Reduction to periodically adjourn the assessment of disaster risk.

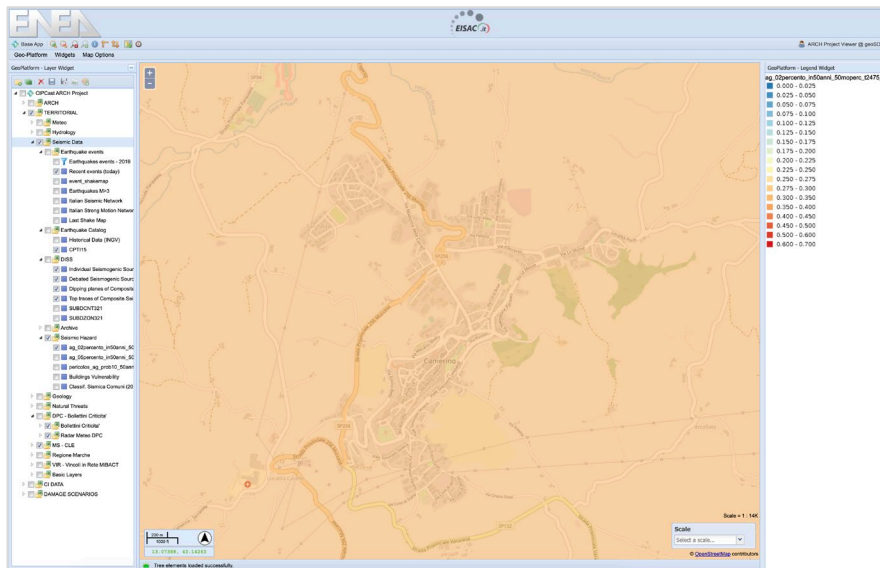
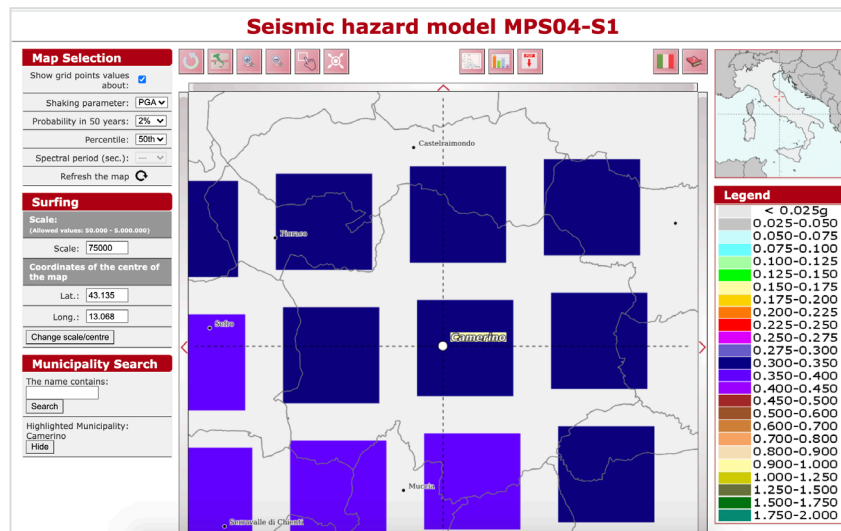


Figure 56. Expected PGA in Camerino in the range 0.3-0.35 [g] for earthquake events with 2% probability of occurrence in 50 years (Return Period $T_R = 2475$ years) according to the Italian PSHA model and maps³⁷ that have been all made available in ARCH DSS.

³⁸ https://www.mit.gov.it/sites/default/files/media/notizia/2020-05/1_Testo_Linee_Guida_ponti.pdf

The choice of the metric to be employed for the ground motion representation, that can be either quantitative or qualitative depends on the quality of the analysis performed and on the vulnerability model chosen for the assessment of the seismic response of the exposed assets to the ground shaking. The earthquake ground motion, can be described in term of either qualitative parameters. Examples of quantitative/engineering parameters include, among others, the peak ground acceleration, *PGA* [m/s^2] or [%g], peak ground velocity *PGV* [m/s], peak ground displacement *PGD* [m], elastic spectral acceleration, *Sa* [m/s^2], elastic spectral velocity, *Sv* [m/s],, elastic spectral displacement, *Sd* [m].

Macroseismic Intensity, *I* is instead a qualitative metric and therefore non-dimensional, provides a description of the effects of the earthquake at a particular location, as evidenced by observed damage on the natural and built environment, and by the human and animal reactions at that location. Thanks to its qualitative nature it is the oldest measure of the earthquake. Macroseismic Intensity scales have been extensively used when adopting empirical-based model for assessing the building stock seismic vulnerability and for estimating the possible earthquake-induced damage to it.

Section 3.1.1 provides a simplified overview on the methods and metrics to be used for generating ground shaking models and maps³⁹. In particular Par. 3.1.1 clarifies the DSHA adopted in the ARCH project and embedded in ARCH DSS for modelling ground shaking and for generating ground shaking maps. Section 3.1.2 provides an overview of the data used for implementing in the HA of Camerino Municipality the approach described in Par. 3.1.1. Section 3.1.3 presents a summary of the obtained results.

3.1.1. Methods

In the ARCH project a deterministic seismic hazard model has been implemented to enable the representation of the geographical and physical extent of the ground motion produced by an earthquake. Figure 57 represents the workflow used in the ARCH DSS to generate deterministic ground motion maps for both real and user-defined events. The workflow can be summarized in three basic steps:

1. Characterization of the specific earthquake event under analysis: i.e. hypocenter location and characteristics of the seismogenic source (i.e. location and characteristics of faults or fault systems) that has generated the earthquake (for a historic event) or that might generate the earthquake (for user-defined scenarios); the magnitude of the energy that has been released (for a real event) or that can be potentially be released (for user-defined events);
2. Characterization of specific local site conditions, that might lead to amplification, i.e. to an increase in the size of the ground motion;
3. Selection and implementation of a Ground Motion Prediction Equation (GMPE), i.e. attenuation relations, describing how the earthquake ground motion decreases as the distance between the earthquake source and the site under analysis increases, while accounting for the possible amplification due to the ground propagation properties (point 2 above).

³⁹ An exhaustive overview is out of the scope of this report; several references of scientific journal paper and report are provided for the readers who might like to deepen the topic.

As for *Step 1*, i.e. the characterization of the specific earthquake event under analysis: in case of the occurrence of a real event, data are automatically collected and collated by the ARCH DSS. A web-service, developed through ObsPy toolbox [40], [41] gets the measured characteristics of the occurred earthquakes in near real-time; characteristics of seismic events with a magnitude greater than 3 and an epicenter located within (or close to) European countries are then stored in the ARCH DSS geodatabase. To this end, the system continuously polls the earthquake catalogues managed by the European Mediterranean Seismological Centre (EMSC) [42] and by the National Institute of Geophysics and Volcanology (INGV) [43] to obtain information according to the International Federation of Digital Seismograph Networks (FDSN) standard protocols [44]. For user-defined seismic event scenarios ARCH HArIS tool provides end-users with several geo-datasets (as described in Deliverable D4.3) to support them to appropriately select the characteristics of the simulated earthquake (e.g. the maximum historical event from a pertinent seismogenic source, or the maximum earthquake compatible with the known tectonic framework, etc.). These datasets, relating to both the Italian and the European territories, include representations of historic earthquakes [45],[46],[47], known seismogenic sources [48],[49], and probabilistic seismic hazard PSHA maps used as a reference in seismic design codes [50], [51], [52]. All the beforementioned datasets have been imported and embedded in ARCH DSS (e.g. Figure 58 and 60).

As far *Step 2*, i.e. as the characterization of the specific geological and geomorphological conditions of the territory under analysis is concerned, geodatabases, reporting the results of seismic microzoning studies [53] that provide spatial information about local effects related to geological and geotechnical conditions on ground motion (e.g., [54] [55]) and of hydrogeological hazards (landslides and floods) [56] are embedded in the ARCH DSS geodatabase. In particular, two different V_{S30} maps are included: worldwide topographic slopes [57],[58] that are also reported as a regional detail in the world map published by the US Geological Survey, USGS [59] and seismic soil classification of Italy obtained by terrain geomorphological classification integrated with a large amount of data obtained by seismic microzoning dataset [60].

Figure 56 represents the workflow adopted and built in the ARCH DSS hazard assessment module for the assessment of the deterministic ground shaking maps in Peak Ground Acceleration (PGA) using GMPE by [61] and for the PGA to I_{MCS} and I_{EMS98} conversion [62].

Step 3 requires the selection of a GMPE used in seismic hazard analysis to evaluate the expected level of ground shaking at any given site for the earthquake event de-fined in Step (1). The ground shaking can be described in term of the level of acceleration, velocity, and displacement of the earth's surface induced by the earthquake waves. As mentioned before, conventionally used shaking intensity measures IMs include, among others: Peak Ground Acceleration, PGA ; Peak Ground Velocity, PGV ; Peak Ground Dis-placement, PGD . The values of these IMs are generally provided as median values by GMPEs, with their associated uncertainty both due to the inherent randomness, referred to as aleatory variability, and to the epistemic uncertainty because of lack of knowledge.

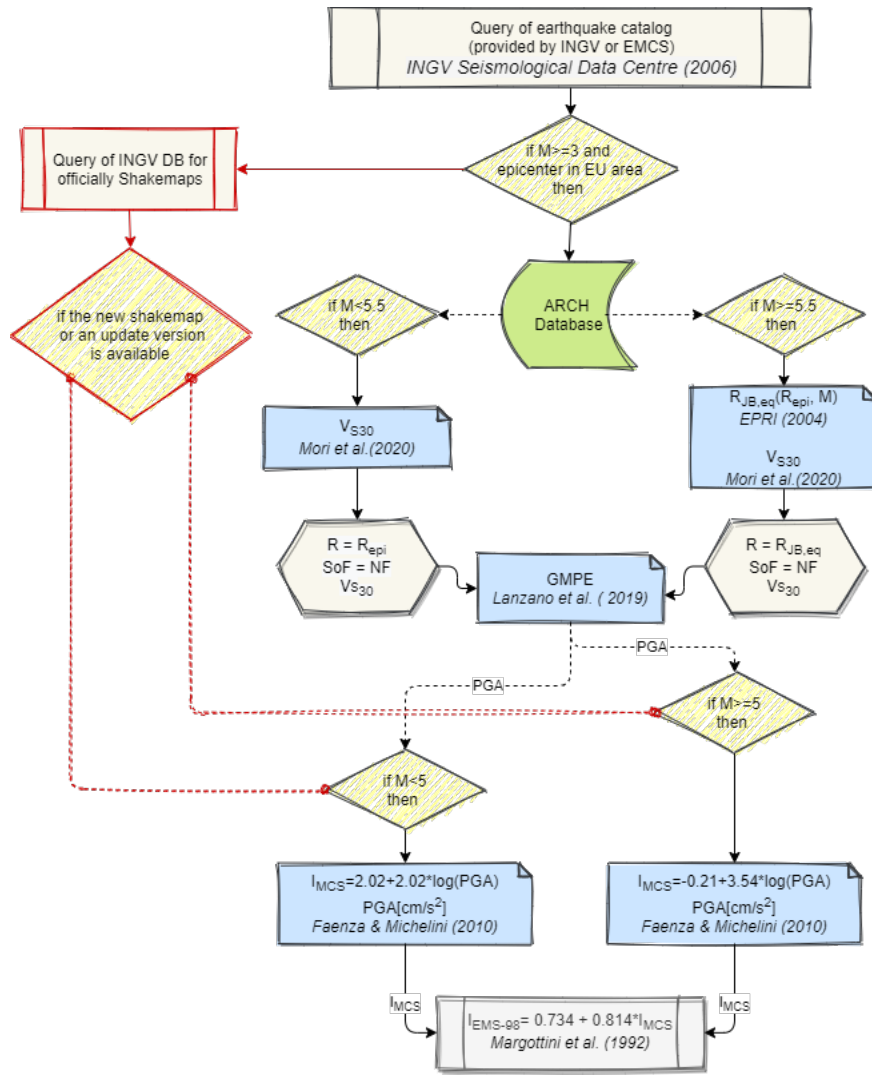


Figure 57. Workflow of ARCH DSS hazard assessment module: assessment of deterministic ground shaking maps in Peak Ground Acceleration (PGA) using GMPE by [61] and PGA to I_{MCS} and I_{EMS98} conversion [62].

The values of these IMs generated by depend on different characteristics and parameters as represented in Figure 55 and described in Equation 5, namely: moment magnitude, (M_w); style of faulting (SoF), i.e. main focal mechanism normal fault, thrust or strike-slip; distance from the site under analysis to the seismic source R that can be represented by point-source distance metrics such as hypocentral distance and epicentral distance or the rupture distance, i.e. the closest distance to an extended rupture of plane fault (RRup), or Joyner-Boore distance (RJB), i.e. the closest distance to the surface projection of an extended fault [53]; a simplified term representative of the site effects on the amplification of the ground motion (A), e.g. the average shear-wave velocity in the uppermost 30 m (V_{S30}), among others.

$$IMs = f(M_w, SoF, R, A) \quad (5)$$

In the current version of the ARCH DSS, the most recent GMPEs for the Italian territory have been implemented, namely [61], [63], [64] among others.

Once ground motion maps are assessed in terms of the shaking intensity measure PGAs, ground motion to intensity conversion equations are implemented in the ARCH DSS to obtain Macroseismic Intensity, I , maps. In particular, the relationship proposed by [56] allows to obtain Macroseismic Intensity estimation with regard to Mercalli-Cancani-Siberg Macroseismic Intensity scale I_{MCS} [65]. A further correlation [66] is applied to convert I_{MCS} to intensities measured according to the European Macroseismic Scale I_{EMS-98} [67] that is the official Macroseismic Intensity scale adopted in Europe.

3.1.2. Data

The Central area of Italy, where Camerino Municipality is located is highly seismically active (Figure 58). In 2016, this area experienced one of the most disruptive seismic sequence of recent time. The sequence started on August 24th, 2016, when an earthquake with a moment magnitude $M_w=6.0$, referred to as “*Amatrice earthquake*” and a hypocentral depth of 8 km, followed by an $M_w=5.4$ aftershock, caused 299 deaths and significant destruction of numerous towns and villages in Central Italy. On October 26th, two earthquakes ($M_w=5.4$ and $M_w=5.9$) occurred, in an adjacent area along Umbria and Marche region boundaries. The $M_w=5.9$ 26th October event is referred to as “*Visso earthquake*”. A further main shock of $M_w=6.5$ occurred on October the 30th in the Umbria region, referred to as “*Norcia earthquake*”. Strong earthquake sequences to the one experienced by Camerino in 2016 are not at all a novelty; earthquake sequences with very similar characteristics in term of the magnitude of the energy released, the location of the epicentre as well as the impacts caused to the population and built environment have stroke Camerino in the centuries as showed in Figure 59.

Five different earthquake events have been simulated for Camerino Municipality in the framework of the ARCH project: 4 real earthquake events and 1 user-defined event.

The 4 real events include 2 historical events and 2 more recent events whose data have been retrieved from the CPTI15-DBMI15 v3.0 Parametric Catalogues of Italian Earthquakes^{42,43} and from the DISS Database of Individual Seismogenic Sources respectively, both accessible through ARCH DSS (Figures 58 and 60), thanks to ad hoc embedded webservices.

For the 2 historical events the known ones that have been causing the stronger impacts in Camerino have been selected (Figure 59), namely:

- the *1279 Appenino umbro marchigiano earthquake* that stroke 30/04/1279 with a magnitude at the epicentre equal to $M_w=6.2$, causing in Camerino a macroseismic intensity $I=9$;
- the *1799 Appenino marchigiano earthquake* that stroke 28/07/1799 with a magnitude at the epicentre equal to $M_w=6.18$, causing in Camerino a macroseismic intensity $I=9$.

The Parametric Catalogues of Italian Earthquakes provides almost all the data needed for the implementation of a GMPE aiming to simulate a ground shaking maps; namely origin, time, location (epicentral coordinates) and magnitude of historical earthquakes as reported in Table 13. As for the hypocentre depth, it is unknown and has been therefore assumed to be equal to 5Km for both the events

The 2 recent earthquakes simulated:

- the *2016 Visso Earthquake* ($M_w=5.9$) that stroke 18/04/2016 causing in Camerino a macroseismic intensity $I=7.5$.

- the *2021 Fiordimonte Earthquake* (Mw=3.3) that stroke 26/10/2016 causing in Camerino a a macroseismic intensity I=2.4;

The selection of the 2 recent earthquakes has been motivated by the following reasons. The *2016 Visso earthquake* has been chosen as a case study for the seismic simulation over the cultural heritage in the HA of Camerino-San Severino. The choice has been motivated by the widespread damage caused to the cultural heritage buildings and cultural sites in the analysed area. Visso earthquake induced, in fact, the collapse of the tower of “Santa Maria in Via” church (already severely damaged by the previous earthquake events of the sequence) that is one of the focus points selected in the ARCH project by Camerino Municipality.

Table 13. Parameters defining the 5 earthquake events selected for the simulation of deterministic seismic hazard maps in Camerino

Simulation parameters:	2021 Fiordimonte	2016 Visso	1799 Appennino marchigiano	1279 Appennino umbro-marchigiano	Camerino-synth
References	INGV Shakemap ⁴⁰⁴¹	INGV Shakemap ⁴²	Historical Catalogue ⁴³	Historical Catalogue ⁴⁴	DISS – ID: ITIS049 ⁴⁵ Historical Catalogue ⁴⁶
Date and Time GMT	18/04/2021 17:25:59	26/10/2016 19:18:07	28/07/1799 22:05	30/04/1279 18:00	N/A
Mw	3.3	5.9	6.18	6.2	5.8*
Lat.	43.03	42.9087	43.193	43.093	43.093*
Lon.	13.09	13.1206	13.151	12.872	12.872*
Hypocentre Depth [km]	8.2	9.6	5*	5*	3*
GMPE	[61]	[61]	[61]	[61]	[61]
Output:Metric	PGA [%g]	PGA [%g]	PGA [%g]	PGA [%g]	PGA [%g]

*user-defined parameter

⁴⁰ <http://shakemap.rm.ingv.it/shake4/viewLeaflet.html?eventid=26473301>

⁴¹ <http://cnt.rm.ingv.it/event/26473301>

⁴² <http://shakemap.rm.ingv.it/shake4/viewLeaflet.html?eventid=8669321>

⁴³ https://emidius.mi.ingv.it/CPTI15-DBMI15/eq/17990728_2205_000

⁴⁴ https://emidius.mi.ingv.it/CPTI15-DBMI15/eq/12790430_1800_000

⁴⁵ http://diss.rm.ingv.it/dissnet/CadmoDriver?_action_do_single=1&_state=find&_token=NULLNULLNULLNULL&_tabber=0&_page=pGGSources_I&IDSource=ITIS049

⁴⁶ https://emidius.mi.ingv.it/CPTI15-DBMI15/eq/12790430_1800_000

The *2021 Fiordimonte earthquake* has been selected aiming to compare the resulting simulated shake maps with the shake maps recorded by INGV thanks to the urban seismic network installed in Camerino, as part of the ARCH project, and already fully operation at the time when the *2021 Fiordimonte earthquake* event stroke. The comparison between the ARCH DSS simulated shaking maps and the shaking maps obtained by the interpolation of the recorded accelerations by the Italian National Seismic Network^{40, 42} and by the Camerino Urban seismic network (limited to the Fiordimonte earthquake) will be discussed in the ASRCH deliverable D5.3.

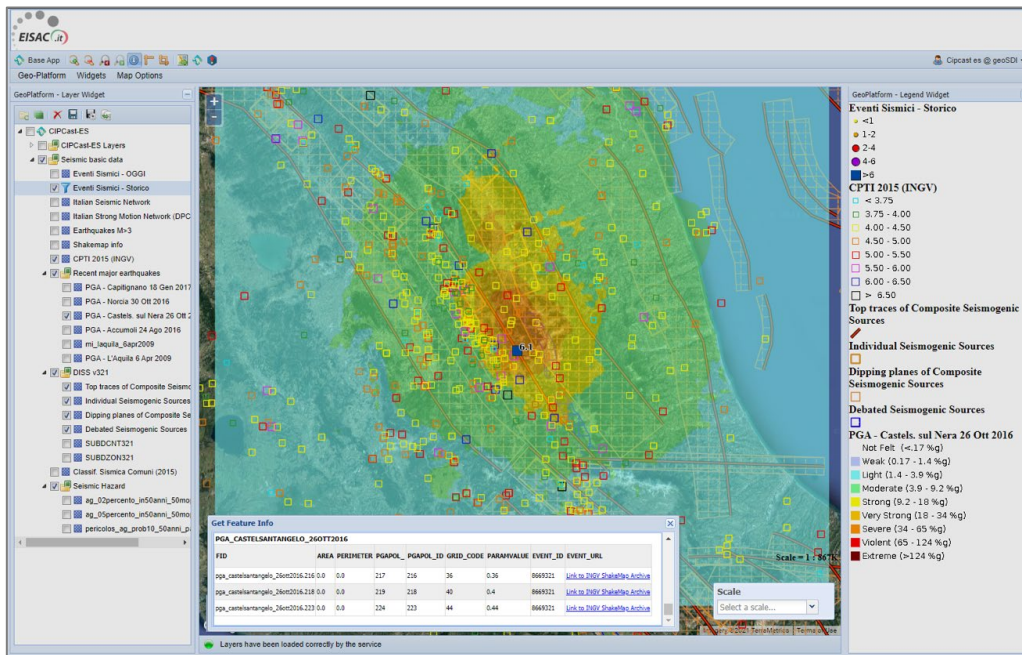


Figure 58. ARCH DSS screenshot representing data from DISS geodatabase of seismic sources and CPTI15-DBMI15 v3.0 Parametric Catalogues of Italian Earthquakes (for Mw>3 events);

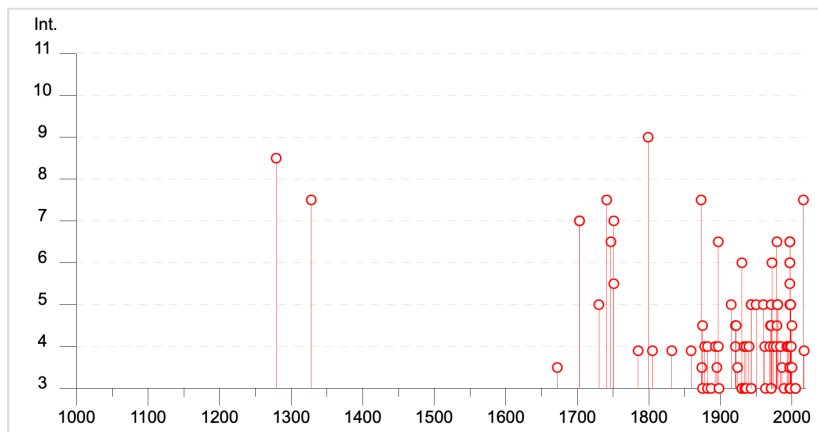


Figure 59. Diagram of known historical earthquakes that have affecting Camerino Municipality in the time range from 1000 to 2000 (source⁴⁷).

Finally 1 user-defined earthquake event, referred to in the following as *Camerino-synth* has been simulated; this aiming to define a realistic scenario, the parameters defining the

⁴⁷ https://emidius.mi.ingv.it/CPTI15-DBMI15/query_place/

earthquake event (i.e. epicentre coordinates; hypocentral depth; magnitude M_w and fault type) have been selected making reference to the faults and historical earthquakes identified in the surrounding of Camerino area (Figure 60 and Table 13).

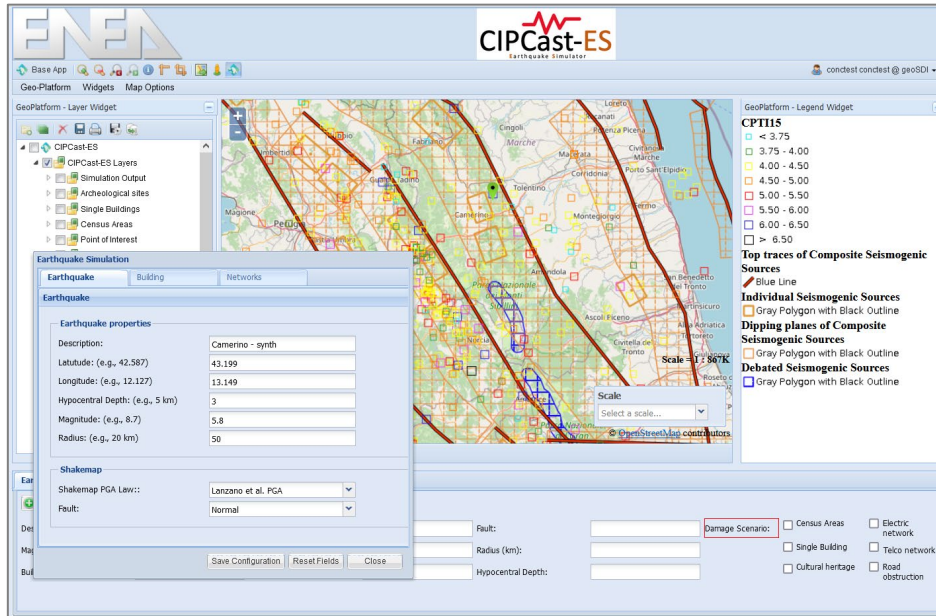


Figure 60. Definition of the earthquake event parameter for running the simulation of an end-user defined earthquake event referred to as “camerino-synth” (Table 13).

3.1.3. Results

ARCH DSS has been used to simulate, according to the methods introduced in Section 3.3.1, the ground shaking map generated by the 5 selected earthquake events (Table 13). As an example, Figure 61 shows the location of the epicenter of the user-defined earthquake event *Camerino-synth* while the simulation for the creation of the ground shaking map is running. Figure 62 shows the resulting ground shaking map for the *Camerino-synth* user-defined event highlighting a “very strong” to “severe” ground shaking expected for Camerino, i.e. about $PGA=28,8\%g=2.82m/s^2$. Figure 63 shows the resulting ground shaking map for the 2016 Visso earthquake event in term of PGA highlighting a “strong” to “very strong” ground shaking expected for Camerino, about $PGA=14.52\%g=1.42m/s^2$.

Appendix B includes the figures representing the resulting ground shaking maps for the further earthquake events simulated, namely; *2021 Fiordionte*; *1799 Appennino marchigiano*; and *1279 Appennino umbro-marchigiano*.

Table 14 reports the results obtained for Camerino in terms of PGA [%g] and [m/s^2]. As said in the introduction (Section 1) large uncertainties might affect hazard assessment processes. As such the results provided in Table 14 and in the following Figures have to be regarded just as indicative. A comparison of the obtained results with the ones recorded by the national and urban accelerometric networks (limited to the recent events are concerned i.e. *2021 Fiordimonte* and *2016 Visso*) is in progress and will be the subject of a scientific publication.

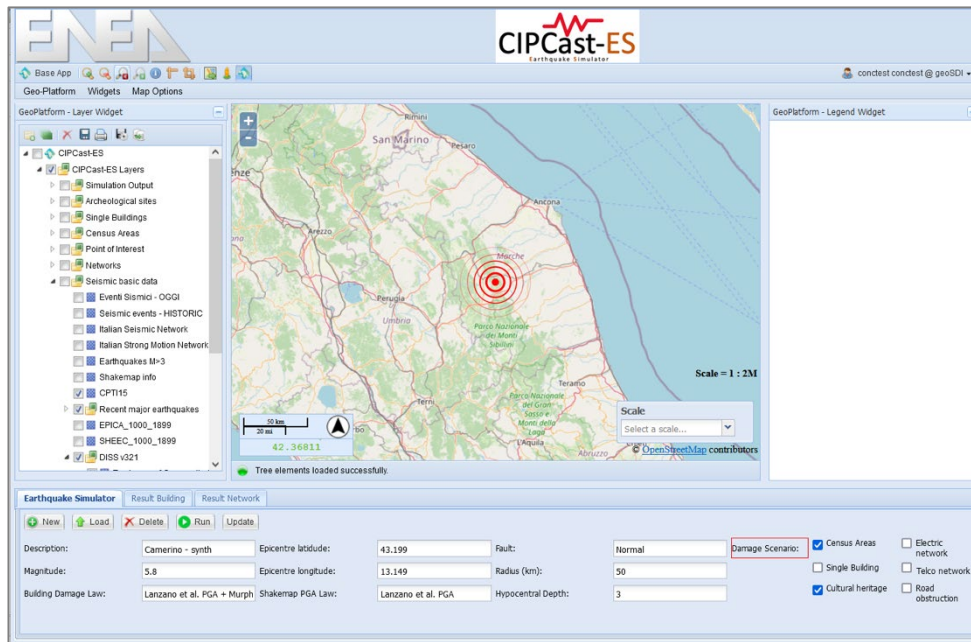


Figure 61. Screenshot of ARCH DSS while the simulation for producing ground shaking map for the “Camerino-synth” event is running.

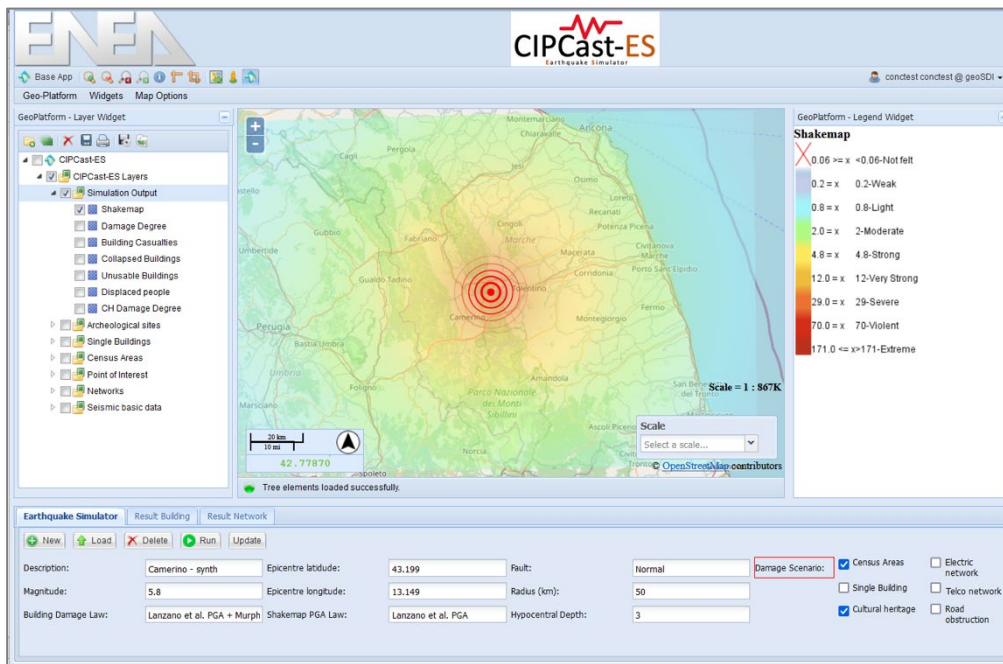


Figure 62. Screenshot of ARCH DSS resulting ground shaking map [%g] for the “Camerino-synth”.

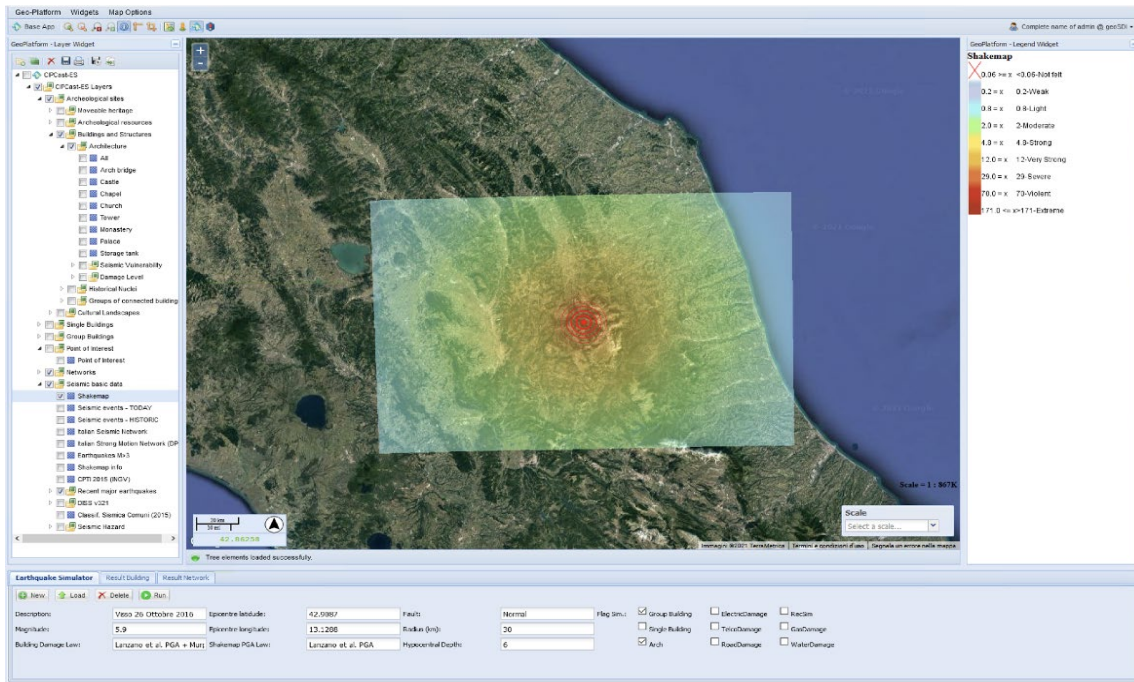


Figure 63. Ground-shaking map for the Visso Earthquake (PGA in [%g]) simulated using the ARCH DSS (26 October 2016, Mw=5.9, Lat 42,91 N, Long 13,13 E).

Table 13. Parameters defining the 5 earthquake events selected for the simulation of deterministic seismic hazard maps in Camerino

Earthquake event	ARCH DSS Simulated In Camerino* PGA[m/s^2]	ARCH DSS Simulated In Camerino* PGA[%g]	INGV shakemaps PGA[%g] in Camerino**
2021 Fiordimonte	0.25	2.61	0.5
2016 Visso	1.42	14.52	13.8
1799 Appennino marchigiano	3.32	33.92	N/A
1279 Appennino umbro-marchigiano	3.44	35.15	N/A
Camerino-synth	2.82	28.8	N/A

As reported in Section 3.1.1, in post-event emergency management and response circumstances simulated ground shaking maps can be substituted and/or integrated with the ground shake maps resulting from national or urban [68] accelerometric seismic networks as soon as they are made available by INGV. The availability of simulated maps from ARCH DSS for real event allows to have a very first overview on the potential extent and severity in the immediate aftermath of an earthquake the event (as INGV official map are made available usually around 45 minutes after the event); as an example these maps can allow to estimate immediately earthquake induced impacts on Camerino HAs and surrounding areas where

several MIBACT bound cultural heritage are identified (Figure 64). The assessment of impact scenarios will be part of D5.3; Figure 64 is provided here just as an example.

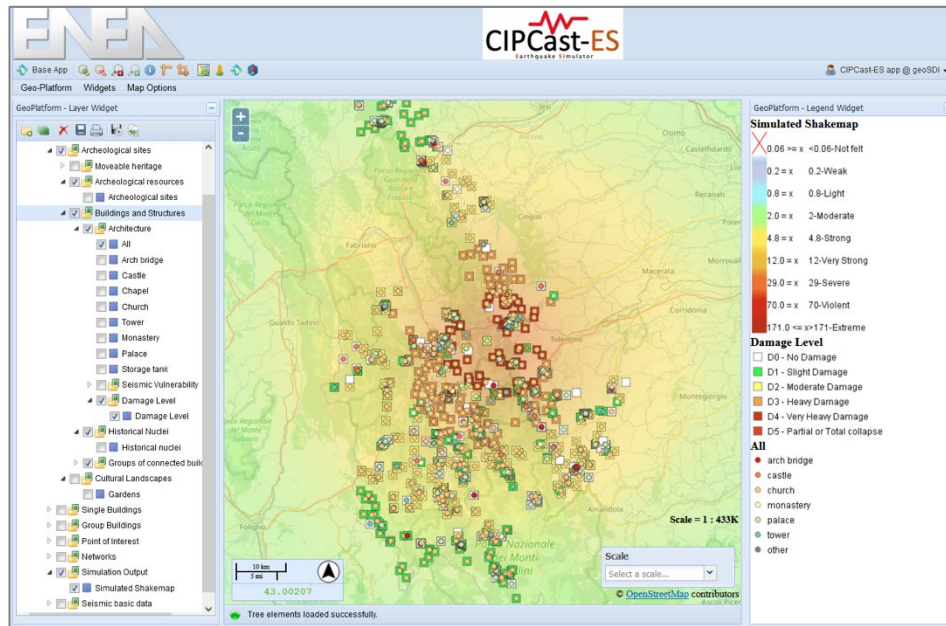


Figure 64. Simulated impact scenario by ARCH DSS induced by “camerino-synth” on the cultural heritage exposed asset in the Camerino-San Severino District.

3.2. Earthquake-induced landslide hazard models and maps for impact assessment

An Italian National Landslide Inventory (IFFI in Italian “*Inventario dei Fenomeni Franosi*”⁴⁸, is available in Italy providing a complete and homogeneous overview on the distribution of landslides happened (both historical and recent events) national wide, with regard to both the recording of information and mapping of the landslides. The IFFI Project was carried out by the Regions and Autonomous Provinces of Italy, in collaboration with the Soil Defence Department Geological Service of Italy of APAT (now in ISPRA). The Marche Region, where the Camerino Municipality is located, makes available the IFFI as Landslide WebGIS⁴⁹ freely accessible, providing on the regional cartographic basis, a detailed picture of the distribution of landslides within the regional territory. For the Marche Region, the data included in the IFFI and Marche Region WebGIS spam from the second half of the 90s to the early 2000s. The vector cartographic base displayed at the different scales derives from the information contained in the Regional Technical Map (CTR scale 1:1000), increasing the magnification level increases the level of detail of the representation, until the CTR is displayed in its printable version. Within the IFFI and Marche Landslide WebGIS the landslide phenomena are characterised and represented as follow:

- Collapse/Overturn (red);

⁴⁸ http://www.isprambiente.gov.it/site/it-IT/Pubblicazioni/Rapporti/Documenti/rapporto_2007_78.html

⁴⁹ <https://giscartografia.regione.marche.it/ProgettoIFFI/>

- Rotational/translational scrolling (yellow);
- Slow pouring (green);
- Quick pouring (light green);
- Complex (orange);
- Deep slope gravitational deformation, DGPV, in Italian “*Deformazione gravitativa profonda di versante*” (dotted orange).

Figure 65 represents a screenshot from the Marche Landslide WebGIS focussed in Camerino. The same set of data and information can be accessed and shared via the recently released (May 2021) ISPRA IdroGEO platform⁵⁰ (Figure 66).

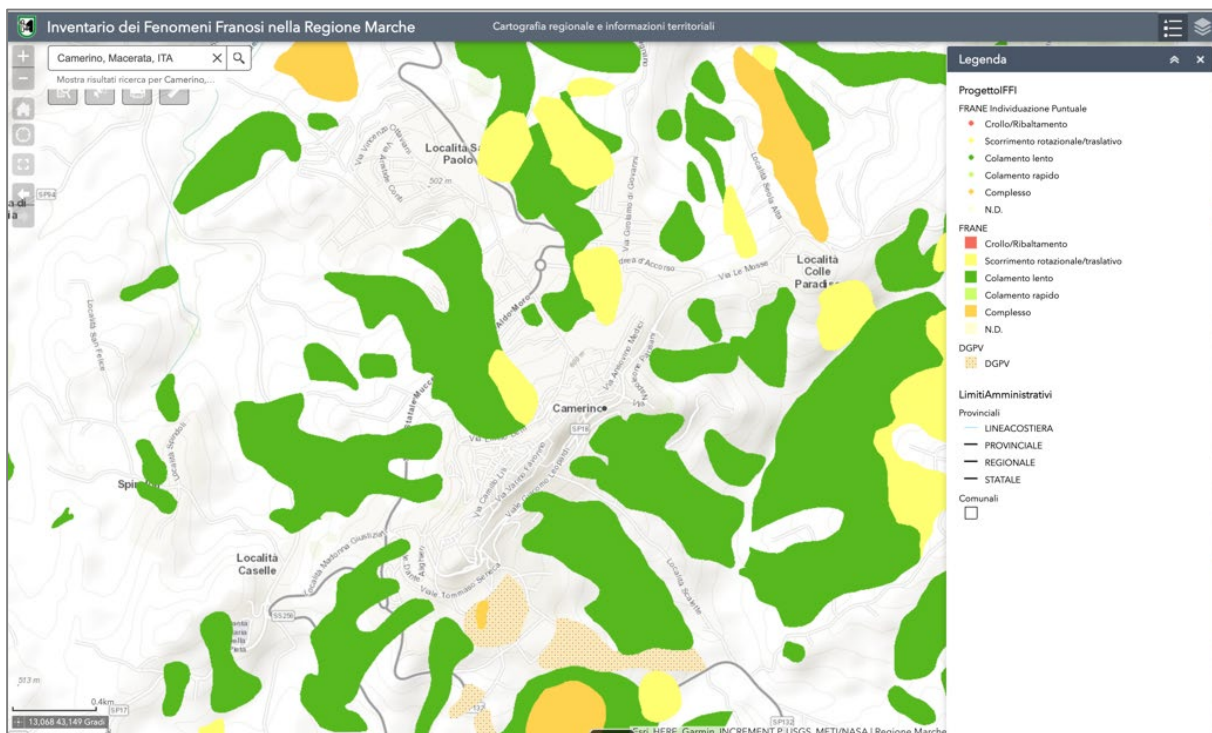


Figure 65. Landslide identified in Camerino according to the Italian National Landslide Inventory IFFI reported by Regione Marche Landslide Web GIS⁴⁹.

From Figure 65 and Figure 66 it is clear that the Historic Area (HA) of Camerino has been mainly interested by Rotational/translational scrolling (yellow) and Slow pouring (green) phenomena. A deep slope gravitational deformation, DGPV, can be noted in south-east area of Camerino HA.

These landslide phenomena, further to the HAs in itself are potentially affecting also the Landscape Asset (Beni Paesaggistici Vincolati) AV165, of Camerino bound by the MiBACT, Italy Ministry of Cultural Heritage and Activities and Tourism (MiBACT), as shown by a dedicated Landscape Asset webGIS available from Marche Region (Figure 67).

⁵⁰ <https://idrogeo.isprambiente.it/app/pir?@=42.55833077471979,19.281774108881752,0>

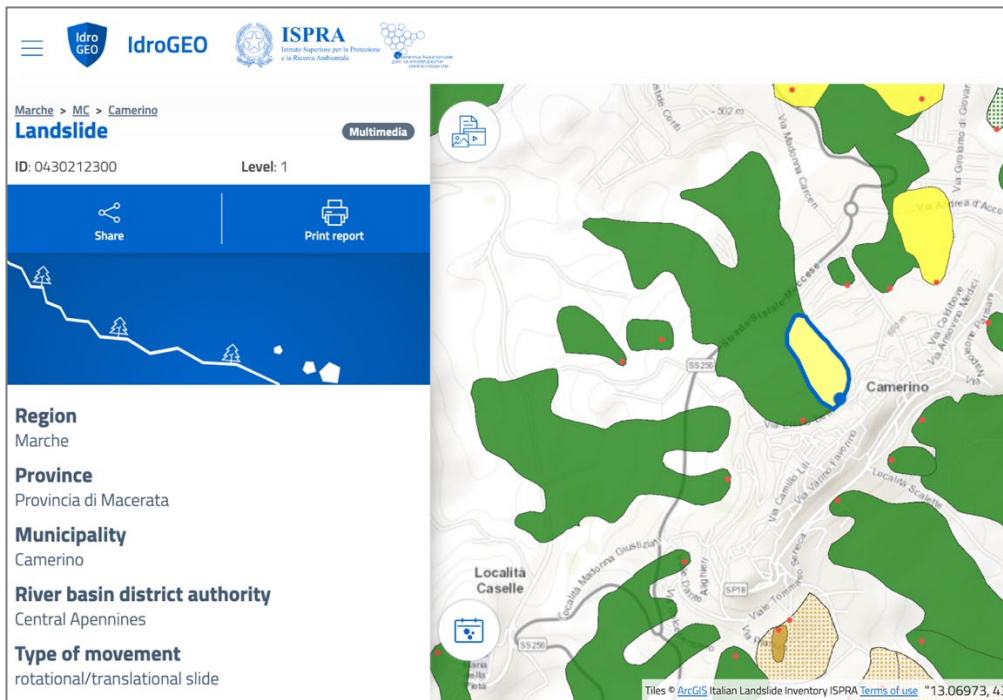


Figure 66. Landslide identified in Camerino according to the Italian National Landslide Inventory IFFI represented in the ISPRa IdroGEO platform⁵¹.

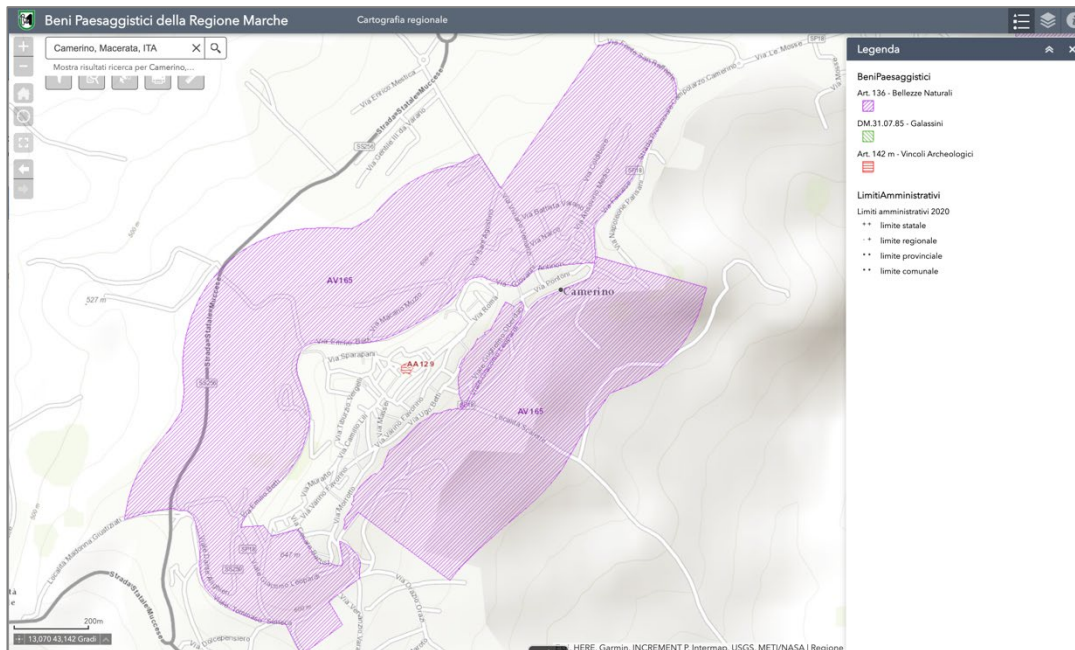


Figure 67. Protected Landscapes assets identified in the surrounding of Camerino historic area that is affected by different landslide phenomena as for Figure 65.

A Web Processing Service, WPS, i.e. an interoperable and interchange protocol for sharing geographical datasets⁵² is available for the IFFI Landslide Inventory; this has allowed to make

⁵¹ <https://idrogeo.isprambiente.it/app/pir?@=42.55833077471979,19.281774108881752,0>

⁵² In compliance with EU Directive 2007/2/EC INSPIRE (Infrastructure for Spatial Information in Europe)

the IFFI inventory available in the ARCH DSS prepared for Camerino Municipality in the framework of the ARCH project (Figure 68).



Figure 68. Landslide identified in Camerino and surrounding area according to the Italian National Landslide Inventory IFFI embedded in ARCH DSS.

This will allow the overlaying the information and data related to observed landslides phenomena with the exposure and vulnerability layers in order to assess potential impacts induced by these observed and still on-going landslide phenomena as part of Task 5.3. The results of these analysis will be included in deliverable D5.3.

It is worth highlighting, however, that the same Italian National Landslide Inventory IFFI has been included in the ReSTART⁵³, "Territorial Resilience of the Central Apennines Earthquake Reconstruction" technological platform (Figure 69) that has been created following the 2016-2017 earthquake sequence to provide a cognitive framework of natural phenomena in real time, in support of governance models for territorial planning. ReSTART aims to be usable by all municipalities and by anyone involved in the post-earthquake reconstruction activities. ReSTART has been conceived and realized by the *Central Apennine District Basin Authority* in collaboration with the affected Regions to make technical-scientific skills available to the Commissioner Structure for reconstruction, by providing an updated overview of the hydrogeological risk of the area towards a more resilient reconstruction.

⁵³ <https://www.restartgis.it/>



Figure 68. Landslide identified in Camerino and surrounding area according to the Italian National Landslide Inventory IFFI and represented in the ReSTART54 technological platform.

Further to the Italian National Landslide Inventory IFFI inventory providing the complete mapping of already ensued landslides, the Marche Region worked, in compliance with an institutional task required by the Italian Government, to define the landslide hazard areas aiming to inform the Hydrogeological Planning Plans (PAI). PAI landslide mapping targets the areas of possible evolution of landslide phenomena and areas potentially susceptible to new landslide phenomena. The adopted classification of the *Landslide Hazard* is common for the entire national territory according to hazard 5 classes, namely:

- P4, very high (red);
- P3, high (orange);
- P2, medium (yellow);
- P1 moderate (green); and
- AA attention areas

A WebGIS tool of the PAI (Figure 69) has been set by Marche Region and its freely accessible⁵⁵. From Figure 69 it can be inferred that the hazard level for all the landslide phenomena identified in Camerino has been judged as *P1*, i.e. *moderate* (green).

⁵⁴ <https://www.restartgis.it/>

⁵⁵ http://webgispcn.autoritabacino.marche.it/mapserverPCFS/viewer.php?BBOX=-1&winwidth=1629&winheight=980&sysrif=&service=../maps/rit_PA1-PS2006

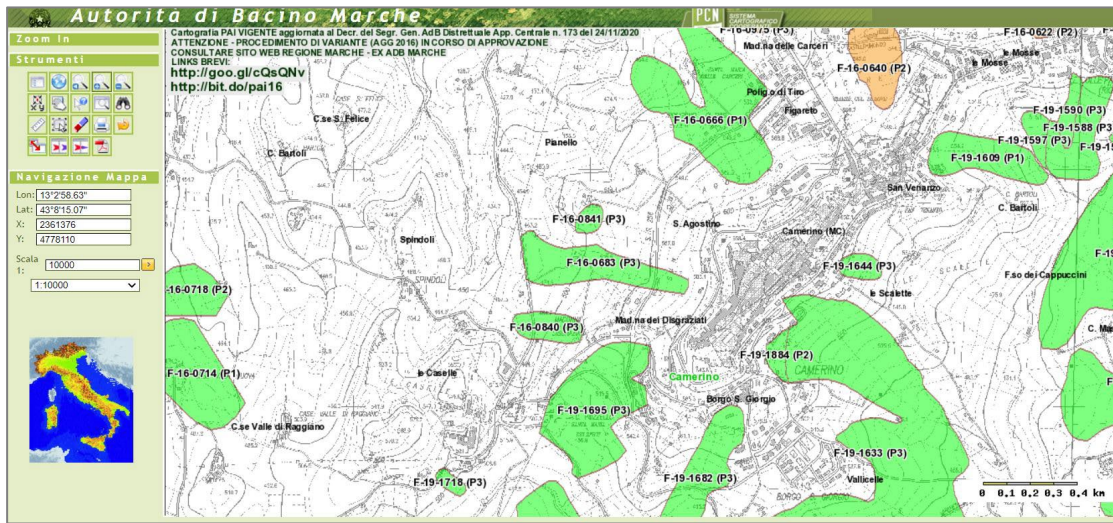


Figure 69. Landslide hazard in Camerino according to PAI WebGIS provided by Marche Region. ⁵¹

Similarly to what done for the IFFI Inventory, the PAI Marche inventory of landslide hazard as well as of landslide risk has been embedded in ARCH DSS thanks to the availability of an ad-hoc WPS, Web Processing Service. Figure 70 shows in fact the Marche PAI included in ARCH DSS.

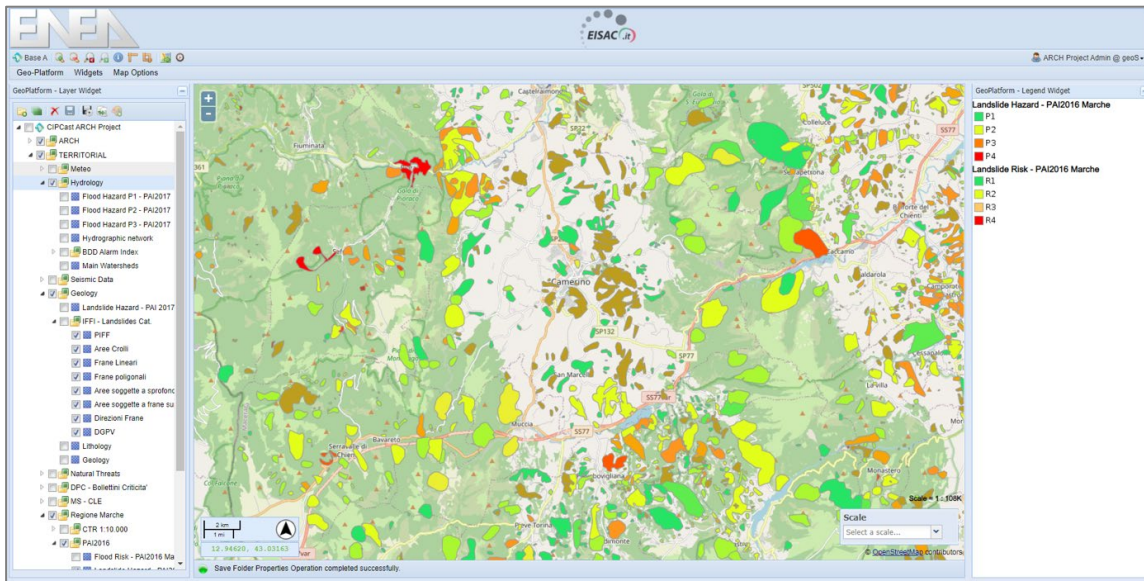


Figure 70. ARCH DSS: Landslide hazard and Landslide risk identified in Camerino and surrounding area according to PAI2016 Marche.

The PAI inventory of landslide hazard and risk has been included also in the ISPRA IdroGEO platform⁵⁶ (Figure 71) that provides a count of the asset exposed to the landslide risk, e.g. for Camerino: an area of the territory equal to 129.88km²; 3092 families for a total of 6902 people; 2904 buildings; 661 industries and services; and 341 cultural buildings.

⁵⁶ <https://idrogeo.isprambiente.it/app/pir?@=42.55833077471979,19.281774108881752,0>

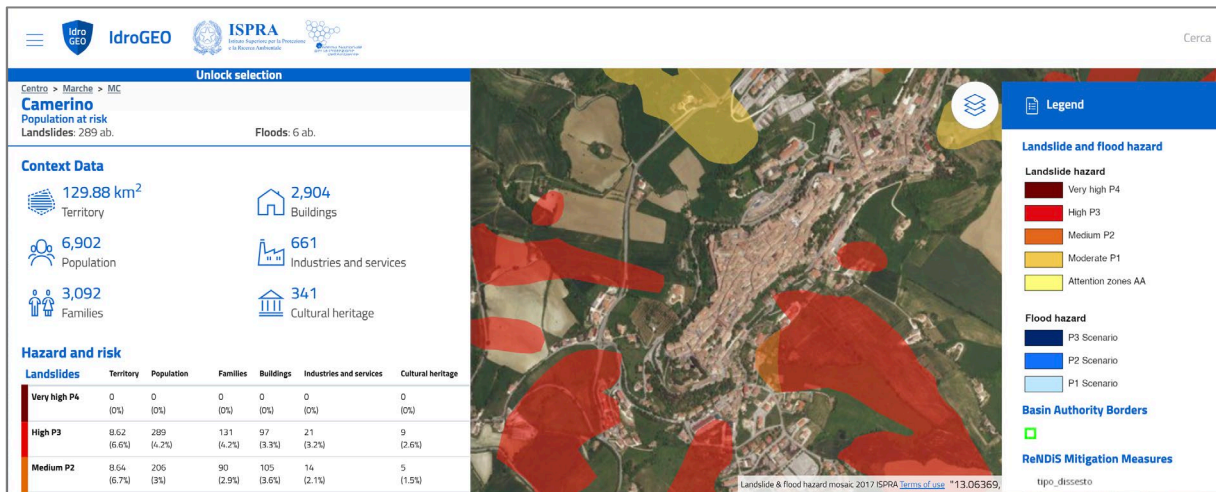


Figure 70. Landslide hazard and Landslide risk identified in Camerino and surrounding area according to the ISPRa IdroGEO platform⁵⁹.

As a further steps as part of Task 5.3 the potential for earthquake-induced ground failures and landslides for the 5 simulated earthquake scenarios (Section 3.1) and their possible impacts on the population and built environment, with special focus to the cultural heritage patrimony of Camerino HA and surrounding cultural districts will be implemented by combining the data from both the IFFI and PAI inventory acquired in ARCH DSS with the simulated ground shaking maps. This is indeed a risk to be estimated and accounted for considering all what presented above and the occurrences that have been already observed. As a matter of fact, the Italian catalogue of *Earthquake-induced Ground Failures*, *CEDIT*⁵⁷, indicated that the September-October, 1997 produced earthquake-induced ground changes in Camerino (Figure 71).

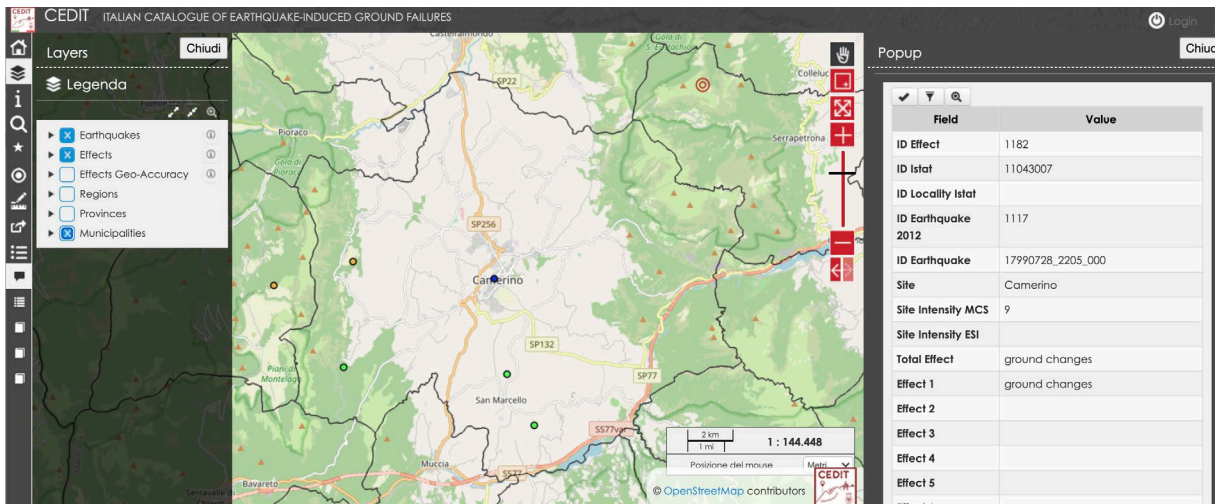


Figure 71. Italian catalogue of *Earthquake-induced Ground Failures*, *CEDIT*⁵⁸ reporting on earthquake-induced ground changes in Camerino

⁵⁷ <https://gdb.ceri.uniroma1.it/index.php/view/>

3.3. Earthquake-induced Soil-structure interaction: Hazard models and maps for

The interaction between soil and housing structures in a predefined area can be evaluated and in some ways quantified, using the most detailed maps possible of parameters and indices that are present, with different weights, in the building design formulas.

The predisposition of the buildings to being damaged by earthquakes, depending on several aspects, which regard the typology and construction methods, the quality of materials, the maintenance, and adaptation intervention. All these information can be collected in the HARIS database. In the dynamic behaviour of a building, another important role is played by the foundation site; indeed, the local geomorphological and geo-structural setting may produce relevant amplification phenomena on the ground motion, with an increase of the shaking level. This phenomenon, also known as site response, is mainly due to the focalization of the seismic energy during the transfer from the deep soils to the soft superficial ones [e.g. 68]. These amplification effects are able to induce significant amplifications in the ground motion on small distances such as within urban areas or historic centres [69-74].

The understanding of these local phenomena with effects on the ground motion is extremely important to assess the expected damage level at the urban scale. With this awareness, on one side the RUSN (Real-Time Seismic Network) was deployed in Camerino (cf. D4.1 [75]) to record the shaking level on different sites of the historic centre when an earthquake occurs and produce shaking maps which take into account the local amplifications [68] - method and results are illustrated in D4.3 [77]. On the other side, the geo-structural setting of the hill was investigated with geophysical techniques in order to improve its knowledge and then, the *a priori* evaluation of the potential effects on the ground motion. In fact, the geological setting of the site was previously analysed for the elaboration of the three levels of Seismic Microzonation (SM), after the 2016-2017 central Italy seismic sequence. Furthermore, the velocity map of the seismic Primary waves (V_P) was elaborated exploiting an electrical resistivity map obtained through deep geophysical prospecting (3D electrical tomography) [78],[79]. The correlation between P wave velocity and electrical resistivity values was obtained using the well-known Faust equation (first time in complex and urban contexts). The resulting seismic wave velocity map will serve as a basis for future applications and research developments.

3.3.1. Seismic Microzonation (SM): methods and results

Seismic Microzonation (SM) is a key tool for planning strategies for risk mitigation; it represents the assessment of Local Seismic Hazard by identifying and mapping, at scale 1:10.000 or higher, zones with homogeneous seismic behaviour within a given geographic area. SM studies are complementary to the Regional Seismic Hazard (RSH) studies, which calculate with probabilistic and deterministic methods ground motion parameters at a site under conditions of rigid and flat soil (NTC 08). In the 2008, the Conference of Regions and Autonomous Provinces of Italy and the Civil Protection Department published the “*Guidelines for Seismic Microzonation*”⁵⁹ (2015) that are in Italy is a national reference document for

⁵⁹ <https://www.centromicrozonazioneismica.it/it/download/category/9-guidelines-for-seismic-microzonation>

studies to estimate the seismic risk of a territory. The seismic microzonation (SM) identifying zones with homogeneous seismic behaviour. The identified microzones are classified basing on the expected local ground motion in case of earthquake, and are subdivided into:

- *stable zones*, where no substantial deviations are expected from the ground motion produced by a seismic event on rigid and flat soils;
- *stable zones prone to local amplification*, where ground motion is amplified because of local stratigraphic and morphological conditions;
- *instability-prone zones*, where permanent instabilities, slope instability, liquefaction, differential settlement, active and capable faults, are expected.

Three levels for SM studies of increasing complexity are determined.

- *Level 1*: it consists of a collection of existing data that are processed to divide the investigated area into qualitatively homogeneous Microzones. This level of analysis is a preparatory level for the next levels and only in some cases can be considered exhaustive. The result of Level 1 is the Map of Seismically Homogeneous Microzones at scale of 1:5000 – 1:10000.

- *Level 2*: in this level, insights for the uncertainties identified in the Level 1, are conducted, and quantitative elements associated with the homogeneous zones are introduced. The quantitative elements are amplification factors, calculated with simplified methods (schedules and empirical laws). The result of this Level is the Seismic Microzonation Map at scale of 1:5000 – 1:10000.

- *Level 3*: it represents the level of maximum detail that should be applied 1) to stable zones prone to local amplification (under complex geological and geotechnical conditions) when problems cannot be solved using the aforementioned schedules, when a global detailed analysis may be useful, for buildings or structures of particular importance and strategic function, and 2) to zones prone to particularly severe instabilities owing to the complexity of phenomenon and/or to their local widespread character. The results are amplification factors calculated by quantitative numerical methods (response spectra, acceleration) for each stable zones prone to local amplification, and indexes of instability for each instability-prone zones. The product of this Level is the Detailed Seismic Microzonation Map covering particular issues or areas at suggested higher scale ($\geq 1:5000$).

The products of the Seismic Microzonation in Camerino (Figure 72) are all available for download as raster maps⁶⁰ as well as the technical report that illustrates the obtained results⁶¹. All the SM maps have been imported in ARCH tools THIS and ARCH DSS (Figure 73) since they represent a key source for estimating amplification of ground motion, possible resonance effects and soil-structure interaction phenomena that will be estimated in D5.3.

⁶⁰ <https://www.comune.camerino.mc.it/documenti-cms/microzonazione-sismica-di-livello-3-del-comune-di-camerino-ai-sensi-dellordinanza-del-commissario-straordinario-n-24/?a=>

⁶¹ <https://www.comune.camerino.mc.it/wp-content/blogs.dir/11/files/RELAZIONE-MS3-Camerino-REV-2.pdf>

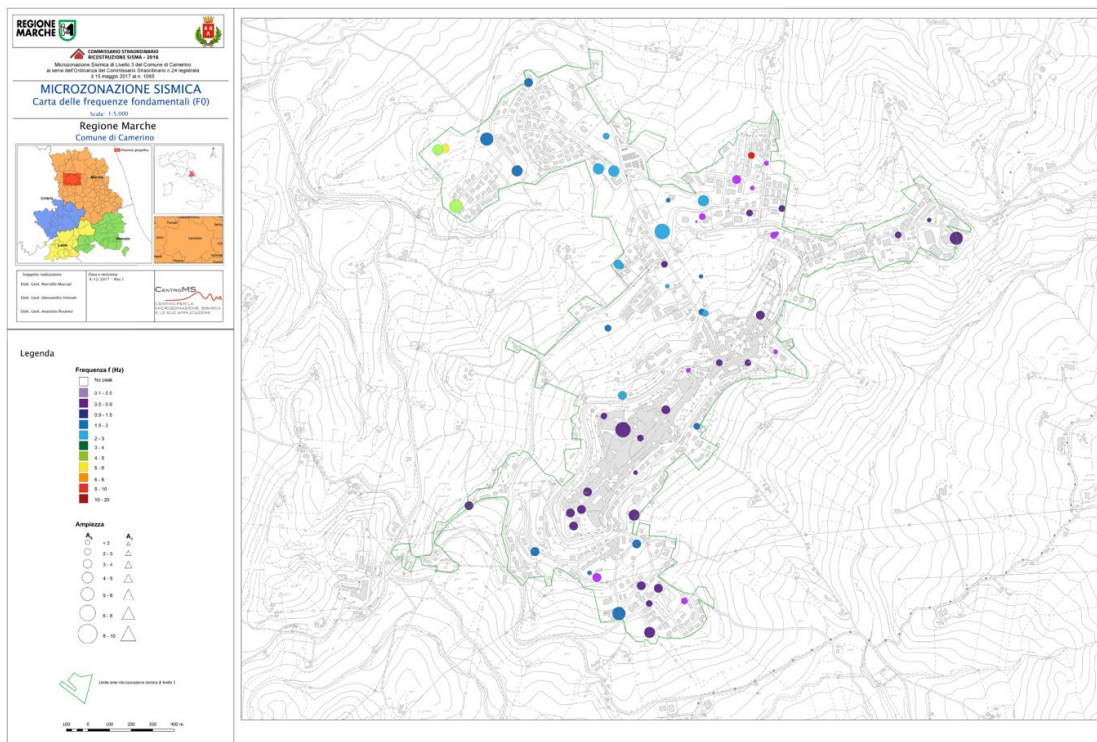
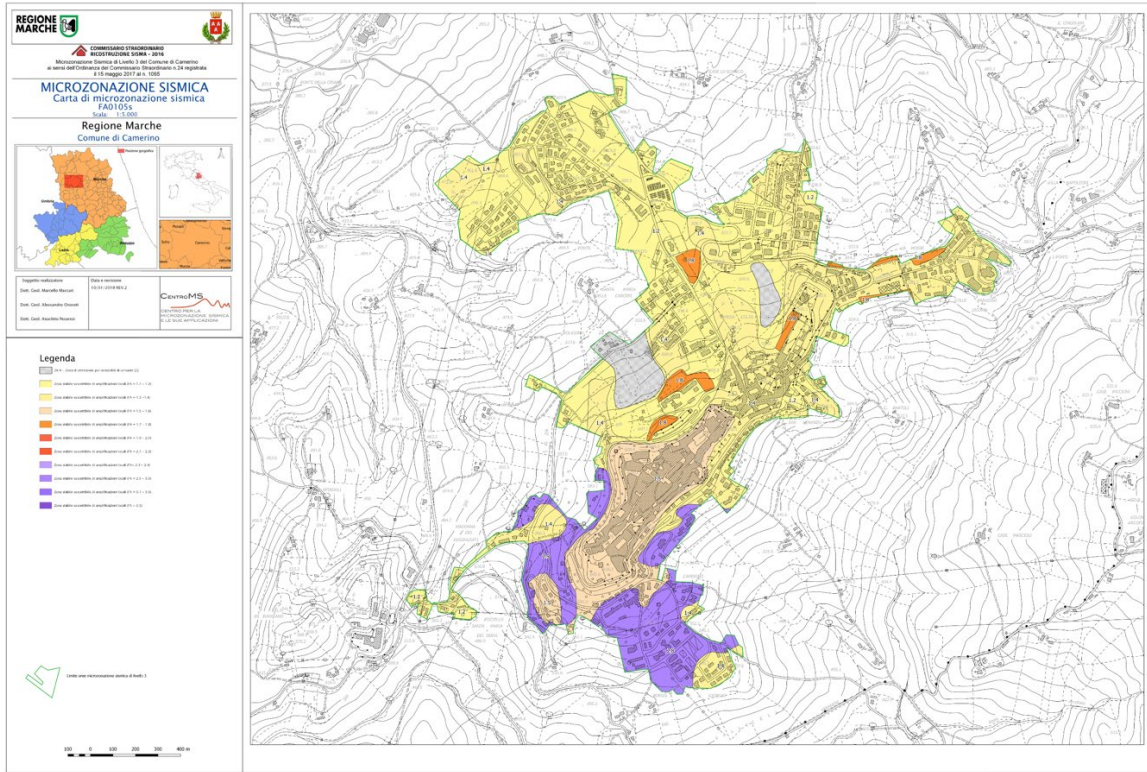
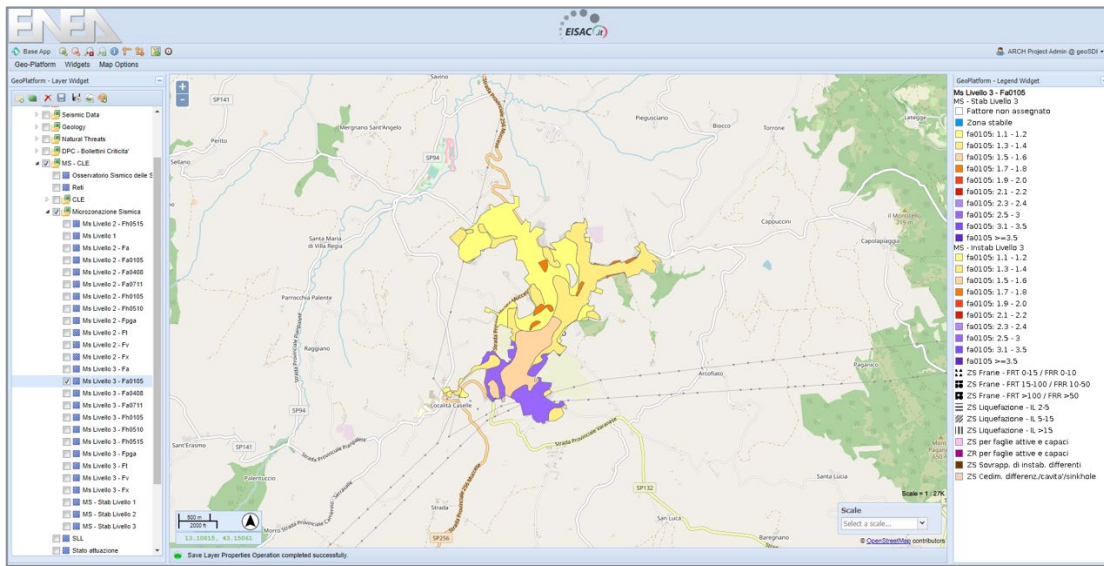


Figure 72. Example of the Seismic Microzonation available for the historic centre of Camerino.



ge 0.1-

Figure 73. ARCH DSS Map of the fundamental frequencies obtained on (and around) the historic centre of Camerino (after Seismic Microzonation [8])

3.3.2. Geophysical investigation: methods and results for Camerino Municipality hill

The characterization of the geological bedrock was realized by carrying out geophysical prospecting and in particular a 3D electrical tomography. For this purpose, the Fullwaver device of the IRIS Instruments company, specific for deep investigation, was used (Figure 74).



Figure 74. The Fullwaver equipment: example of receiver (left) and of an injection station.

More in particular, the Fullwaver devices have been designed for the measurement of resistivity on large 3D surfaces which can be affected by sharp topography. Depending on the size of the area to investigate, 10 or more devices can be randomly located on the surface of the investigation, performing a continuous measurement; each device an acquisition system is associated with three electrodes (P1-P2-P3) constituting the electric dipoles. In the meantime, the operator moves a transmitter (typically VIP) and the Fullwaver on the same surface, to perform a different injection. In the present study, 19 points with injection electrodes (TX-1 to TX-19) were defined and 15 receivers (RX-1 to RX-15) were positioned (Figure 76).

in a future step once the empirical data have been calibrated with those resulting from the in situ analyses.

3.3.2.2. Data: resistivity values and their representation through 3D models

The results of the acquisition are shown in Figure 77. The 3D resistivity model elaborated, agrees quite faithfully with the proposed geological model.

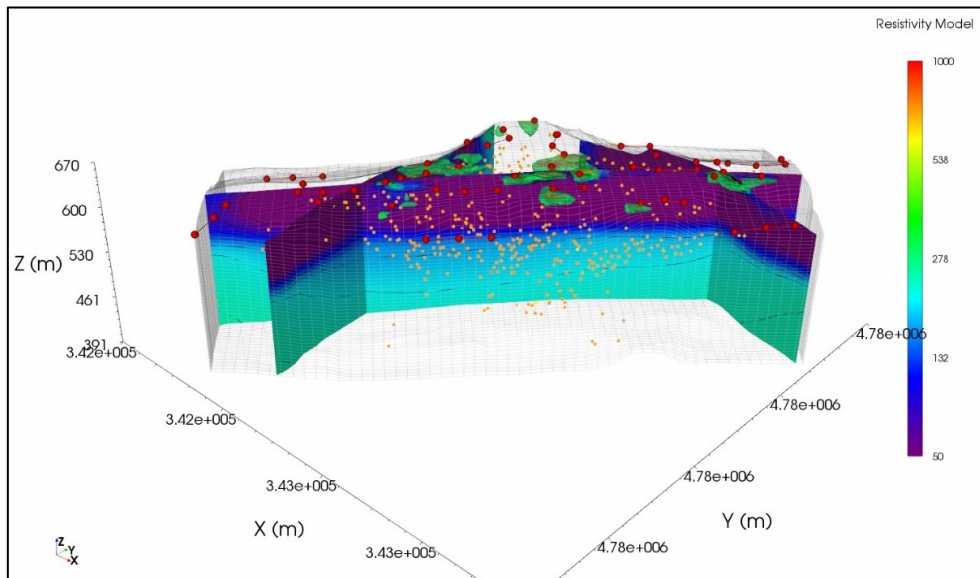


Figure 77. 3D electrical tomography: resistivity model of the study area (values of resistivity expressed in term of [Ωm])

As can be seen from the image, the almost tabular setting of the bedrock appears very evident; the progressively increasing resistivity values with depth (from 50 [Ωm] – purple, to 150-200 [Ωm] - light blue) agree with the lithotypes observed, which pass from arenaceous and pelitic-arenaceous to marly and marly-calcareous. Nevertheless, the presence, at variable depths, of areas with higher resistivity (around 300 [Ωm]) within the arenaceous-pelitic and pelitic lithotypes, perhaps associated with voids and cavities, should be fully understood.

Even more interesting indications come from the analysis of the resistivity values recorded in the first meters below the buildings. Through processing in a GIS environment, it was possible to extract a 2D slice interpolated at around 10-15m below the surface (Figure 78).

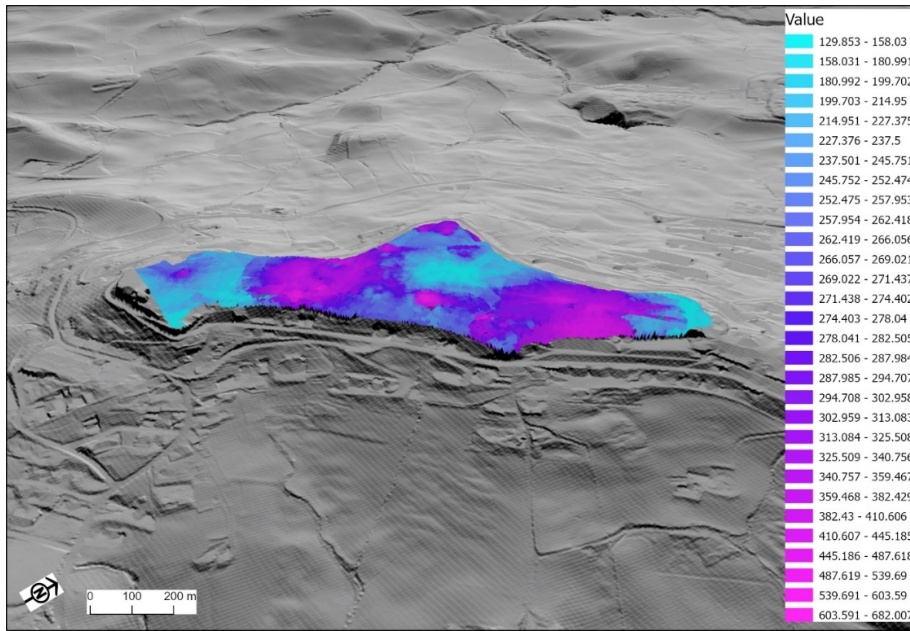


Figure 78. 2D slice extracted from the model and showing the values of resistivity [Ωm] at around 10-15m of depth.

The image clearly shows how strong lateral variations in resistivity exist at this depth, with values ranging between 130 and 600 [Ωm].

3.3.3. Results: P-wave velocity maps

By starting from the resistivity map described above, Faust's formula was then applied to obtain a map of the P-waves velocities [ft/s] for the entire area of the historic centre of Camerino. By default, the values of KR1-3 have been chosen respectively 3000, 6 and 6. The results, processed in a GIS environment using the ArcGIS Pro software (licensed by ESRI), are illustrated in Figure 79.

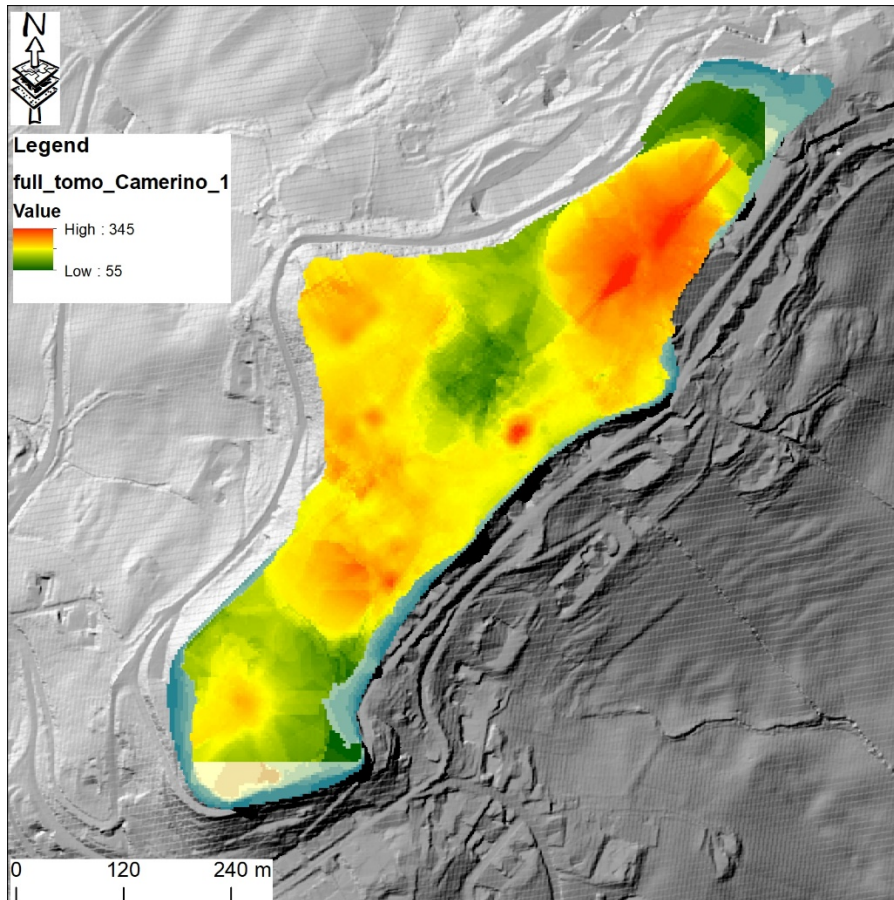


Figure 79. Map of the P-waves velocities [ft/s] resulting from the application of the methodology above described.

As previously mentioned, the next step will be to calibrate the results obtained by implementing Faust Equation with the ones resulting from in situ measurements via traditional instruments and to integrate them with the results obtained by the SM studies available for Camerino (Section 3.3.1) and the evidence from the signals recorded by the urban seismic network installed by INGV in the framework of the ARCH project [68].

4. References

- [1] White, G., F., (1973), Natural hazards research. In Directions in Geography, Methuen and Co., London, Methuen and Co., London, UK, 193-216.
- [2] UNDRO, (1980) Natural disasters and vulnerability analysis : report of Expert Group Meeting, 9-12 July 1979.
- [3] Cardona, O.D., M.K. van Aalst, J. Birkmann, M. Fordham, G. McGregor, R. Perez, R.S. Pulwarty, E.L.F. Schipper, and B.T. Sinh, (2012), Determinants of risk: exposure and vulnerability. In: Managing the Risks of Extreme Events and Disasters to Advance Climate Change Adaptation. A Special Report of Working Groups I and II of the Intergovernmental Panel on Climate Change (IPCC). Cambridge University Press, Cambridge, UK, and New York, NY, USA, 65-108..
- [4] UNDHA, (1992), Internationally agreed glossary of basic terms relating to disaster management. UNDHA, Geneva, Switzerland.

- [5] Birkmann, J., (2006), Measuring vulnerability to promote disaster-resilient societies: conceptual frameworks and definitions. In: *Measuring Vulnerability to Natural Hazards: Towards Disaster Resilient Societies*. United Nations University Press, Tokyo, Japan, 9-54
- [6] Lavell, A., M. Oppenheimer, C. Diop, J. Hess, R. Lempert, J. Li, R. Muir-Wood, and S. Myeong, (2012) Climate change: new dimensions in disaster risk, exposure, vulnerability, and resilience. In: *Managing the Risks of Extreme Events and Disasters to Advance Climate Change Adaptation. A Special Report of Working Groups I and II of the Intergovernmental Panel on Climate Change (IPCC)*. Cambridge University Press, Cambridge, UK, and New York, NY, USA, 25-64.
- [7] IPCC (2014), Summary for Policymakers. *Climate Change 2014: Impacts, Adaptation, and Vulnerability. Part A: Global and Sectoral Aspects. Contribution of Working Group II to the Fifth Assessment Report of the Intergovernmental Panel on Climate*
- [8] Mysiak, J., Torresan, S., Bosello, F., Mistry, M., Amadio, M., Marzi, S., Furlan, E., & Sperotto, A. (2018), Climate risk index for Italy. *Philosophical transactions. Series A, Mathematical, physical, and engineering sciences*, 376(2121). <https://doi.org/10.1098/rsta.2017.0305>
- [9] Ouzeau, G., Soubeyroux, J.-M., Schneider, S., Vautard, R. and Planton, S. (2016) Heat waves analysis over France in present and future climate: Application of a new method on the EURO-CORDEX ensemble. *Climate Services*, 4, 1-12.
- [10] Charron (2016), A guidebook on climate scenarios. Using climate information to guide adaptation research and decisions. Ouranos, Quebec. www.ouranos.ca.
- [11] Peres, D. J., Senatore, A., Nanni, P., Cancelliere, A. and Mendicino, G. (2020) Evaluation of EURO-CORDEX (Coordinated Regional Climate Downscaling Experiment for the Euro-Mediterranean area) historical simulations by high-quality observational datasets in southern Italy: insights on drought assessment. *Natural Hazards and Earth System Science*, 20, 3057-3082.
- [12] Cattiaux, J., Douville, H. and Peings, Y. (2013) European temperatures in CMIP5: origins of present-day biases and future uncertainties. *Climate Dynamics*, 41, 2889-2907.
- [13] Patel, M., Kok, K. and Rothman, D.S. Participatory scenario construction in land use analysis: An insight into the experiences created by stakeholder involvement in the Northern Mediterranean. *Land Use Policy*, 24, 546-561.
- [14] Rothfusz, L.P. (1990) The Heat Index "Equation" or, More Than You Ever Wanted to Know About Heat Index". Technical attachment, SR 90-23, 1990. http://www.srh.noaa.gov/images/ffc/pdf/ta_htindx.PDF.
- [15] Murage, P., Hajat, S. and Kovats, R.S. (2017) Effect of night-time temperatures on cause and age-specific mortality in London. *Environmental Epidemiology*, 1, 1-7.
- [16] Lücknerath, D., Streberova, E., Bogen, M., Rome, E., Ullrich, E. and Pauditsova, E. (2020) Climate Change Impact and Vulnerability Analysis in the City of Bratislava: Application and Lessons Learned. In *Critical Information Infrastructures Security. CRITIS 2019. Lecture Notes in Computer Sciences, Volume 11777*. Springer.
- [17] Yang, X., Grönlund, A. and Tanzilli, S. (2002) Predicting Flood Inundation and Risk Using Geographic Information System and Hydrodynamic Model,. *Geographic Information Sciences*, 8, 48-57.
- [18] Filipova, V., Rana, A. and Singh, P. (2012) Urban flooding in Gothenburg - A Mike 21 Study. In *Journal of Water Management and Research*, Volume 68. pp. 175-184.
- [19] DHI (2017) MIKE 21 Flow Model & MIKE 21 Flood Screening Tool. Hydrodynamic Module Scientific Documentation.
- [20] Copernicus Land Monitoring Service, (2018) Urban Atlas 201. Available at: 2018. <https://land.copernicus.eu/local/urban-atlas/urban-atlas-2018>.
- [21] Papaioannou, G., Efstratiadis, A., Vasiliades, L., Loukas, A., Papalexiou, S.M., Koukouvinos, A., et al. (2018) An Operational Method for Flood Directive Implementation in Ungauged Urban Areas. *Hydrology*, 5, 1-23.

- [22] Neris, J., Tejedor, M., Rodríguez, M., Fuentes, J. and Jiménez, C (2013) Effect of forest floor characteristics on water repellency, infiltration, runoff and soil loss in Andisols of Tenerife (Canary Islands, Spain). *CATENA*, 108, 50-57.
- [23] Shukla, M.K., Lal, R., Owens, L.B. and Unkefer, P. (2012) Land use and management impacts on structure and infiltration characteristics of soils in the North Appalachian region of Ohio. *Soil Science*, 168, 167-177.
- [24] Wang, G., Fang, Q., Wu, B., Yang., H. and Xu, Z. (2015) Relationship between soil erodibility and modeled infiltration rate in different soils. *Journal of Hydrology*, 528, 408-418.
- [25] Richter C. F. (1935) An instrumental earthquake scale, *Bulletin of the Seismological Society of America*. (25) 1-32.
- [26] Federal Emergency Management Agency (FEMA) HAZUS99 Technical Manual; Service Release 2; FEMA: Washington, DC, USA, 2001.
- [27] Newman, J.P.; Maier, H.R.; Riddell, G.A.; Zecchin, A.; Daniell, J.E.; Schaefer, A.M.; van Delden, H.; Khazai, B.; O’Flaherty, M.J.; Newland, C.P. (2017) Review of literature on decision support systems for natural hazard risk reduction: Current status and future research directions. *Environ. Model. Softw.*, 96, 378–409.
- [28] Matassoni, L.; Fiaschi, A.; Giovinazzi, S.; Pollino, M.; La Porta, L.; Rosato, V. (2017) A geospatial decision support tool for seismic risk management: Florence (Italy) case study. In *Computational Science and Its Applications—ICCSA 2017; Lecture Notes in Computer Science, Part II, LNCS 10405*; Springer International Publishing: Cham, Switzerland, 2017; pp. 278–293.
- [29] Bocchini, G.M.; Pomonis, A.; So, E.; King, A.B.; Giovinazzi, S. The GEM Earthquake Consequences Database and New Zealand’s Contributions (2014) NZSEE Conference. Available online: https://www.researchgate.net/publication/283934626_The_GEM_earthquake_consequences_database_and_New_Zealand\T1\textquoterights_contributions (accessed on 17 February 2021).
- [30] Vecere, A.; Monteiro, R.; Ammann, W.J.; Giovinazzi, S.; Santos, R.H.M. (2017) Predictive models for post disaster shelter needs assessment. *Int. J. Disaster Risk Reduct.*, 21, 44–62. [
- [31] Balbi, A.; Galasco, S.; Giovinazzi, S.; Lagormarsino, S.; Parodi, S. “Scenario Sismico”: A Tool For Real Time Damage Scenarios (2006) In *Proceedings of the First European Conference on Earthquake Engineering and Seismology*, Geneva, Switzerland, 3–8 September; 912.
- [32] Pollino, M.; Fattoruso, G.; La Porta, L.; Della Rocca, A.B.; James, V. (2012) Collaborative Open Source Geospatial Tools and Maps Supporting the Response Planning to Disastrous Earthquake Events. *Future Internet*, 4, 451–468.
- [33] Steiniger, S.; Hunter, A.J.S. (2011) Free and Open Source GIS Software for Building a Spatial Data Infrastructure. In *Geospatial Free and Open Source Software in the 21st Century*; Bocher, E., Neteler, M., Eds.; Springer: Berlin/Heidelberg, Germany, 247–261.
- [34] Coletti, A.; De Nicola, A.; Di Pietro, A.; La Porta, L.; Pollino, M.; Rosato, V.; Vicoli, G.; Villani, M.L., (2020) A comprehensive system for semantic spatiotemporal assessment of risk in urban areas. *J. Conting. Crisis Manag*, 28, 178–193.
- [35] Pollino, M.; Cappucci, S.; Giordano, L.; Iantosca, D.; De Cecco, L.; Bersan, D.; Rosato, V.; Borfecchia, F. (2020) Assessing Earthquake-Induced Urban Rubble by Means of Multiplatform Remotely Sensed Data. *ISPRS Int. J. Geo-Inf*, 9, 262.
- [36] Giovinazzi, S.; Marchili, C.; Di Pietro, A.; Giordano, L.; Costanzo, A.; La Porta, L.; Pollino, M.; Rosato, V.; Lückerkath, D.; Milde, K.; Ullrich, O. (2021) Assessing Earthquake Impacts and Monitoring Resilience of Historic Areas: Methods for GIS Tools. *ISPRS Int. J. Geo-Inf.* (10), 461. <https://doi.org/10.3390/ijgi10070461>
- [37] Francesco Mulargia, Philip B. Stark and Robert J. Geller. Why is Probabilistic Seismic Hazard Analysis (PSHA) still used? (2016). *Physics of the Earth and Planetary Interiors*. Vol. 264:63-75. DOI: 10.1016/j.pepi.2016.12.002.

- [38] Peresan, A., Zuccolo, E., Vaccari, F., Gorshkov, A., Panza, G., (2011) Neo-Deterministic Seismic Hazard and Pattern Recognition Techniques: Time-Dependent Scenarios for North-Eastern Italy. *Pure and Applied Geophysics*. 168. 583-607. 10.1007/s00024-010-0166-1.
- [39] Dolce, M., Prota, A., Borzi, B. et al. Seismic risk assessment of residential buildings in Italy. (2021), *Bull Earthquake Eng* 19, 2999–3032. <https://doi.org/10.1007/s10518-020-01009-5>
- [40] Beyreuther, M.; Barsch, R.; Krischer, L.; Megies, T.; Behr, Y.; Wassermann, J. ObsPy: A Python Toolbox for Seismology. *Seismol. Res. Lett.* 2010, 81, 530–533.
- [41] Megies, T.; Beyreuther, M.; Barsch, R.; Krischer, L.; Wassermann, J. ObsPy—What can it do for data centers and observatories? *Ann. Geophys.* 2011, 54, 47–58.
- [42] EMSC Seismic Portal. Available online: <https://www.emsc-csem.org/Project/#seismic> (accessed on 30 November 2020).
- [43] INGV Seismological Data Centre. Rete Sismica Nazionale (RSN). Italy. Available online: <http://cnt.rm.ingv.it/instruments/network/IV> (accessed on 6 May 2021).
- [44] FDSN Services. Available online: <http://fdsn.org/services/> (accessed on 30 November 2020).
- [45] Guidoboni, E.; Ferrari, G.; Tarabusi, G.; Sgattoni, G.; Comastri, A.; Mariotti, D.; Ciuccarelli, C.; Bianchi, M.G.; Valensise, G., CFTI5Med, the new release of the catalogue of strong earthquakes in Italy and in the Mediterranean area.
- [46] Stucchi, M.; Rovida, A.; Capera, A.A.G.; Alexandre, P.; Camelbeeck, T.; Demircioglu, M.B.; Gasperini, P.; Kouskouna, V.; Musson, R.M.W.; Radulian, M.; et al. The SHARE European Earthquake Catalogue (SHEEC) 1000–1899. *J. Seismol.* 2013, 17, 523–544.
- [47] Grünthal, G.; Wahlström, R.; Stromeyer, D. The SHARE European Earthquake Catalogue (SHEEC) for the time period 1900–2006 and its comparison to the European-Mediterranean Earthquake Catalogue (EMEC). *J. Seismol.* 2013, 17, 1339–1344.
- [48] DISS Working Group. Database of Individual Seismogenic Sources (DISS), Version 3.2.1: A Compilation of Potential Sources for Earthquakes Larger than M 5.5 in Italy and Surrounding Areas. Istituto Nazionale di Geofisica e Vulcanologia. 2018. Available online: <http://diss.rm.ingv.it/diss/> (accessed on 26 January 2021).
- [49] Basili, R.; Kastelic, V.; Demircioglu, M.B.; Moreno, D.G.; Nemser, E.S.; Petricca, P.; Sboras, S.P.; Besana-Ostman, G.M.; Cabral, J.; Camelbeeck, T.; et al. The European Database of Seismogenic Faults (EDSF) Compiled in the Framework of the Project SHARE. Available online: <http://diss.rm.ingv.it/share-edsf/> (accessed on 6 May 2021).
- [50] Italian Seismic Map. Available online: http://esse1-gis.mi.ingv.it/s1_en.php (accessed on 30 November 2020).
- [51] Giardini, D.; Wössner, J.; Danciu, L. Mapping Europe's Seismic Hazard. *Eos* 2014, 95, 261–262.
- [52] Toro, G.; Abrahamson, N.; Schneider, J. Letter to the editor. *Seismol. Res. Lett.* 1997, 68, 481–482.
- [53] Open Data Ricostruzione Sisma. 2016. Available online: <https://sisma2016data.it/microzonazione/> (accessed on 30 November 2020).
- [54] Lanzo, G.; Silvestri, F.; Costanzo, A.; D'Onofrio, A.; Martelli, L.; Pagliaroli, A.; Sica, S.; Simonelli, A. Site response studies and seismic microzoning in the Middle Aterno valley (L'aquila, Central Italy). *Bull. Earthq. Eng.* 2011, 9, 1417–1442.
- [55] Costanzo, A.; Caserta, A. Seismic response across the Tronto Valley (at Acquasanta Terme, AP, Marche) based on the geophysical monitoring of the 2016 Central Italy seismic sequence. *Bull. Int. Assoc. Eng. Geol.* 2019, 78, 5599–5616.
- [56] ISPRA Hydro-Geological Hazards. <https://idrogeo.isprambiente.it/app/page/open-data> (accessed on 30 November 2020).
- [57] Wald, D.; Allen, T.I. Topographic Slope as a Proxy for Seismic Site Conditions and Amplification. *Bull. Seismol. Soc. Am.* 2007, 97, 1379–1395.
- [58] Michelini, A.; Faenza, L.; Lauciani, V.; Malagnini, L. Shakemap Implementation in Italy. *Seismol. Res. Lett.* 2008, 79, 688–697.

- [59] Worden, C.B.; Wald, D.J.; Sanborn, J.; Thompson, E.M. Development of an open-source hybrid global Vs30 model. In Proceedings of the Seismological Society of America Annual Meeting, Pasadena, CA, USA, 21–23 April 2015.
- [60] Mori, F.; Mendicelli, A.; Moscatelli, M.; Romagnoli, G.; Peronace, E.; Naso, G. A new Vs30 map for Italy based on the seismic microzonation dataset. *Eng. Geol.* 2020, 275, 105745.
- [61] Lanzano, G.; Luzi, L.; Pacor, F.; Felicetta, C.; Puglia, R.; Sgobba, S.; D'Amico, M. A Revised Ground-Motion Prediction Model for Shallow Crustal Earthquakes in Italy. *Bull. Seismol. Soc. Am.* 2019, 109, 525–540.
- [62] Faenza, L.; Michelini, A. Regression analysis of MCS intensity and ground motion parameters in Italy and its application in ShakeMap. *Geophys. J. Int.* 2010, 180, 1138–1152.
- [63] Joyner, W.; Boore, D.M.; Porcella, R. Peak horizontal acceleration and velocity from strong motion records including records from the 1979 Imperial Valley, California, earthquake. *Open File Rep.* 1981, 71, 2011–2038.
- [64] Bindi, D.; Pacor, F.; Luzi, L.; Puglia, R.; Massa, M.; Ameri, G.; Paolucci, R. Ground motion prediction equations derived from the Italian strong motion database. *Bull. Earthq. Eng.* 2011, 9, 1899–1920.
- [65] Sieberg, A. *Geologie der Erdbeben. Handbuch Geophysik* 1930, 2, 552–555.
- [66] Margottini, C.; Molin, D.; Serva, L. Intensity versus ground motion: A new approach using Italian data. *Eng. Geol.* 1992, 33, 45–58.
- [67] Grünthal, G. European Macroseismic Scale 1998. In *Chaiers du Centre Européen de Géodynamique et de Seismologie*; Grünthal, G., Musson, R.M.W., Schwarz, J., Stucchi, M., Eds.; Conseil de l'Europe: Luxembourg, 1998; Volume 15, 100p, ISBN 2-87977-008-4.
- [68] Costanzo, A.; Falcone, S.; D'Alessandro, A.; Vitale, G.; Giovinazzi, S.; Morici, M.; Dall'Asta, A.; Buongiorno, M.F. A Technological System for Post-Earthquake Damage Scenarios Based on the Monitoring by Means of an Urban Seismic Network. *Sensors* 2021, 21, 7887. <https://doi.org/10.3390/s21237887>
- [69] Lanzo, G.; Silvestri, F.; Costanzo, A.; D'Onofrio, A.; Martelli, L.; Pagliaroli, A.; Sica, S.; Simonelli, A. Site response studies and seismic microzoning in the Middle Aterno valley (L'Aquila, Central Italy). *Bull. Earthq. Eng.* 2011, 9, 1417–1442.
- [70] Caserta, A.; Doumaz, F.; Costanzo, A.; Gervasi, A.; Thorossian, W.; Falcone, S.; La Piana, C.; Minasi, M.; Buongiorno, M.F. Assessing soil-structure interaction during the 2016 central Italy seismic sequence (Italy): Preliminary results. *Ann. Geophys.* 2016, 59, 1–7.
- [71] Costanzo, A.; Caserta, A. (2019) Seismic response across the Tronto Valley (at Acquasanta Terme, AP, Marche) based on the geophysical monitoring of the 2016 Central Italy seismic sequence. *Bull. Eng. Geol. Environ.*, 78, 5599–5616.
- [72] Costanzo, A.; D'Onofrio, A.; Silvestri, F. (2019) Seismic response of a geological, historical and architectural site: The Gerace cliff (southern Italy). *Bull. Eng. Geol. Environ.*, 78, 5617–5633.
- [73] Ferraro, A.; Grasso, S.; Maugeri, M.; Totani, F. Seismic response analysis in the southern part of the historic centre of the City of L'Aquila (Italy) (2016) *Soil Dyn. Earthq. Eng.*, 88, 256–264.
- [74] Brando, G.; Pagliaroli, A.; Cocco, G.; Di Buccio, F. (2020) Site effects and damage scenarios: The case study of two historic centers following the 2016 Central Italy earthquake. *Eng. Geol.*, 272, 105647.
- [75] Maccari, M.; Onorati, A.; Pesaresi, A. Geological-Technical Map in the 3th Level of the Seismic Microzonation of Camerino. Available online: http://www.comune.camerino.mc.it/wp-content/blogs.dir/11/files/Carta_geologico_tecnica-10000.pdf.
- [76] Krukowski, A.; Vogiatzaki, E.; Costanzo, A.; Buongiorno, F.; Bignami, C.; D'Alessandro, A.; Falcone, S.; Musacchio, M.; Silvestri, M.; Vitale, G.; Morici, M.; Dall'Asta, A.; Zona, A.; Giovinazzi, S., (2021) ARCH-D4.1 - Sensing and Repositories. Deliverable of the H2020 ARCH project, GA no. 820999, 2019.

- [77] Costanzo, A., Falcone, S., Krukowski, A., Peña Cerezo, N., Giordano, L., Giovinazzi, S., Krukowski, P., (2021) ARCH-D4.3 - Threats and Hazard Information System. Deliverable of the H2020 ARCH project, GA no. 820999, 2019
- [78] Meju, Max & Gallardo, Luis & Mohamed, Adel. (2003). Evidence for correlation of electrical resistivity and seismic velocity in heterogeneous near-surface materials. *Geophysical Research Letters*. 30. 1373-1373. 10.1029/2002GL016048
- [79] Marzán, I., Martí, D., Lobo, A., Alvarez-Marrón, J., Carbonell, R., (2019) Cluster analysis of Vp seismic velocity, and resistivity: Subsurface model building. <http://hdl.handle.net/10261/204059>
- [80] Faust, L.Y. (1953), A velocity function including lithologic variation. *Geophysics*, 18, 271–288.
- [81] Crain, E.R., (2000) Editing Logs—Editing with Resistivity. In *Crain's Petrophysical Handbook*; Crain, E.R., Ed.; Available online: <https://www.spec2000.net/> (accessed on 27 July 2021).

6. Annex: Thermal model maps for the grey and black scenario

Maximum and minimum temperature distribution maps have been generated for each of periods (1981-2011, 2011-2041, 2041-2070, 2071-2100) to observe the distribution trend of temperature along the area of study. Additionally, each grey/black land use scenario values have been subtracted to the current land use scenario to better visualized spatially the differences between scenarios, as reported below in Figures from 80 to 96.

6.1. Historic data

Grey Scenario

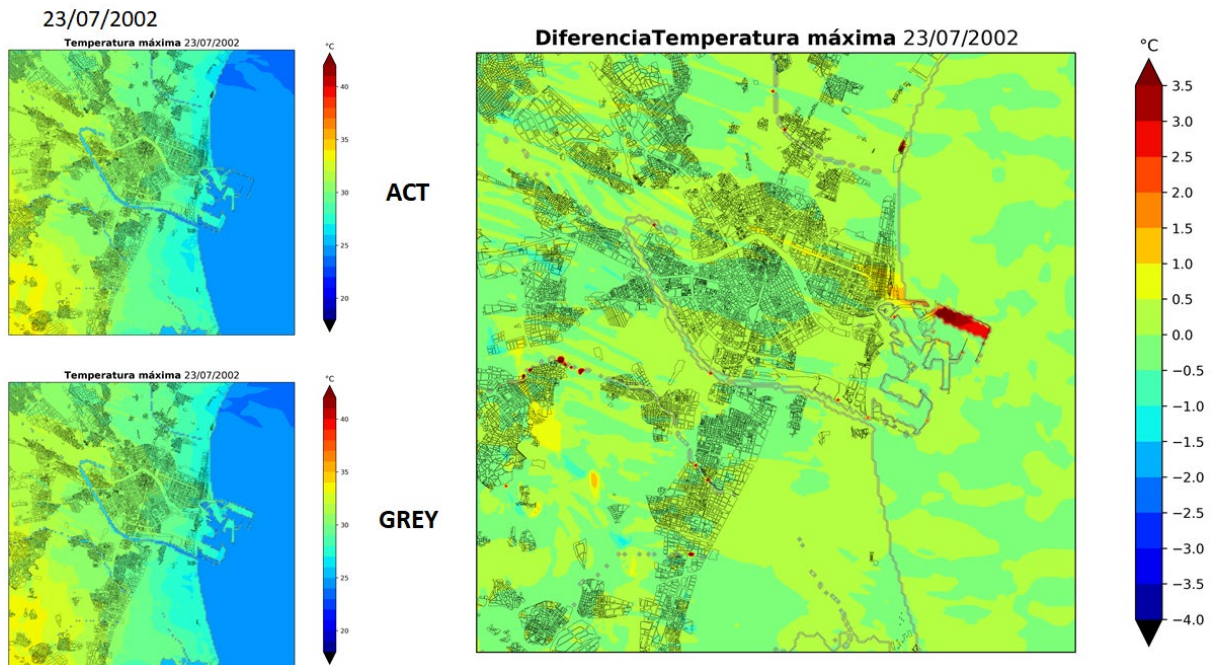


Figure 80. Maximum temperature values and differences between grey and current scenario (1981-2010).

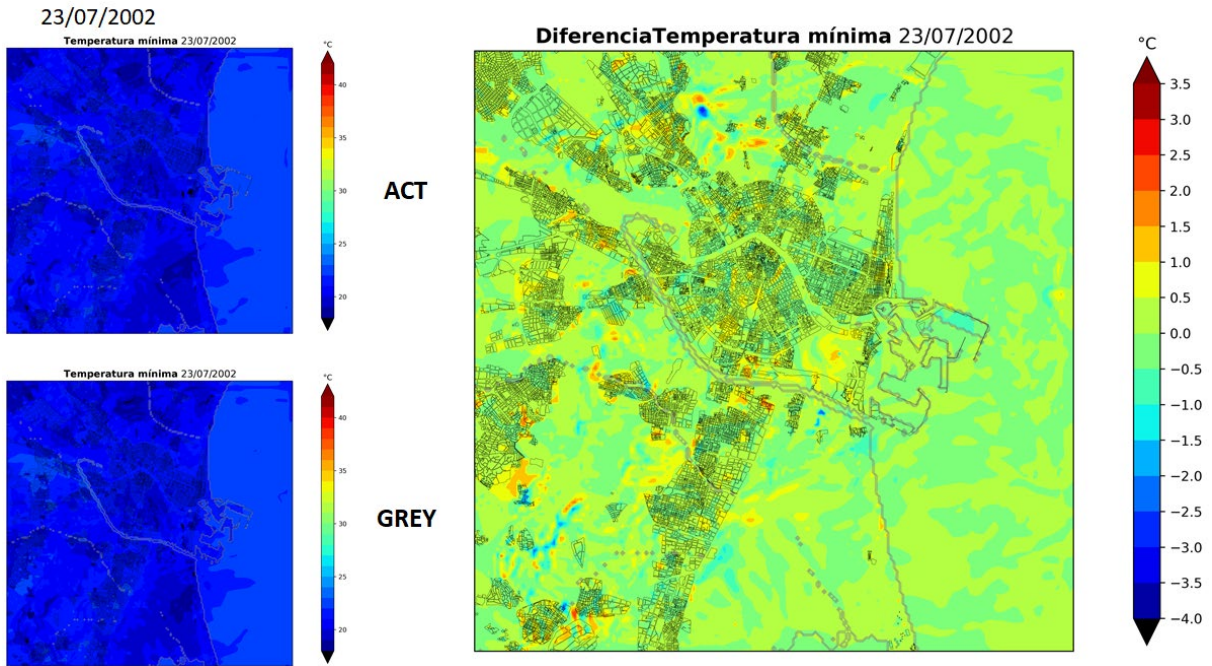


Figure 81. Minimum temperature values and differences between grey and current scenarios (1981-2010).

Black Scenario

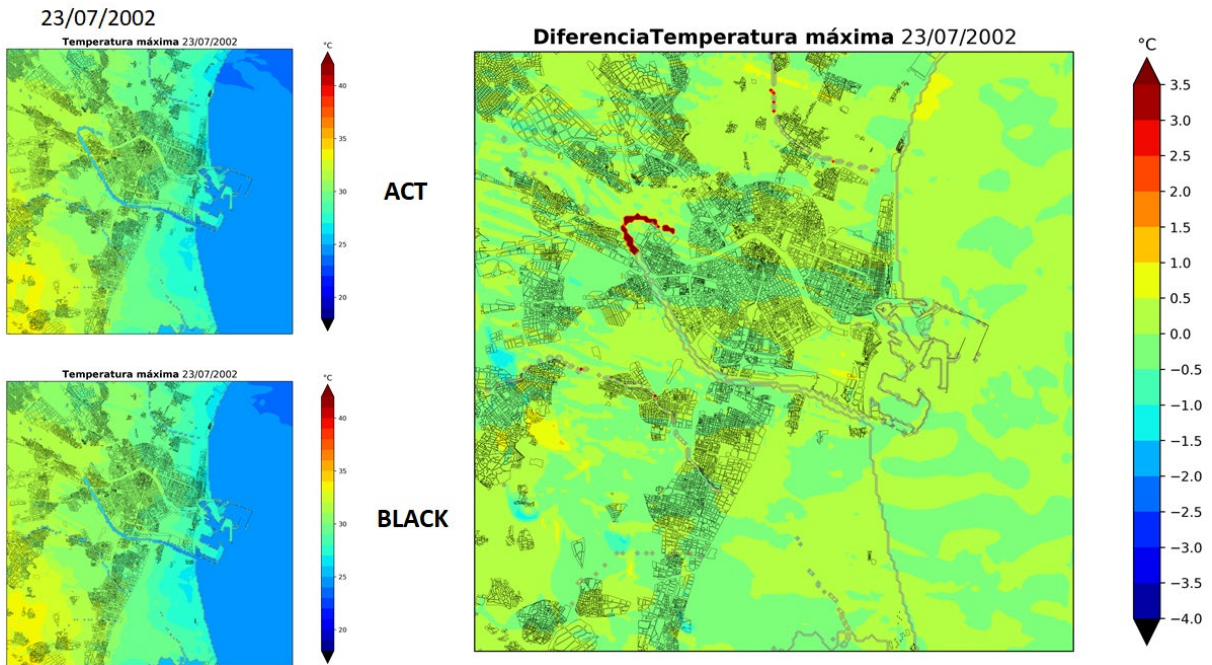


Figure 82. Maximum temperature values and differences between black and current scenario (1981-2010)

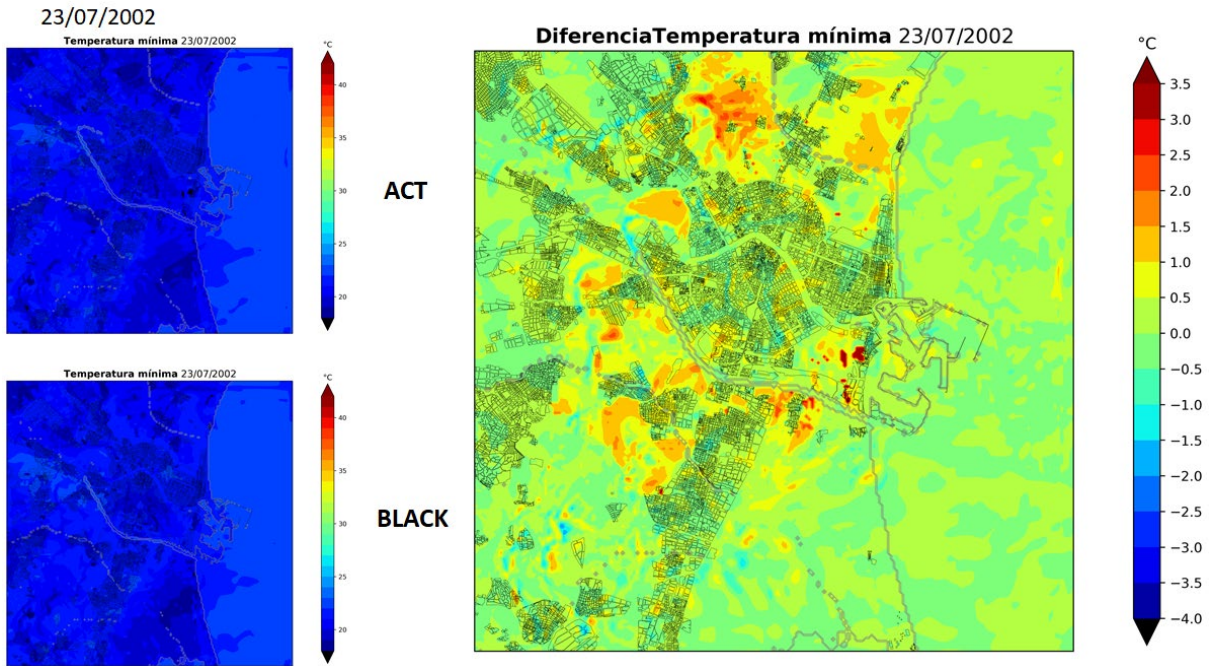


Figure 83. Minimum temperature values and differences between black and current scenario (1981-2010).

Hourly distribution of temperature per scenario

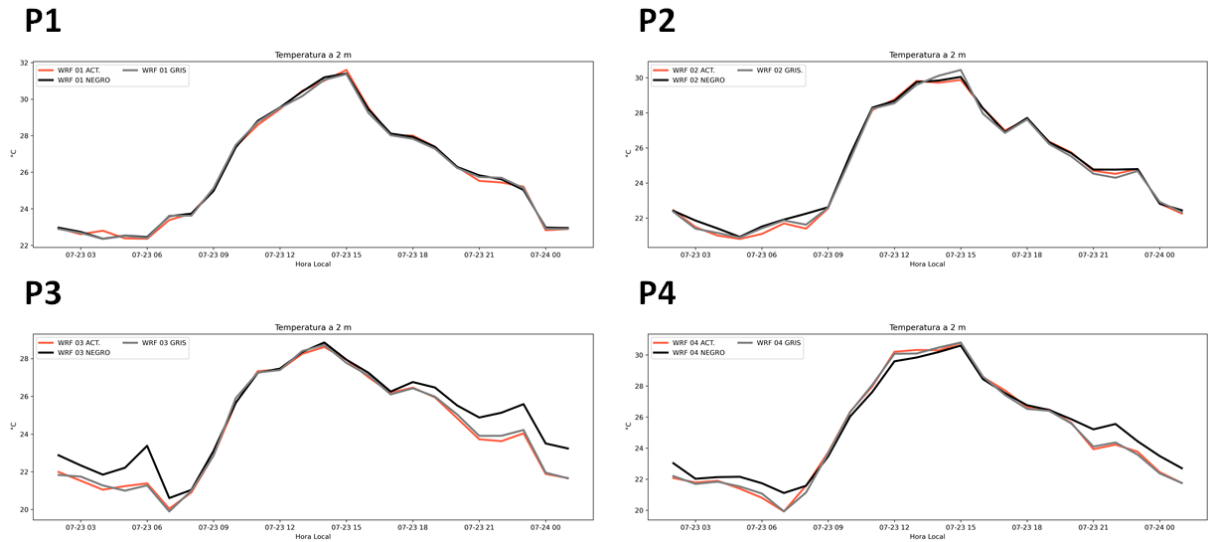


Figure 84. Each plot represents the hourly distribution of 2m temperature for each geographical point for 1981-2010. (Red line represents the current land use scenario, grey line represents the grey land use scenario and black line represents the black land use scenario).

6.2. Near Future (2011-2040)

Grey Scenario

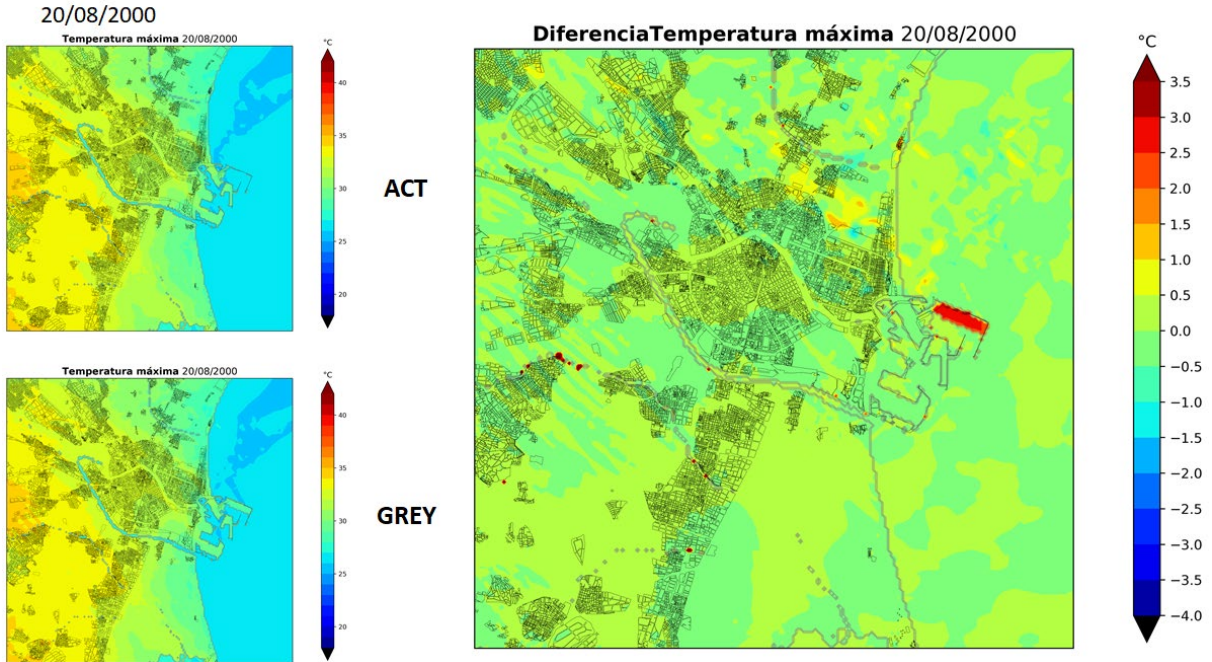


Figure 85. Maximum temperature values and differences between grey and current scenario (2011-2040).

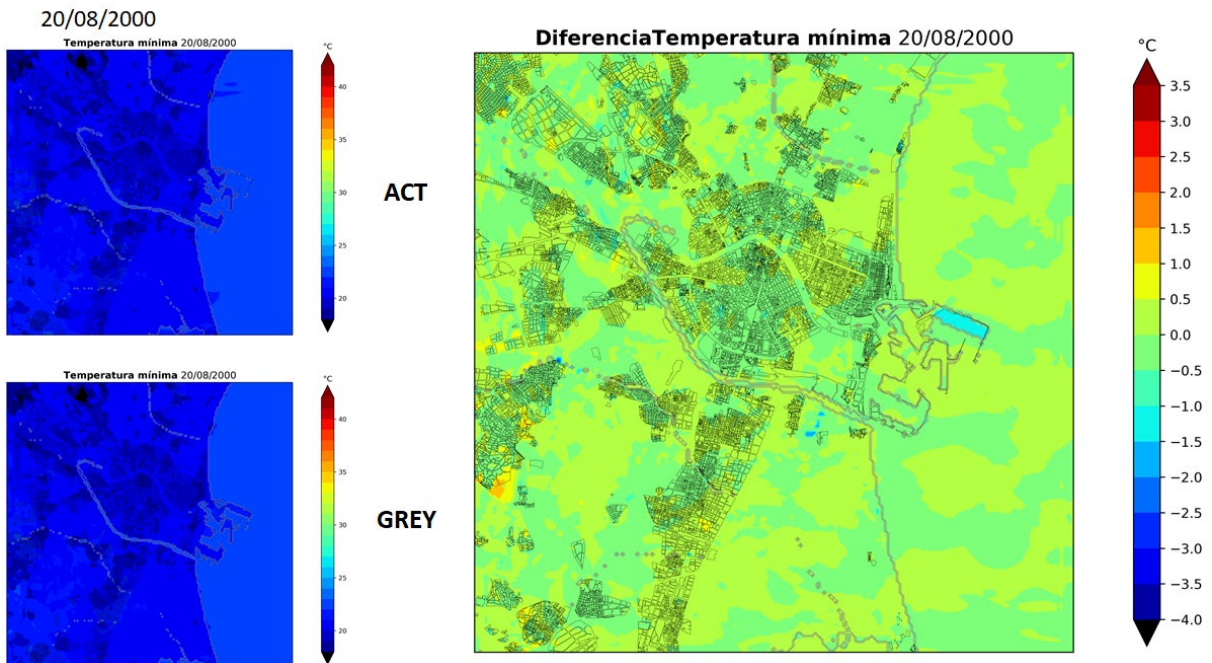


Figure 86. Minimum temperature values and differences between grey and current scenario (2011-2040).

Black Scenario

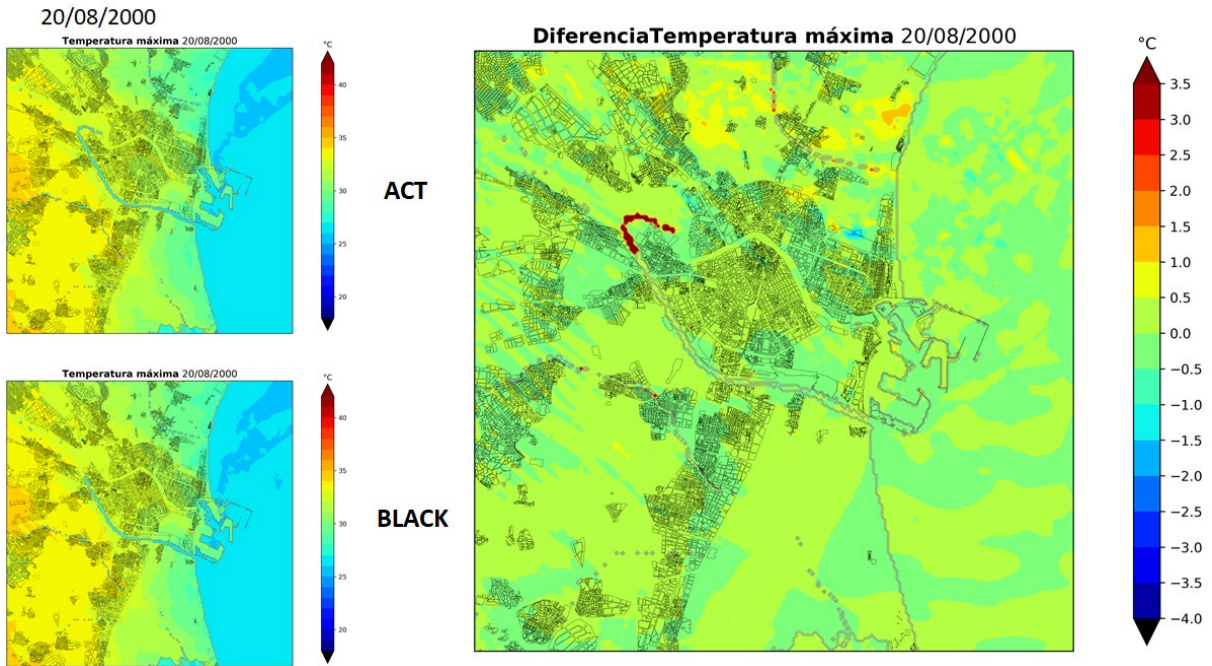


Figure 87. Maximum temperature values and differences between black and current scenario (2011-2040).

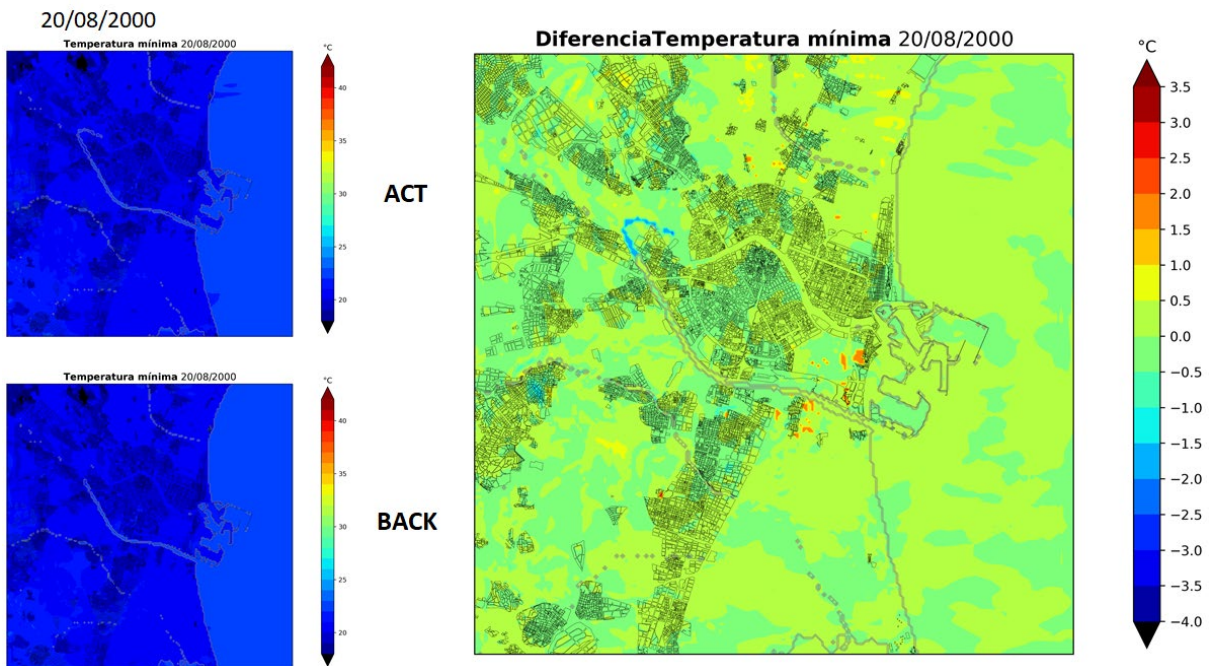


Figure 88. Minimum temperature values and differences between black and current scenario (2011-2040).

Hourly distribution of temperature per scenario

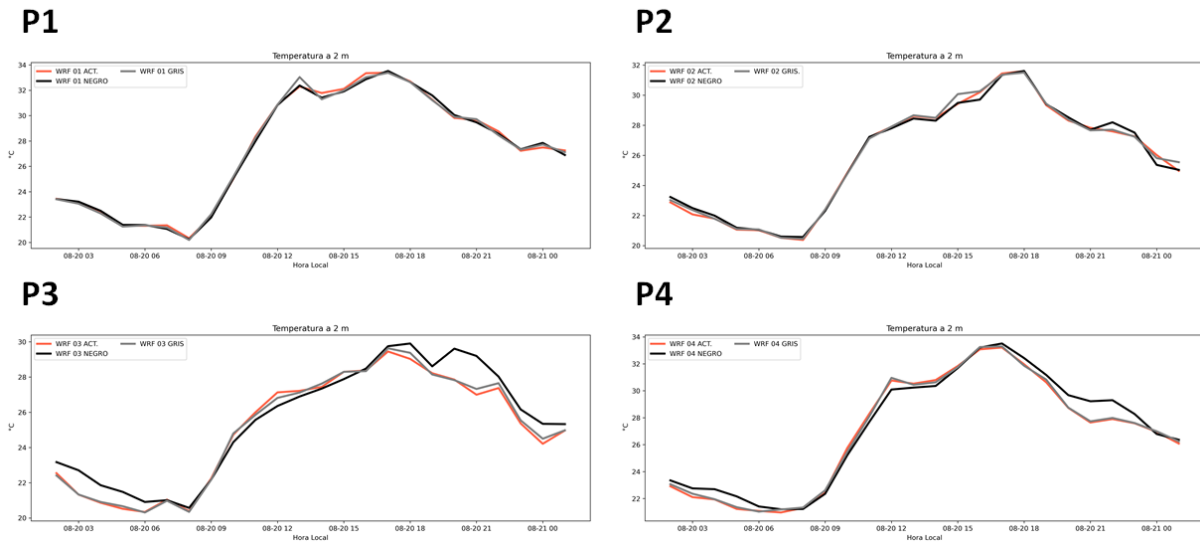


Figure 89. Each plot represents the hourly distribution of 2m temperature for each geographical point for 2011-2040. (Red line represents the current land use scenario, grey line represents the grey land use scenario and black line represents the black land use scenario)

6.3. Next Future (2041-2070)

Grey Scenario

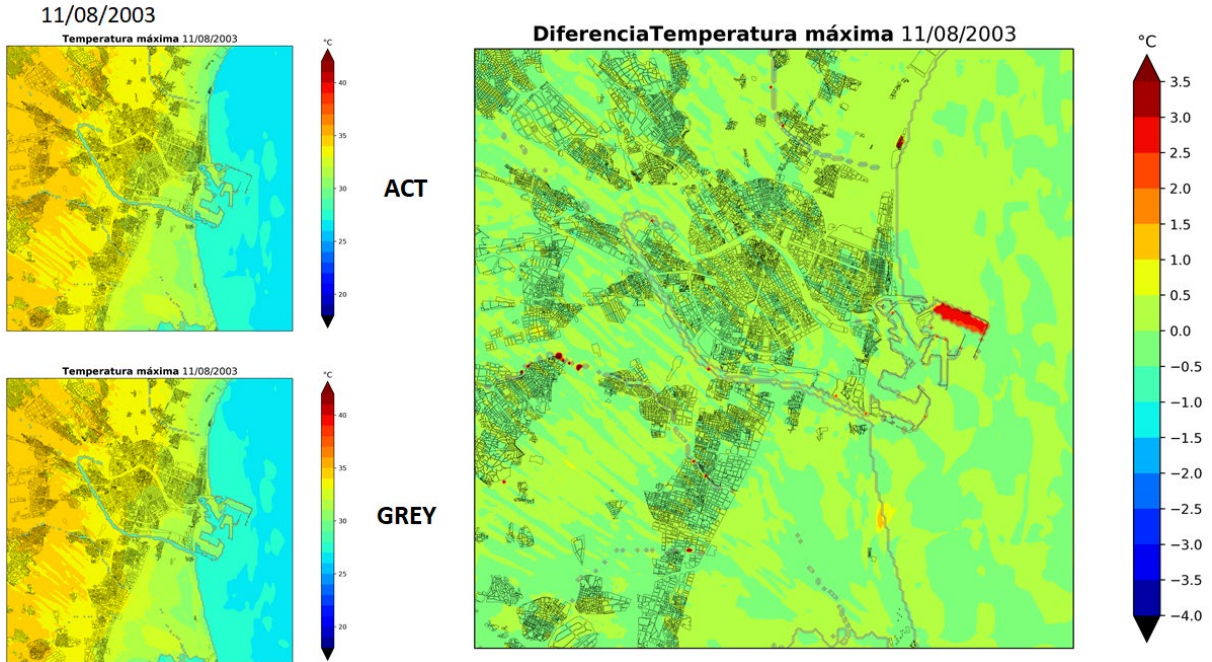


Figure 90. Maximum temperature values and differences between grey and current scenario (2041-2070).

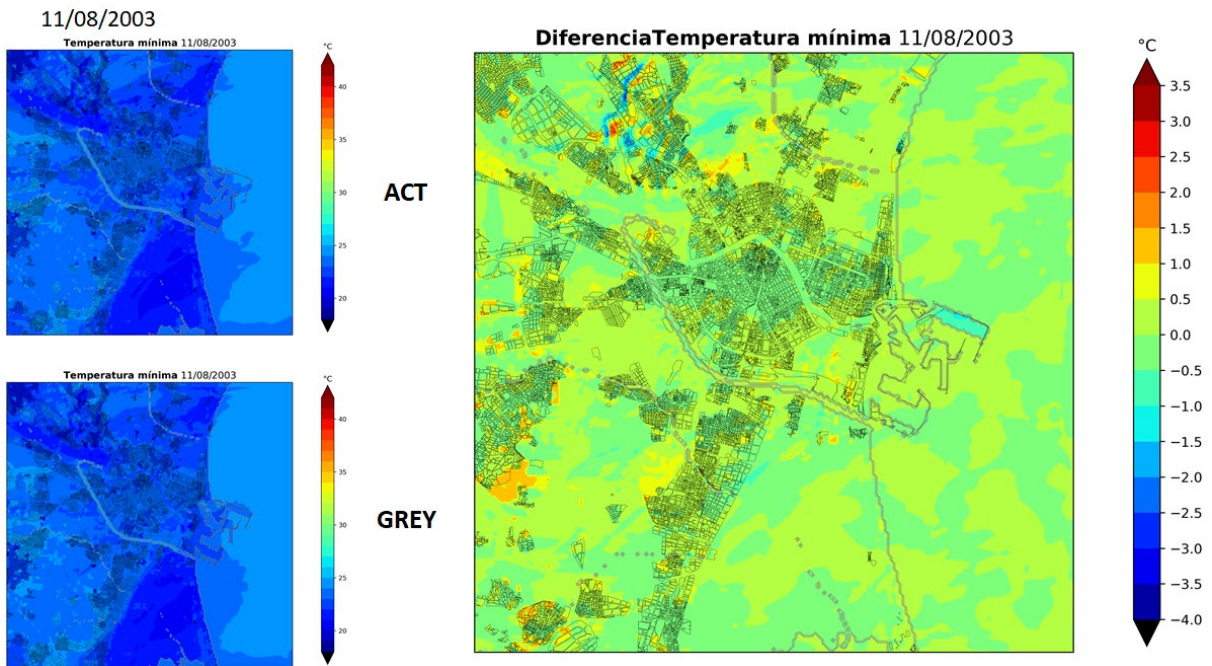


Figure 91. Minimum temperature values and differences between grey and current scenario (2041-2070)

Black Scenario

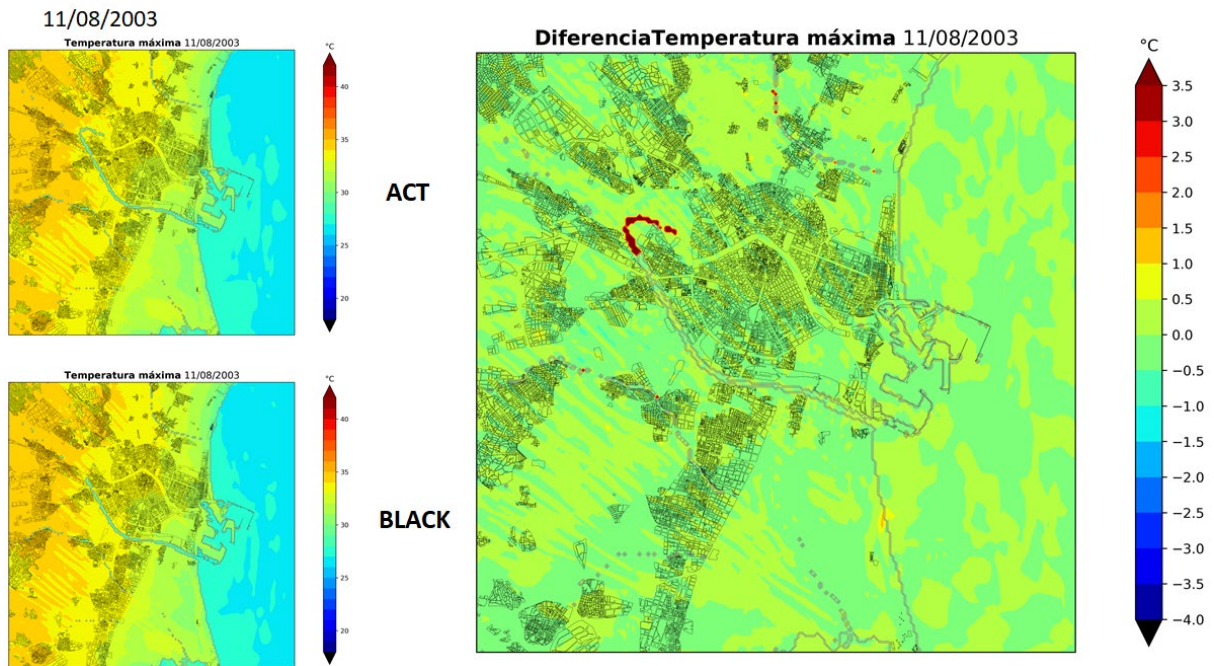


Figure 92. Maximum temperature values and differences between black and current scenario (2041-2070).

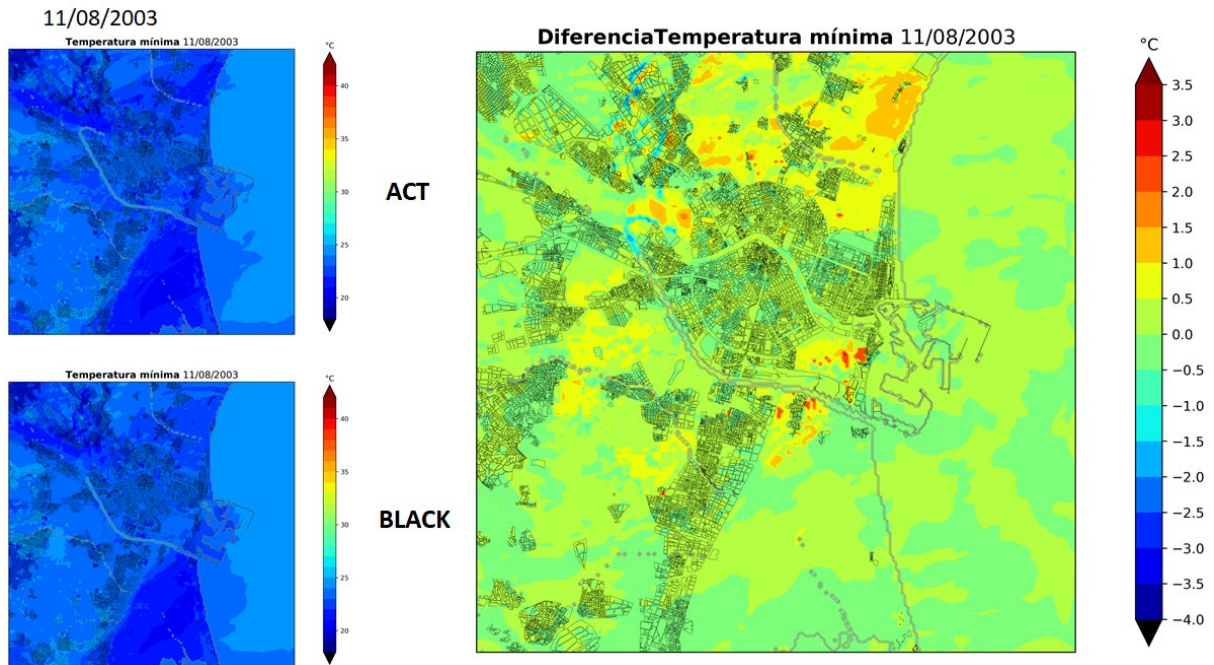


Figure 93. Minimum temperature values and differences between black and current scenario (2041-2070).

Hourly distribution of temperature per scenario

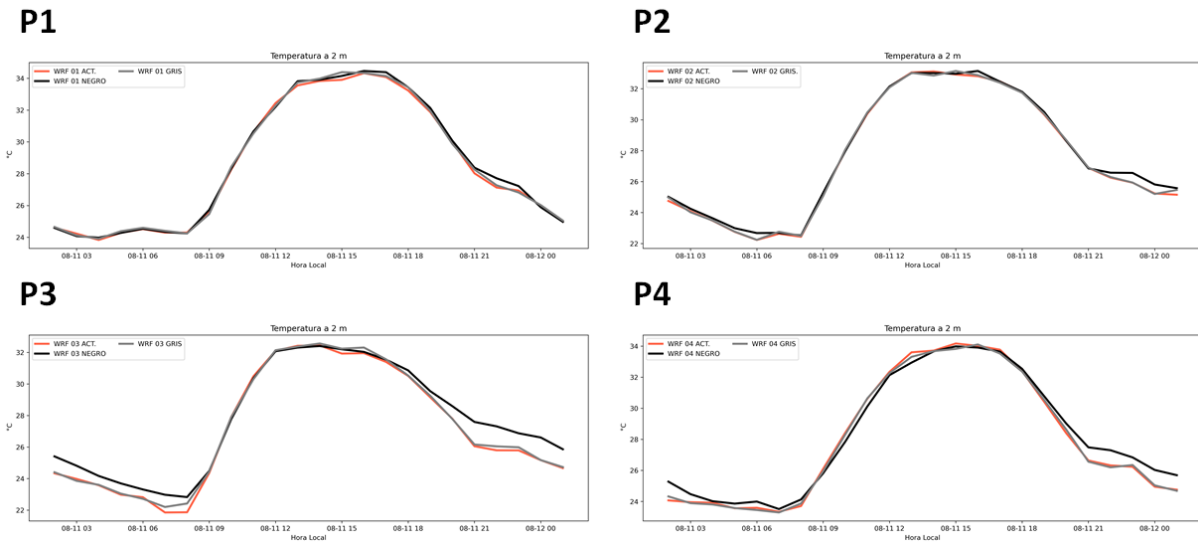


Figure 94. Each plot represents the hourly distribution of 2m temperature for each geographical point for 2041-2070. (Red line represents the current land use scenario, grey line represents the grey land use scenario and black line represents the black land use scenario).

6.4. Far Future (2071-2100)

Grey Scenario

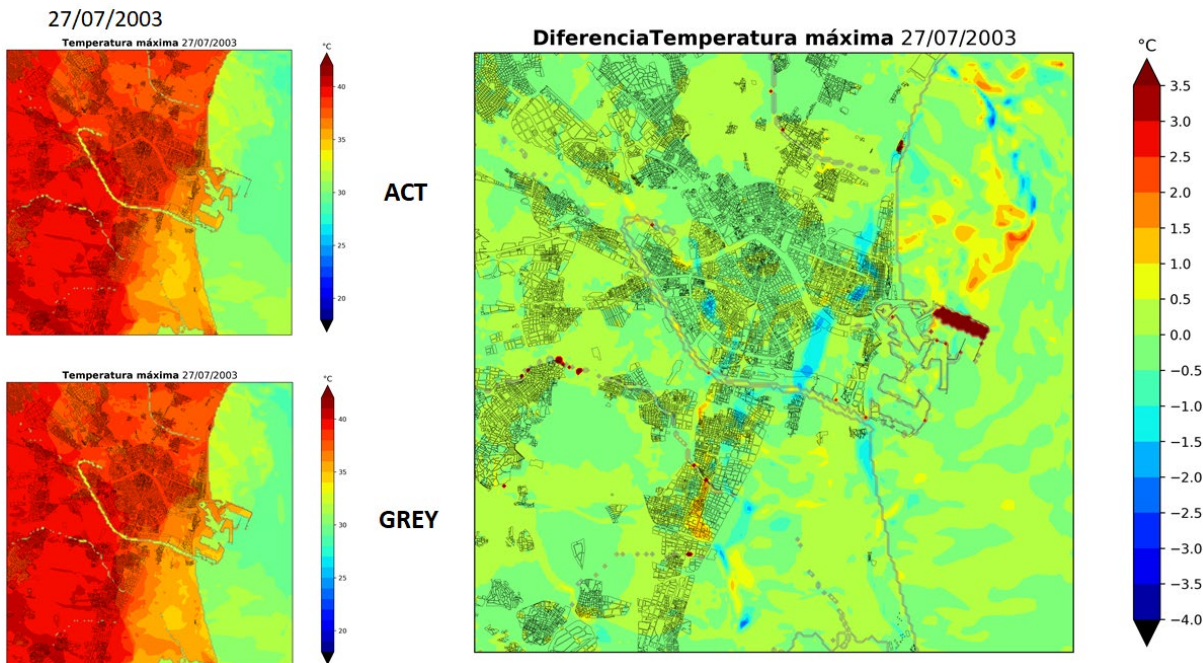


Figure 95. Maximum temperature values and differences between grey and current scenario (2071-2100).

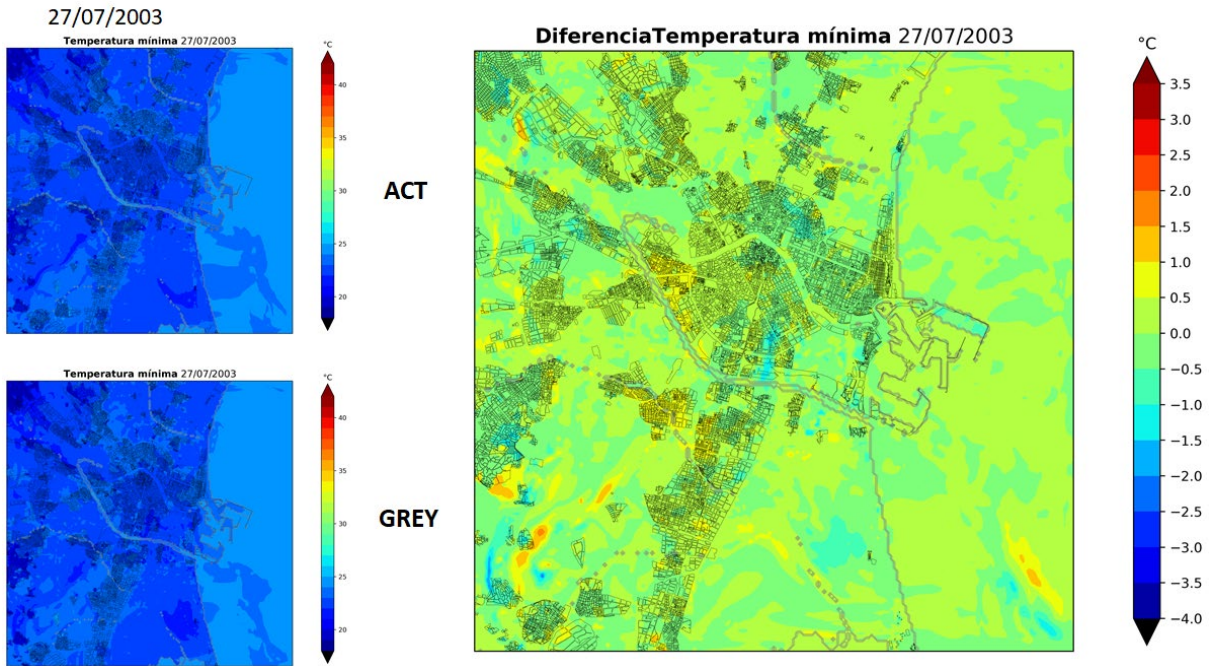


Figure 96. Minimum temperature values and differences between grey and current scenario (2071-2100).

Black Scenario

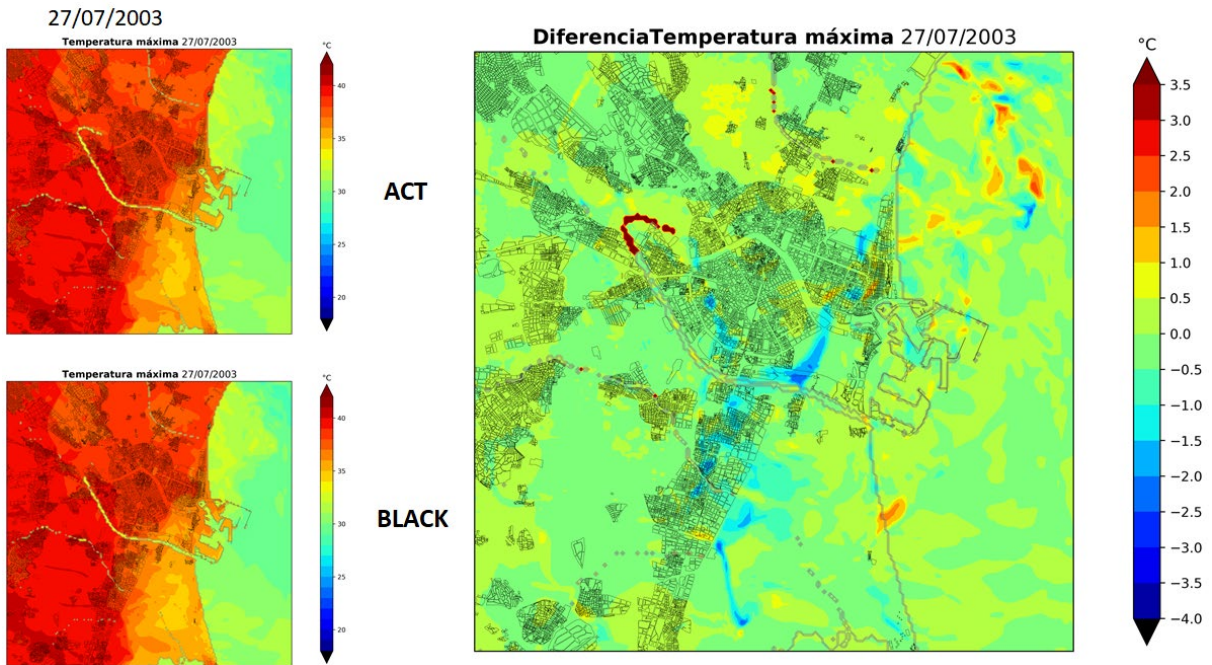


Figure 97. Maximum temperature values and differences between black and current scenario (2071-2100).

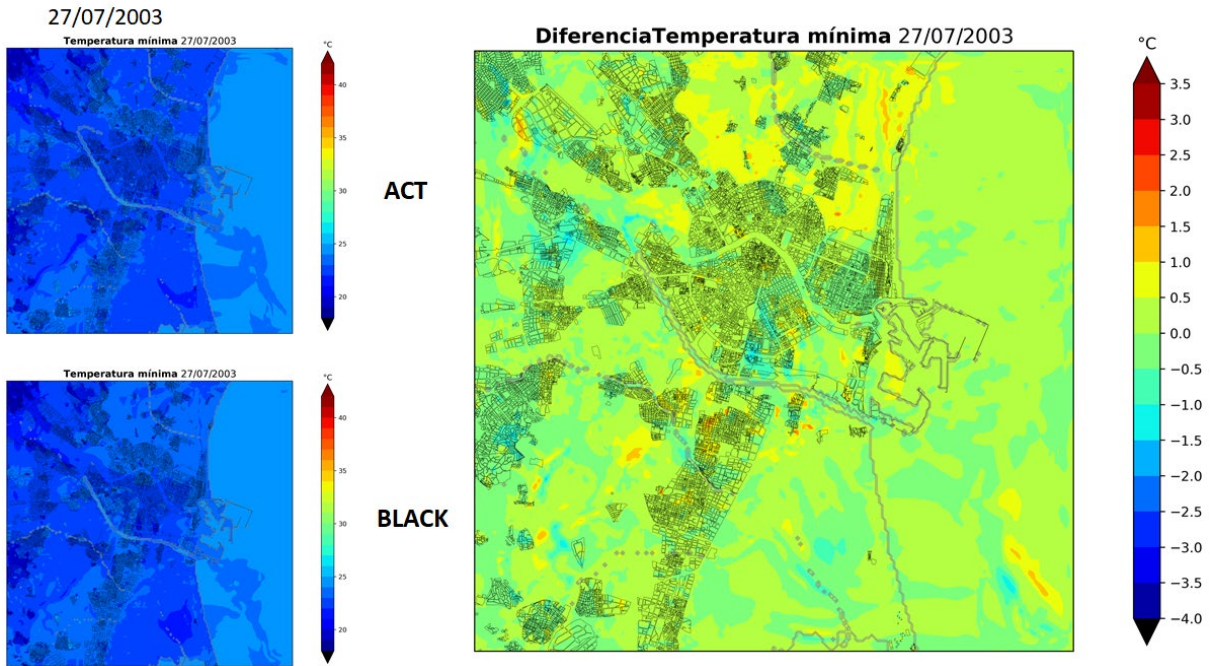


Figure 96. Minimum temperature values and differences between black and current scenario (2071-2100).

Hourly distribution of temperature per scenario

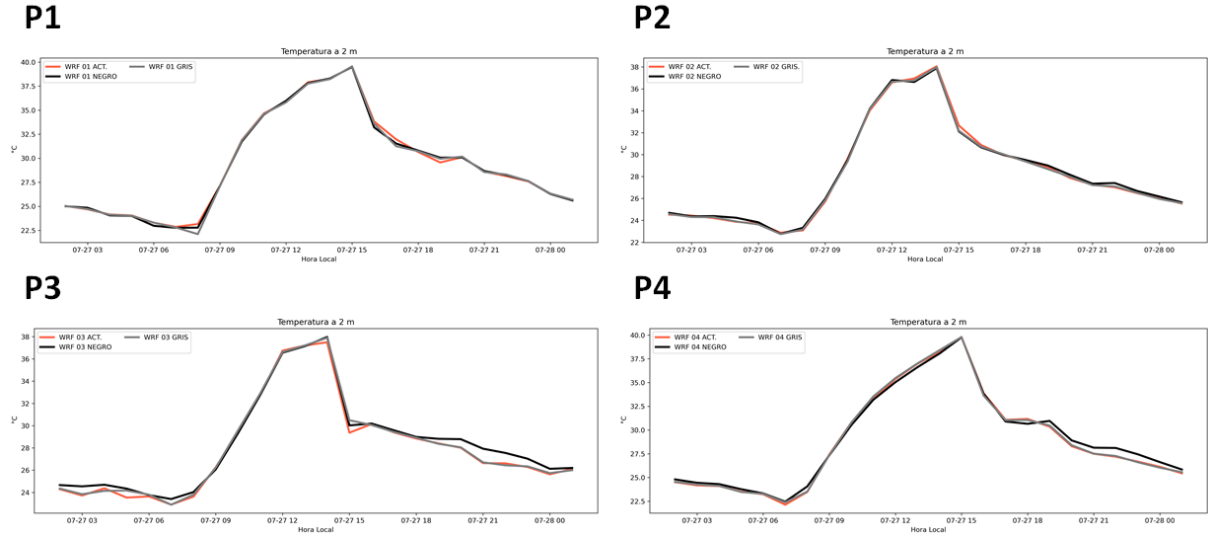


Figure 97. Each plot represents the hourly distribution of 2m temperature for each geographical point for 2071-2100. (Red line represents the current land use scenario, grey line represents the grey land use scenario and black line represents the black land use scenario).

7. Annex: Earthquake-induced ground shaking maps

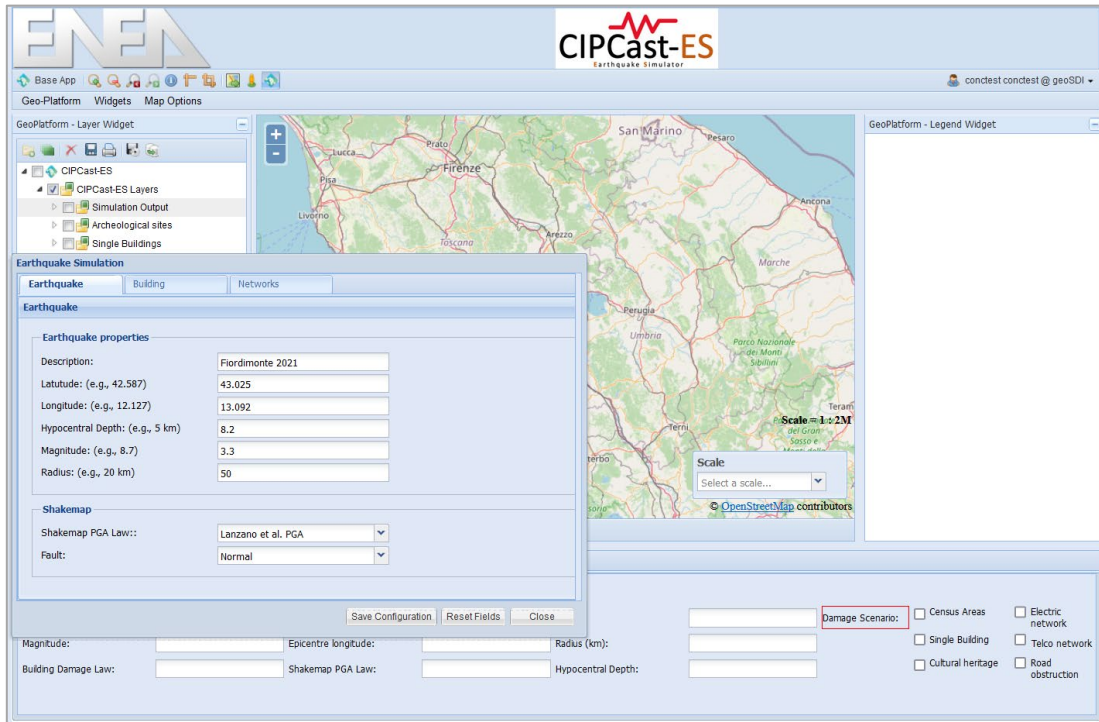


Figure 98. ARCH DSS end-user interface for defining the parameters of the earthquake event to be simulated filled out with the parameters of the Fiordimonte (MC) 2021-04-18 17:25:59 earthquake (Table 13).

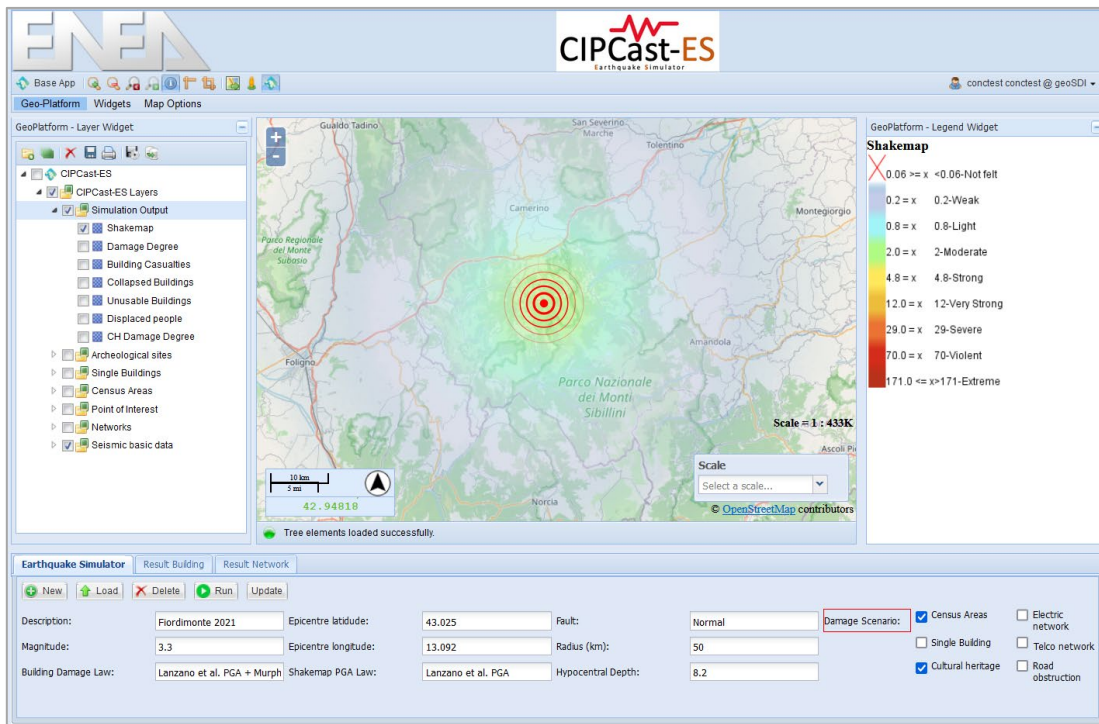


Figure 99. Screenshot of ARCH DSS ground shaking map [%g] resulting for the Fiordimonte (MC) 2021-04-18 17:25:59 Earthquake (Table 14).

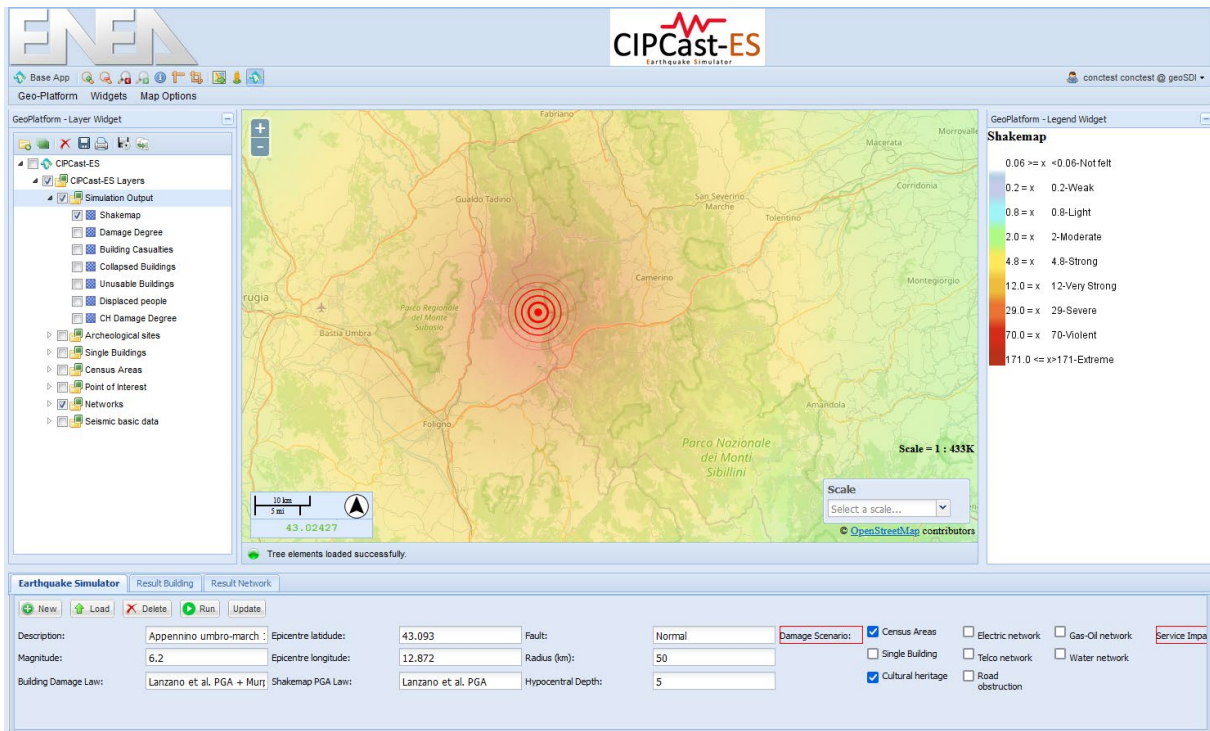


Figure 100. Ground-shaking map (PGA in [%g]) for the 1279 Appennino umbro-marchigiano earthquake 30/04/1279 simulated using the ARCH DSS.

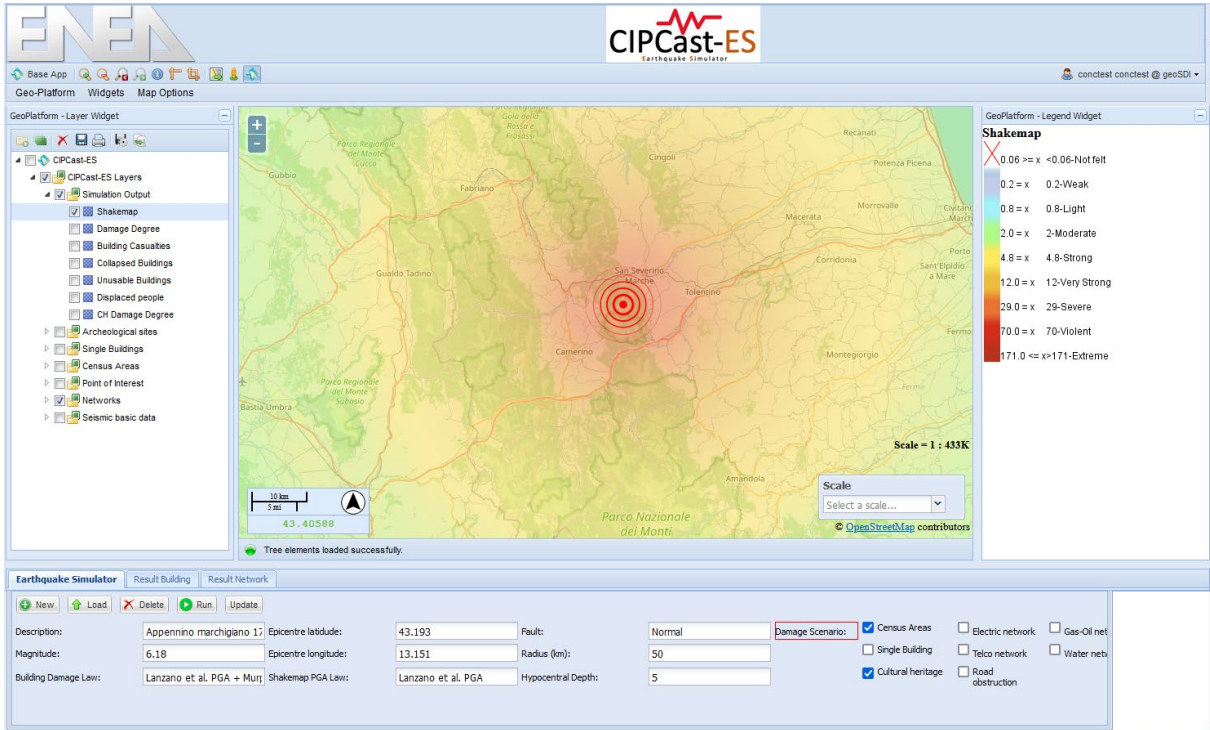


Figure 101. Ground-shaking map (PGA in [%g]) for the 1799 Appennino marchigiano earthquake 28/07/1799 simulated using the ARCH DSS.